Topics in 2-D Separated Vortex flows

Thesis by
Saleh Ahmed Tanveer

In Partial Fulfillment of the Requirement
for the Degree of
Doctor of Philosophy

California Institute of Technology
Pasadena, California
1984
(Submitted October 26, 1983)

ACKNOWLDEDGEMENT

First of all, I wish to thank my advisor Professor P.G.Saffman for his guidance and expertise which was crucial at every stage of progress of this thesis. Not only did he suggest the topic, but also followed it through with great patience and care. His sincere concern for me as an individual and constant encouragement made it very enjoyable for me to work with him.

I also like to express my gratitude to Caltech for financially supporting me through Graduate Teaching and Research assistantships and for giving me the opportunity in the first place to attend Caltech and share its facilities.

Further thanks to the faculty and fellow students in the deparment of Applied Mathematics especially Dr. Bengt Fornberg for some useful suggestions. Special thanks to Mrs. Edith Huang of the computing center for bearing with a computer novice.

Last of all, I like to express gratitude to my parents for their love, care and sacrifice without which I would have never got this far.

ABSTRACT

This thesis is concerned with vortices in steady two dimensional inviscid incompressible flow. In the first three chapters, separated vortex flows are considered in the context of inviscid flow past two dimensional airfoils for which the action of the vortex is to induce large lift. In the fourth and last chapter, we consider vortices in uniform flow in the absence of any physical bodies.

In chapter I, we consider two configurations of vortices for flow past a flat plate with a forward facing flap attached to its rear edge. In the first case, case (a), we consider a potential vortex in the vicinity of the airfoil, while for case (b), we consider a vortex sheet coming off the leading edge of the plate and reattaching at the leading edge of the flap such that the region between the vortex sheet and the airfoil is stagnant. For case (a), the Schwarz-Christoffel transformation is used to find exact solutions to the flow problem. It is found that by suitably placing a potential vortex of appropriate strength it is possible to satisfy the Kutta condition of finite velocity at both the leading edges of the plate and the flap in addition to satisfying it at the trailing edge, provided the plate flap combination satisfies a geometric constraint. The action of the potential vortex is to create a large circulatory region bounded by the airfoil and the streamline that separates smoothly at the leading edge of the plate (due to the Kutta condition) and reattaches smoothly at the leading edge of the flap (from the Kutta condition again). The circulation induced at infinity for such a flow and hence the lift on the airfoil is found to be very large. For case (b), where the vortex sheet location is unknown, a hodograph method is used to find exact solutions. It is found that once a geometric constraint is satisfied, flows exist for which the Kutta condition is satisfied at the trailing edge of the plate-flap combination. As in (a), large values of lift are obtained. However, in both cases (a) and (b), the adverse

pressure gradient of top of the flap is recognized as a source of potential difficulty in the experimental realization of the calculated flow.

In chapter II, successive modifications are made to the airfoil considered in chapter I. Exact solutions are once again obtained by a variation of the hodograph method of chapter I. The lift for these airfoils is found to be significantly larger than the one in chapter I. Because the trailing edge is no longer a stagnation point, it is felt that these flows may be easier to realize experimentally.

Chapter III is concerned with the so-called Prandtl-Batchelor flow past the plate-flap geometry of chapter I. The flow consists of an inner region which has a constant vorticity. The region outside of the airfoil and the vortex sheet coming off the leading edge of plate and reattaching at the leading edge of the flap (as in chapter I) is once again irrotational. The common boundary between the exterior flow and the inner flow, i.e. the vortex sheet, is unknown a priori and is determined by continuity of pressure, which translates into a nonlinear boundary condition on an unknown boundary. By extending the function theoretic approach of complex variables to this problem, we reduce the entire problem into one of determining one unknown function of one variable on a fixed domain from which everything else can be calculated. This is then solved numerically. Our calculations provide what we believe to be the first such calculation of a Prandtl-Batchelor flow. The calculations also provide a more realistic model for the vortex sheet flow considered in chapter I.

Chapter IV deals with a steadily translating pair of equal but opposite vortices with uniform cores and vortex sheets on their boundaries, moving without the presence of any physical boundary. The solutions were found for such flows using the function theoretic approach introduced earlier in chapter III for flows where the velocity on the vortex sheet is not a constant. The solutions form a continuum between the hollow vortex case of Pocklington (1898) and those of

Deem & Zabusky (1978) and Pierrehumbert (1980) who consider uniform core with no vortex sheet. The iterative scheme for numerical calculation, however, turns out to have severe limitations, as it fails to converge for the cases with no vortex sheet or when the vortex sheet strength is small. In the last section of the chapter, a more traditional approach due to Deem & Zabusky is taken to calculate a pair of touching vortices with uniform core and no vortex sheet on the boundary and an error in Pierrehumbert's (1980) calculations is pointed out.

In appendix I, we point out some errors in Pocklington's paper on the motion of a hollow vortex pair. The errors are corrected and the results are found to be then in agreement with results using the method in chapter IV.

Table of contents

Chapter I

Vortex Induced lift on a plate with a forward facing flap.

1.1. Introduction

Aerodynamicists have long been concerned with increasing the lift on an aircraft without paying the price of large drag. Smith (1975) summarizes some of the efforts of past researchers in designing airfoils with high lift characteristics. One of the major hurdles in the design of high lift wings is the lack of full understanding of flow past wings. In general, such flows are very complex exhibiting compressibility, viscosity and three dimensional features which are beyond the scope of theoretical techniques available today. In the limit of zero viscosity and compressibility, however, the steady state equations for fluid motion past simple geometries simplify substantially to allow analytical solutions in some cases. Based on solutions to the two dimensional inviscid incompressible potential flow equations for which the vorticity is confined to a vortex sheet around the body and possibly a point vortex, the lift and other such characteristics of a whole class of airfoils can be calculated. An extensive literature exists on such solutions in two dimensions (see Thwaites, 1960 for example), where the methods of complex variables can be readily applied. The proximity of such calculations to real characteristics of an airfoil depends on how well the flow assumptions are satisfied. We now examine these assumptions one by one.

The assumption of a two dimensional flow precludes consideration of highly swept wings or low aspect ratio wings. Only flows past high aspect ratio wings with small cross-wise variations in the wing shape may be expected to be approximately two dimensional. The assumption of incompressibility restricts us to low speed airfoils for which the Mach number is small compared to unity. The zero viscosity assumption is more delicate since it is well known that even for fluids with very small viscosity the approximation of the actual flow by a

totally inviscid flow is not uniform. For large Reynolds number (low viscosity), there exists a small region around any body, known as the boundary layer, where the effect of viscosity is important because of large velocity gradients (Prandtl,1904). However, the boundary layer shrinks to zero size with increasing Reynolds number and therefore the inviscid flow solutions might be expected to provide the outer solution to the actual high Reynolds number flow past a body. It turns out, however, that this is true only for a few cases such as uniform flow past a streamlined body where the boundary layer stays attached to the body. The drag in such cases arises as a skin friction from the boundary layer and therefore is not determinable from the inviscid potential flow. Since the skin friction goes to zero in the limit of infinite Reynolds number, the prediction of zero drag for inviscid flow is consistent with the actual features of steady infinite Reynolds number limit of attached flows. Unlike the drag prediction, the inviscid solutions allow the possibility of an arbitrary circulation around the body which leads to an arbitrary lift force. The well known Kutta condition of finite velocity, which is justified from experimental study of actual flows, is used to determine this unknown circulation and therefore the lift.

For most flows, however, the boundary layer does not stay attached because of conditions of large positive pressure gradient streamwise which causes the boundary layer equations to become singular (Goldstein,1948). This effect is illustrated in figure 1.1, where the uniform flow past a flat plate is experimentally studied for different angles of attack. As the angle of attack is increased beyond a few degrees boundary layer separation occurs on top of the plate. The separation bubble gets larger with increasing angle of attack and eventually extends far beyond the airfoil. For flow past other thin airfoils these features remain generally unchanged even though careful designing of the shape retards separation to some extent. The Kutta lift on a flat plate airfoil per unit span

based on attached inviscid potential flow is $\pi \sin\alpha \rho U^2 l$, where α is the angle of attack, l the length of the plate, ρ the fluid density and U the magnitude of the uniform stream at infinity. Therefore the nondimensional lift coefficient $C_L = 2\pi \sin\alpha$ and increases with the angle of attack. In the past, considerable efforts were made to realize an attached potential flow at large angles of attack so that the prediction of large lift coefficient comes true. Such efforts have included installation of active mechanisms such as blowing and suction on top of the wing or inclusion of slots and slats besides careful designing of the wing shape so as to have desired pressure profile on the wing surface (see Thwaites, 1960 for example). These efforts have had some success, but the theoretical limits of lift characteristics and the lift to drag ratio that is expected from attached inviscid flow is far from being realized. The boundary layer invariably separates at large angles of attack causing vorticity in the boundary layer to be convected to the main stream leading to large values of drag and loss in lift. This condition known as stall leads to loss of control of the aircraft and usually occurs around 15° for conventional thin airfoils. It remains a big stumbling block in the design of efficient VTOL or STOL aircrafts. In recent years, there have been some studies of the problem of generating high lift at low angles of attack by creating a flow in which there is a vortex attached to the wing. Based on experiments with gliders, W.Kasper (see J.Cox,1973) claimed that very high lift could be generated by designing wings that have an extensive vortex region on top of the wing. Boundary layer separation still occurs, but the hope is that the vortex may allow or cause it to reattach, preventing the formation of a large wake and loss of lift.

The first task, of course, is to demonstrate the existence of ideal flows with the required property of a separating and reattaching streamline. Rossow (1978) considered an incompressible inviscid two dimensional flow model where

a vortex-sink combination is placed behind a leading edge flap so as to cause the separated boundary layer to reattach close to the trailing edge of the wing. This forms a large separation bubble on top of the wing resulting in high values for the lift coefficient. Inspired by Kasper's claim, Saffman and Sheffield (1977) considered a flow with a point vortex over a flat plate and Sheffield (1978) studied the case of the Joukowski airfoil. As with Rossow's model, the vortex creates a large eddy region on top of the wing leading to high values of the lift coefficient. Saffman and Sheffield, however, present no clues as to how the point vortex flow could be realized though evidence of stability to two dimensional disturbances is presented.

In this chapter, we study inviscid, incompressible, steady two dimensional flows past a flat plate AO of length l_1 with a forward facing flap OB of length l_2 attached at O such that the angle AOB equals β. At infinity, the flow asymptotes to a uniform stream of magnitude U making an angle α (angle of attack) with AO. Two cases are considered here :

(a) A point vortex of strength κ in equilibrium in the flow situated at a point (x_o, y_o), with smooth separation and reattachment at A and B and a stagnation point at O, i.e. Kutta conditions at all edges, (fig 1.2a). Besides O there is one other stagnation point on the lower plate at P, which is unknown apriori.

*(b) A vortex sheet AB of constant strength q per unit length, which separates at A and reattaches at B (fig. 1.2b) such that the region between the vortex sheet and the airfoil is stagnant. Point P on AO is another stagnation point besides O.

It is hoped that for case (a) the installation of a flap at the trailing edge will allow the experimental realization of the high lift characteristics demonstrated

* This case was previously considered by Hurley and Skeat (1957) using a different method. We were in ignorance of their work at the time this flow was initially calculated.

earlier by Saffman and Sheffield, while for case (b) the attachment of a flap may serve as a natural mechanism for reattaching a separated boundary layer thus forming an extensive vortex region on top of the airfoil as originally suggested by Kasper. The results show the possibility of achieving high lift if the flow models considered here can be physically attained.

1.2. The point vortex case

1.2.1. Formulation of the problem

For the inviscid, incompressible two dimensional flow being considered, since the vorticity is confined to isolated points, we may introduce the complex velocity potential $W(z) = \varphi + i\,\psi$, where φ is the velocity potential and ψ is the stream function, each of which are harmonic functions of (x,y), the physical coordinates (as in fig.1.2a). W is an analytic function of z except at isolated points were flow singularites exist. The uniform flow at infinity at an angle α with respect to the x-axis admits $W(z)$ whose asymptotic behavior as $z \to \infty$ is given by

$$W(z) \to U\,z\,e^{-i\alpha} + \frac{i\Gamma}{2\pi}\log z + O(1) \tag{1.1}$$

where Γ is the clockwise circulation at infinity and U is the magnitude of the free stream. Further, in the neighborhood of the point vortex located at $z = z_o$,

$$W(z) \to \frac{i\kappa}{2\pi}\log(z - z_o) + O(1) \tag{1.2}$$

where κ is the clockwise circulation of the point vortex. At the plate-flap boundary we have the requirement that it be a streamline

$$\text{Im } W = constant \tag{1.3}$$

For given U and α and plate-flap geometry there is a four parameter family of solutions $W(z)$ depending on Γ, κ, Re z_o and Im z_o for which (1.1), (1.2) and (1.3) can be satisfied. However, we are looking for flows as sketched in fig.1.2a where the point vortex at z_o is in equilibrium in the flow and the velocities are finite at

A, B and O. These impose five independent real conditions on four real parameters and is therefore impossible to satisfy unless a geometrical constraint is imposed on the plate-flap combination. It will be seen that if α, β are considered as known, there is a specific l_2/l_1 which allows a flow of the type considered. All the other nondimensional features of the flow including Γ/Ul_1, κ/Ul_1, x_o/l_1, y_o/l_1 and the location of the stagnation point P relative to the plate are determined in terms of α and β once the geometric constraint is satisfied.

1.2.2. Method of solution

The exterior of the geometry AOB in the physical z-plane can be mapped on to the upper half plane (fig 1.4) by the Schwarz-Christoffel transformation

$$z = -a\int_0^{\zeta} d\zeta \, \frac{(\zeta-\zeta_1)\,\zeta^{-1+\beta/\pi}\,(\zeta-\zeta_3)\,(\zeta-\zeta_4)^{1-\beta/\pi}}{(\,1+\zeta^2\,)^2} \tag{1.4}$$

where ζ_1, 0, ζ_3, ζ_4 are reals corresponding to the points A, O, B, O (fig.1.2a) in the clockwise sense, and a is a positive real number when ζ_4 is positive. Since numerical calculations revealed ζ_4 to be always positive for the geometries considered, from here onwards we will assume ζ_4 to be positive and a to be a real positive number. The image of $z = \infty$ is $\zeta = i$. The real numbers ζ_1, ζ_3, ζ_4 and a are determined from:

$$-l_1 = -a\int_0^{\zeta_1} d\zeta \;\; \frac{dz}{d\zeta} \tag{1.5}$$

$$-l_2\, e^{-i\beta} = -a\int_0^{\zeta_3} d\zeta \;\; \frac{dz}{d\zeta} \tag{1.6}$$

$$\frac{1}{(1+\zeta_1^{\,2})} + (\beta/\pi - 2) + \frac{1}{(1+\zeta_3^{\,2})} + \frac{(1-\beta/\pi)}{(1+\zeta_3^{\,2})} = 0 \tag{1.7}$$

$$\frac{\zeta_1}{(1+\zeta_1^{\,2})} + \frac{\zeta_3}{(1+\zeta_3^{\,2})} + \frac{(1-\beta/\pi)\,\zeta_4}{(1+\zeta_4^{\,2})} = 0 \tag{1.8}$$

Equations (1.5) and (1.6) follow from the geometry of the body. Equation (1.7) and (1.8) follow from the requirement that the transformation be 1-1 which demands that the residue of the integrand in (1.4) at the point $\zeta = i$ must vanish. It may be shown after a little algebra that (1.5) through (1.8) guarantee that

the point ζ_4 is mapped to 0 on the outer side of the plate-flap combination while integration of $\frac{dz}{d\zeta}$ along the real axis from $\zeta = -\infty$ to $\zeta = +\infty$ equals zero. Therefore these two necessary conditions need not be imposed in addition to the four equations (1.5) through (1.8).

The Riemann mapping theorem guarantees the existence of a unique mapping as described and therefore we are assured that (1.5) through (1.8) can be solved to obtain ζ_1, ζ_3, ζ_4 and a.

Once ζ_1, ζ_3 and ζ_4 and a are determined from these four equations as functions of l_1, l_2 and β, it is convenient to consider the complex velocity potential W as a function of ζ. It is easy to show that in general a dipole singularity in an original plane corresponds to a dipole singularity in a conformally transformed plane, though its complex magnitude is not invariant. Also, a point vortex remains a point vortex with the same magnitude of circulation under conformal mapping. The sense of the circulation gets reversed when the location of the vortex is at a finite point in one plane and at infinity in the other. Thus, in the upper half ζ plane, we have a point vortex at ζ_o with clockwise circulation κ, where ζ_o is the map of $z = z_o$. The uniform stream and the circulation at $z = \infty$ corresponds to a dipole and a point vortex at $z = \infty$. Therefore, at $\zeta = i$, the image of $z = \infty$, there is a dipole of complex magnitude M and a point vortex with clockwise circulation $-\Gamma$. Since there are no other singularities in the upper half ζ-plane and the real axis is a streamline, where Im $W = 0$ without any loss of generality, we conclude that

$$W(\zeta) = -\frac{M}{(\zeta-i)} - \frac{\overline{M}}{(\zeta+i)} - \frac{i\Gamma}{2\pi}\left(\log(\zeta-i) - \log(\zeta+i)\right) + \frac{i\kappa}{2\pi}\left(\log(\zeta-\zeta_o) - \log(\zeta-\overline{\zeta}_o)\right) \tag{1.9}$$

Consideration of the leading behavior of W in the neighborhood of $\zeta = i$ and comparison with the behavior at $z = \infty$ as in (1.1) gives

$$M = \tfrac{1}{4}\,\alpha U\,(i-\zeta_1)\,i^{\beta/\pi-1}\,(i-\zeta_3)(i-\zeta_4)^{1-\beta/\pi}\,e^{-i\alpha} \tag{1.10}$$

where equations (1.1), (1.4) and (1.9) were used. The Kutta condition of finite velocity $\frac{dW}{dz}$ at A, B and O implies

$$\frac{dW}{d\zeta} = 0 \tag{1.11}$$

at $\zeta=\zeta_1, \zeta_3, \zeta_4$ since $\frac{dz}{d\zeta}$ is zero at those points. The Blasius theorem for force in an irrotational flow implies that for the point vortex to be in equilibrium at $z = z_o$

$$\oint \left(\frac{dW}{dz}\right)^2 dz = \oint \left(\frac{dW}{d\zeta}\right)^2 \left(\frac{dz}{d\zeta}\right)^{-1} d\zeta = 0 \tag{1.12}$$

for a closed contour around $z = z_o$ or $\zeta = \zeta_o$ and no other singularity. Equation (1.11) leads to three real equations.

$$0 = \frac{M}{(\zeta_j - i)^2} + \frac{\overline{M}}{(\zeta_j + i)^2} - \frac{i\Gamma}{2\pi}\left[\frac{1}{(\zeta_j - i)} - \frac{1}{(\zeta_j + i)}\right] + \frac{i\kappa}{2\pi}\left[\frac{1}{(\zeta_j - \zeta_o)} - \frac{1}{(\zeta_j - \bar{\zeta}_o)}\right] , \tag{1.13}$$

for j = 1,3,4. Equation (1.12) implies

$$0 = \frac{4i\kappa\zeta_o}{(1+\zeta_o^2)} - \frac{i\kappa}{(\zeta_o - \zeta_1)} - \frac{i(\beta-\pi)\kappa}{\pi\zeta_o} - \frac{i\kappa}{(\zeta_o - \zeta_3)} - \frac{i(\beta-\pi)\kappa}{\pi(\zeta_o - \zeta_4)} + \frac{4\pi M}{(\zeta_o - i)^2} + \frac{4\pi\overline{M}}{(\zeta_o + i)^2} - \frac{2i\Gamma}{(\zeta_o - i)} + \frac{2i\Gamma}{(\zeta_o + i)} - \frac{2i\kappa}{(\zeta_o - \bar{\zeta}_o)} \tag{1.14}$$

In both (1.13) and (1.14), it is to be understood that M has the value given by (1.10). Altogether (1.11) and (1.12) contain five independent real equations for the four real unknowns Γ, κ, ξ_o and η_o ($\zeta_o = \xi_o + i\eta$) if the shape of the airfoil and the magnitude and direction of velocity at infinity are regarded as given. The system is over determined in general and we expect no solution to exist unless some condition is satisfied between the variables ζ_1, ζ_3 and ζ_4. It is clear from (1.10) and (1.13) that the value of U and α is irrelevant to the question of existence of solutions since each of them just scales Γ and κ linearly. From (1.5) and (1.6), it follows that the absolute magnitude of l_1, l_2 are unimportant.

Indeed, we could set both U and l_1 to unity without any loss of generality. The ratio l_2/l_1 and the angle β determines ζ_1, ζ_3 and ζ_4 and therefore a a relation between l_2/l_1 and β must exist for a solution of the desired type at given angle of attack α.

We choose to regard the angles α and β as given and the ratio $\frac{l_2}{l_1}$ as a further physical unknown along with the strength and position of the free vortex and the circulation at infinity. Then the mathematical system consists of nine real equations from (1.5), (1.6), (1.7), (1.8), (1.13) and (1.14) for ζ_1, ζ_3, ζ_4, α, Γ, κ, ξ_o, η_o, $\frac{l_2}{l_1}$ for given α and β, U and l_1 being set equal to unity. We were unable to prove rigorously that solutions exist and numerical methods were employed to find solutions. Now we present details of the solution procedure.

For fixed α and β, an initial guess for l_2 was taken. Using (1.5) through (1.8) the variables ζ_1, ζ_3, ζ_4^{-1} and $\alpha|\zeta_4|^{1-\frac{\beta}{\pi}}$ were calculated using Newton iteration. Note that the choice of the variables in the Newton iteration was made because ζ_4 could become infinitely large at the same time as α shrinks to zero. The initial guess in the Newton iteration is easy to make for the limiting case l_2, l_1 equal to unity and β equalling π since an exact integration can be done in (1.4) for this case giving $\zeta_1 = -1$, $\zeta_3 = 1$, $\zeta_4 = \infty$ and $\alpha = 2$. Continuation in the parameter β and l_2 allows us to find the proper initial guess for any l_2 and β that we may want. Once ζ_1, ζ_3, ζ_4 and α are determined, the first two equations in (1.13) and the two real equations in (1.14) are used to determine ξ_o, η_o, Γ and κ by using Newton iteration, where M is determined from (1.10). The right hand side of the third equation in (1.13) is used to determine the residual corresponding to l_2 used.

The procedure described in the previous paragraph is repeated for different l_2 in a Newton iterative procedure until convergence is obtained, i.e. until the

residual corresponding to some l_2 is smaller than the desired level of accuracy.

1.2.3. Number of stagnation points

In this section, we will prove that for the flow we are considering, there could be no stagnation points away from the boundary and that there is only one stagnation point P on the airfoil boundary besides 0 (from the exterior * and the interior).

Consider the contour integral

$$\oint_C \left(\frac{1}{2\pi i} \frac{d^2 W}{dz^2} \Big/ \frac{dW}{dz} \right) dz$$

where the contour C is chosen as in Fig.1.3 C is composed of a circular contour C_R of radius R around $z = 0$, straight segments S_1, S_2 drawn very close to each other such that they do not pass through any singularity or zero of the function $\frac{dW}{dz}$ and straight segments L_j, $j = 1,2,...$ coinciding with parts of the airfoil boundary. Further there are small ε radius arcs of circle detours wherever $\frac{dW}{dz}$ is zero or infinite. In our case because of the Kutta condition the velocity is finite everywhere. We will consider the contributions from each of the segments in the limit of zero ε, infinite R and paths S_1 and S_2 overlapping. Since C is a closed contour, it is clear that the above path integral is real. Thus, as far as the contribution from each path segment that is a constituent of C, we will only be concerned with the real part since all the imaginary parts are bound to cancel each other out. In the limit of overlapping paths the contributions from S_1 and S_2 cancel each other out since there are no singularities in between them. Clearly the real part of the contribution of any straight segment L_j, where $j = 1,2,..$ is zero since $\frac{dW}{dz}$ undergoes no change in its argument between the two ends of L_j. At A or B, because of the Kutta condition

* 0 is a stagnation point from the exterior because of the Kutta condition.

$$\frac{dW}{dz} = a_o + a_1 (z - z_{A,B}) + \cdots$$

We will consider only the case of a_o not equal to zero, since the case $a_o = 0$ can be treated as a limiting case of one of the zeroes of $\frac{dW}{dz}$ coinciding with A or B. It is easy to see on local expansion of the integrand that the contribution from each ε circle at A or B equals zero in the limit of zero ε. For calculation of the integral contribution from C_{ε_2}, we notice that for z in the neighborhood of zero from the interior,

$$\frac{dW}{dz} = K z^{\pi/\beta - 1} (1 + O(z))$$

and therefore the integrand becomes $\frac{1}{2\pi i} (\pi/\beta - 1) (\frac{1}{z} + O(1))$ and hence the contribution from C_{ε_2} equals $-\frac{1}{2} + \frac{\beta}{2\pi}$ in the limit of zero ε. Similarly expanding the integrand in the neighborhood of $z = 0$ from the exterior we obtain the contribution from C_{ε_4} equalling $-\frac{\beta}{2\pi}$. For small semicircular detours around each simple zero of $\frac{dW}{dz}$ on the boundary, it is easily seen from local expansion of $\frac{dW}{dz}$ that the contribution equals $-\frac{1}{2}$. Using $W = U z + \log z + O(1)$ at infinity, the contribution from the infinite circle C_R is easily shown to be zero. Summing up all the different contributions to the path integral and equating it to the number of zeroes minus number of poles of the function $\frac{dW}{dz}$ inside the contour, one obtains

$$N_s - 1 = -\tfrac{1}{2} n_s - \tfrac{1}{2}$$

The only non-negative integral values of N_s, the number of interior stagnation points and n_s, the number of stagnation points on the boundary besides 0 (from the exterior and the interior) are 0 and 1 respectively. Thus we have proved that there can be no interior stagnation points and that there is only one stagnation point P on the boundary besides 0. For the flow being con-

sidered, it is found numerically that the stagnation point is always on the plate AO from the exterior.

1.2.4. Results for the point vortex case

Values of Γ/Ul_1, l_2/l_1 are plotted against α in figures 1.5 and 1.6 respectively for five different β values. For the purpose of comparison, the corresponding value of $\Gamma/(Ul_1)$ for a flow without any free vortex but with Kutta condition satisfied only at O is presented in Fig.1.7. We use the notation Γ_k for Γ corresponding to such a flow. The right ends of each of the curves in (1.5) and (1.6) represent the limiting case of the stagnation point P coinciding with O. We did not consider the case of the stagnation point P occurring on the flap. That case was considered uninteresting since it corresponds to an unrealistic physical flow. Table 1.1 show different quantities of interest for three values each of β and α. We did not consider the details of solution for β greater than 90 degrees, though solution exists even in that range. When β approaches 180 degrees, solution ceases to exist. For instance, when α = 5.7 degrees, no solution was found for β greater than 160 degrees. For larger angles of attack α this limit is smaller. Failure of solutions to exist for β close to 180 degrees is consistent with Saffman and Sheffield's findings about the impossibility of satisfying Kutta conditions at both the leading and trailing edge of a flat 2-D airfoil with an equilibrium free vortex in its vicinity.

Fig.1.5 shows that the Γ/Ul_1 obtained for our geometry is generally about an order of magnitude bigger than that for a flat plate with attached flow for which Kutta condition is satisfied at the trailing edge for which $\Gamma/Ul_1 = \pi \sin \alpha$. Comparison with fig. 1.7 shows that the lift is larger in the case of a point vortex than without one even when the leading edges A and B are allowed to have physically unrealistic infinite velocities. The difference is greater for greater values of β. The actual streamlines have been drawn for the case $\beta = 90°$ and $\alpha = 15°$ in

fig.1.8. The square of the ratio of velocity on the flap to the free stream velocity is plotted against the distance from B as a fraction of l_1 in fig.1.9 for four different combinations of α and β. From the local expansion of $\frac{dz}{d\zeta}$ around $\zeta = \zeta_3$ and a similar expansion of $\frac{dW}{d\zeta}$ it can be shown that $\frac{dW}{dz} = K\,(z + l_2\, e^{-i\beta})^{\frac{1}{2}} + \ldots$. and therefore the infinite gradient in fig (1.9) at the left end point is expected. At the right end of the curve, i.e. at $z = 0$, $\frac{dW}{dz} = K\, z^{\beta/(2\pi-\beta)} + \cdots$ and thus there is an infinite gradient on the right end of each of the plots in fig.1.9, which is not visible in the scale used for $\beta = 90°$. From Bernoulli's principle, the plots in fig.1.9 can be interpreted as pressure plots and therefore generally large adverse pressure gradients at the reattachment point B and the trailing edge O can be expected for an attached flow of this type, which suggests that some boundary layer mechanisms has to be installed to realize such a flow experimentally.

1.3. The vortex sheet case:

1.3.1. Mathematical formulation of the problem

We now study the flow sketched in figure 1.2b. As in case (a), P is a stagnation point on the plate AO. Since the region inside APOBA is stagnant, the velocity on the separating streamline must be a constant q, say, which is also the vortex sheet strength. As in case (a), we may introduce the complex velocity potential $W(z)$ defined in the region exterior of APOBA and its boundaries. Once again the asymptotic behavior as $z \to \infty$ is given by equation (1.1). However, there are no other singularities of $W(z)$ in the exterior region. Equation (1.3) is valid on the boundary APOBA. The location of the vortex sheet BA is not known a priori and has to be determined as part of the problem.

1.3.2. Solution procedure

Consider the conformal map $t(z)$ that maps the exterior of the region ABOA in the physical z-plane into the interior of the semicircle (fig.1.10) such that the boundary point B is mapped to -1, O to 0 and A to +1 where BO and AO correspond to the sides of the airfoil and the circular part AB to the vortex sheet, and t_p $(0 \le t_p < 1)$ corresponds to the unknown stagnation point P on the plate AO. By the Riemann mapping theorem, there exists a unique $t(z)$. Further the conformal map

$$T = -\tfrac{1}{2}\,(\,t + 1/t\,) \tag{1.15}$$

maps the interior of the semicircle into the upper half T plane. Now, consider the velocity potential W as a function of T. From equation (1.1) it follows from investigating the dominant behavior of $W(z)$ and the circulation at $z = \infty$ that

$$W(T) \to -M/(T-T_\infty) - i\Gamma/(2\pi)\log(T-T_\infty) \tag{1.16}$$

as $T \to T_\infty$ (image of $z=\infty$), where M is the complex magnitude of the dipole. Since there are no other singular points in the upper half plane and the real T axis corresponds to a streamline it follows that

$$W(T) = -\frac{M}{(T-T_\infty)} - \frac{\overline{M}}{(T-\overline{T}_\infty)} - \frac{i\Gamma}{2\pi}\Big[\log(T-T_\infty) - \log(T-\overline{T}_\infty)\Big] + W_1(T) \tag{1.17}$$

where $W_1(T)$ is analytic in the entire T plane and real on the real axis. Since $\frac{dz}{dT} \to 0$ as $T \to \infty$ and $\frac{dW}{dz}$ is finite there because of the Kutta condition at O, we have $\frac{dW}{dT} \to 0$ as $T \to \infty$. Hence $\frac{dW_1}{dT} \to 0$ as $T \to \infty$. Further $\frac{dW_1}{dT}$ is real on the real axis and therefore can be extended to the whole T-plane. Since $\frac{dW_1}{dT}$ is a bounded analytic function which tends to zero at infinity, it must be identically zero. Therefore, using equations (1.17) and (1.15) we obtain

$$\frac{dW}{dt} = \frac{(1-t^2)}{2}\left[\frac{4Mt_\infty^2}{(t-t_\infty)^2(1-tt_\infty)^2} + \frac{4\overline{M}\,\overline{t}_\infty^2}{(t-\overline{t}_\infty)^2(1-t\overline{t}_\infty)^2} - \frac{i\Gamma(t_\infty-\overline{t}_\infty)(1-t_\infty\overline{t}_\infty)}{\pi(t-t_\infty)(t-\overline{t}_\infty)(1-tt_\infty)(1-t\overline{t}_\infty)}\right]. \tag{1.18}$$

where t_∞ is the image of $z = \infty$ in the t-plane and is related to T_∞ through (1.15). Now, consider the complex velocity $\frac{dW}{dz}$ as a function of t. Extending an idea in Birkhoff and Zarantonello (1957) we define $\Omega(t)$ by

$$\frac{dW}{dz} = q\ t^{\beta/\pi} \frac{(t_p - t)}{(1 - t t_p)} e^{\Omega} \tag{1.19}$$

where the arguments are chosen so that $-\pi \le arg\,(\frac{dW}{dz}) < \pi$ $-\pi \le arg\,(1 - t\ t_p) \le 0$ and $-\pi \le arg\,(t_p - t) \le 0$ for t in or on the semicircle (fig.1.10). It will be seen in section 1.3.3 that there are no interior stagnation points and that there is only one stagnation point P besides 0. Thus $\Omega(t)$ is analytic in the interior of the unit semicircle and continuous up to the boundary since $\frac{dW}{dz}$ is continuous as well. For the flow being considered, $arg\,(\frac{dW}{dz}) = \beta$ on BO, 0 on OP and equals $-\pi$ on PA. Hence considering the argument of both sides in (1.19) we find

$$\text{Im}\ (\Omega) = 0 \tag{1.20}$$

everywhere on BOPA, which implies $\Omega(t)$ can be continued as an analytic function everywhere in the interior of the unit circle in the t-plane with

$$\Omega(t) = \overline{\Omega}(\bar{t}) \tag{1.21}$$

defining Ω for Im t <0. Therefore

$$\Omega(t) = a_0 + a_1\, t + a_2\, t^2 + \ldots \tag{1.22}$$

with a_i real and the power series convergent for $|t| < 1$ Again from the absolute value of equation (1.19) on the unit circle, we have $e^{\text{Re}(\Omega)} = 1$, implying

$$\text{Re}\ (\Omega) = 0 \tag{1.23}$$

on the unit circle. (1.22) and the above implies that $\Omega = 0$. Hence

$$\frac{dW}{dz} = q\ t^{\beta/\pi}\ \frac{(t_p - t)}{(1 - t\ t_p)} \tag{1.24}$$

since $\frac{dz}{dt} = \frac{dW}{dt} / \frac{dW}{dz}$, it follows from equations (1.18) and (1.24) that

$$\frac{dz}{dt} = (1 - t^2)\ t^{-\beta/\pi} \frac{(1 - t t_p)}{2q\,(t_p - t)} \left[\frac{4M t_\infty^2}{(t - t_\infty)^2 (1 - t t_\infty)^2} + \frac{4\overline{M}\ \bar{t}_\infty^2}{(t - \bar{t}_\infty)^2 (1 - t \bar{t}_\infty)^2} \right.$$

$$- \frac{i\Gamma(t_\infty - \bar{t}_\infty)(1 - t_\infty \bar{t}_\infty)}{\pi(t - t_\infty)(t - \bar{t}_\infty)(1 - t t_\infty)(1 - t \bar{t}_\infty)} \Bigg] \qquad (1.25)$$

where t_∞ is the image of $z = \infty$ in the t-plane and is related to T_∞ through (1.15). Stagnation points at $t = 0$ and $t = t_p$ imply that $\frac{dW}{dt} = 0$ at those points, and therefore

$$\frac{4Mt_\infty^2}{(t_p - t_\infty)^2(1 - t_p t_\infty)^2} + \frac{4\bar{M}\,\bar{t}_\infty^2}{(t_p - \bar{t}_\infty)^2(1 - t_p \bar{t}_\infty)^2} = \frac{i\Gamma(t_\infty - \bar{t}_\infty)(1 - t_\infty \bar{t}_\infty)}{\pi(t_p - t_\infty)(t_p - \bar{t}_\infty)(1 - t_p t_\infty)(1 - t_p \bar{t}_\infty)} \qquad (1.26)$$

$$4M + 4\bar{M} = \frac{i\Gamma(t_\infty - \bar{t}_\infty)(1 - t_\infty \bar{t}_\infty)}{\pi t_\infty \bar{t}_\infty} \qquad (1.27)$$

Also, the condition that the relation between z and t is 1-1 means that there should be no residue for $\frac{dz}{dt}$ at $t = t_\infty$, which implies from (1.25) that

$$\frac{i\Gamma}{2\pi} = \frac{2Mt_\infty^2}{1 - t_\infty^2} \Bigg[- \frac{\beta}{\pi t_\infty} - \frac{t_p}{(1 - t_p t_\infty)} + \frac{1}{(t_p - t_\infty)} \Bigg] \qquad (1.28)$$

Besides, we have from geometric considerations

$$\int_0^1 \frac{dz}{dt}\, dt = -l_1 \qquad (1.29)$$

$$\int_{-1}^0 \frac{dz}{dt}\, dt = l_2\, e^{-i\beta} \qquad (1.30)$$

where $\frac{dz}{dt}$ is given by (1.25). From (1.24), we also have

$$U e^{-i\alpha} = q t_\infty^{\beta/\pi} \frac{(t_p - t_\infty)}{(1 - t_p t_\infty)} \qquad (1.31)$$

Equations (1.26) through (1.31) constitute eight real relations for the eight real unknowns Γ, q, t_p, Re t_∞, Im t_∞, Re M, Im M and l_2, where l_1, β, U and α are treated as known. It was not possible to show rigorously that solutions to these system of equations exist. Numerical procedure described in 1.3.4 was used in solving them. Once these constants are found the entire flow is determined. Integration of equation (1.25) on the arc of the semicircle locates the vortex sheet.

It may be noted at this point that it is far from obvious that $z(t)$ defined by (1.25) is the correct mapping function which maps the semicircle into the

exterior of our geometry as desired. Here we will demonstrate the necessary properties of such a mapping function which are not immediately obvious on inspection of equation (1.25):

(i) $\frac{dz}{dt}$ is finite everywhere on the unit semicircle and has simple zeroes at $t = 1, -1$, and a zero at $t = 0$ where $\frac{dz}{dt} = K\, t^{1-\beta/\pi}\,(\,1 + O(t)\,)$.

(ii) $\frac{dz}{dt}$ is negative for $0 < t < 1$ and argument of $\frac{dz}{dt} = -\beta$ for $-1 < t < 0$.

Proof of (i): Clearly from (1.25), $\frac{dz}{dt}$ could be infinite on the unit semicircle only at $t = 0$ and t_p. Since the expression within the square parantheses is zero at those points, it follows that $\frac{dz}{dt}$ is finite everywhere on the unit semicircle and is zero at $t = 0$ where $\frac{dz}{dt} = K\, t^{1-\beta/\pi}\,(\,1 + O(t)\,)$. It is shown in section (1.3.3) that $\frac{dW}{dt}$ can have simple zeroes only at $t = +1, -1$ and at two other points on the real axis, which is imposed in our case at $t = t_p$ and $t = 0$ (in equations (1.26) and (1.27)). Thus $\frac{dz}{dt}$ in (1.25) cannot have any zeroes in the interior of the unit semicircle and can have simple zeroes only at $t = +1$ and -1.

Proof of (ii): Clearly from (1.25), $\frac{dz}{dt}$ is real for $0 \leq t \leq 1$. Since the square parantheses term in (1.25) is zero at $t = t_p$ and $t = 0$ only, it follows that $\frac{dz}{dt}$ must be entirely positive or negative on the positive real axis of the semicircle. However, since equations (1.29) and (1.30) are imposed, we are assured that $\frac{dz}{dt}$ is negative for $0 < t < 1$. Since the square parantheses expression in (1.25) changes sign at $t = 0$, it follows that argument of $\frac{dz}{dt}$ equals $-\beta$ on the negative real axis of the unit semicircle. Thus conditions (i) and (ii) are indeed satisfied by $z\ (t)$ defined by (1.25)

1.3.3. Number of stagnation points

Consider the contour integral

$$\oint_C dt \left(\frac{1}{2\pi i} \frac{d^2 W}{dt^2} \Big/ \frac{dW}{dt} \right)$$

for a contour C as shown in figure (1.11). Small ε radius arc detours are made whereever $\frac{dW}{dt}$ equals zero on the boundary of the unit semi-circle. Since the integral is real, we will only be concerned with the real contribution of each segment that makes up C. Clearly the real contribution of the integral from each of the straight segments L_j is zero since this is simply the difference in the argument of $\frac{dW}{dt}$ across the straight segment. Using local expansion of $\frac{dW}{dt}$ around each simple zero * in the same fashion as in 1.2.3, we find that the contribution from each semicircular detour C_{ε_k} around a simple zero of $\frac{dW}{dt}$ equals $-\frac{1}{2}$. For each quarter circular contour around t = +1 and -1, the contribution is $-\frac{1}{4}$. As far as integral contribution from the circular arc C_1 is concerned, it is convenient to factorize $\frac{dW}{dt} = \frac{(1-t^2)}{t^2} g\ (t)$. It can be seen that $g\ (t)$ is real on the unit circle and undergoes no sign change if we assume that $\frac{dW}{dt}$ has no zeroes on C_1. The case of one or more zeroes of $\frac{dW}{dt}$ on C_1 will not be discussed here though only minor modifications are required in the logic for the end results quoted here to be equally valid. Thus the integral contribution from C_1 is simply the change in the argument of $\frac{(1-t^2)}{t^2}$ between the end points of C_1 divided by 2π and equals $-\frac{1}{2}$ in the limit of zero ε. Collecting all the path contibutions to the closed contour integral and equating it to the number of zeroes minus number of poles of $\frac{dW}{dt}$ inside the contour, we obtain

*The case of multiple zeroes at a point is easily handled as a limit of coalescing zeroes.

$$N_s - 2 = -\frac{1}{2}n_s - \frac{1}{2} - \frac{1}{4} - \frac{1}{4}$$

where N_s is the number of interior simple zeroes and n_s is the number of simple zeroes besides +1 and -1 of the function $\frac{dW}{dt}$. The only non-negative integral possibilities for N_s and n_s are $N_s = 1$,$n_s = 0$ and $N_s = 0$, $n_s = 2$. Since we impose Kutta condition at the trailing edge 0, which requires $\frac{dW}{dt}$ to be zero at $t = 0$, it follows that we could only have the second of the two possibilities, i.e. there are no interior zeroes and there are two simple zeroes besides +1 and -1 on the boundary of the unit semicircle. From general consideration of the properties of the Riemann mapping function $z\ (t)$, it follows that $\frac{dz}{dt}$ is regular at $t = t_p$ and $\frac{dz}{dt} = K\, t^{1-\beta/\pi}\,(1 + 0(t))$ in the neighborhood of $t = 0$. Therefore simple zeroes of $\frac{dW}{dt}$ at $t = 0$ and $t = t_p$ correspond to stagnation points at 0 and P as originally assumed. Also there are no interior stagnation points in the flow.

1.3.4. Results for the vortex sheet case

For given α and β, equations (1.26), (1.27) and (1.31) were used to calculate t_∞, q/U and t_p where M/Γ was eliminated by using (1.28). Newton iteration was used for that purpose and after some trial and error converged solutions obtained. Integrating $\frac{U}{\Gamma}\frac{dz}{dt}$, which is known, Γ/Ul_1 is calculated from (1.29). Equation (1.30), then determines l_2/l_1 and the location of the stagnation point P is determined by integrating (1.25) from 0 to t_p. Thus all the constants characterizing the flow were determined.

Values Γ/Ul_1, l_2/l_1 and q/U are plotted against α in figures (1.12), (1.13) and (1.14) for five different values of β. The right end point of each of this curves correspond to the stagnation point P coinciding with 0. Beyond that, the stagnation point P moved over to the flap. As the angle of attack $\alpha \to 0$ both Γ/Ul_1 and l_2/l_1 went to zero. In view of the low values of the lift no effort was made to

calculate details of the curves in (1.12) through (1.14) for α less that 3 degrees. No numerical solution could be found for $\alpha \leq 0$ suggesting nonexistence of solution in that range. As with the case of point vortex, the values of Γ / Ul_1 and hence the lift coefficient is large. The square of the ratio of velocity on top of the flap and the velocity at infinity is plotted against the distance from B as a fraction of l_1 for different combinations of α and β in figure 1.15. As for the point vortex, there is infinite pressure gradient at B and 0, which is not visible in the scale used for plot in cases where $\beta = 90°$ However, the infinite pressure gradient can be shown analytically by locally expanding $\frac{dz}{dt}$ and $\frac{dW}{dz}$ around $t = -1$ and $t = 0$. Such an expansion also shows that the free-streamline curvature at B in infinite. The large adverse pressure gradient regions are, however, quite localized in the neighborhoods of B and 0 for small α and β. The actual streamlines are plotted the cases $\alpha = 30°$, $\beta = 90°$ and $\alpha = 15°$, $\beta = 30°$ in figures 1.15 and 1.16. Table 1.2 lists the various quantities of interest for different combinations of α and β. Our results were found to be in agreement with Hurley and Skeat (1957), who found an analytical solution to this flow using a different method which makes adhoc assumptions about the flow in a hodograph plane.

1.4. Discussion and conclusion

We considered potential flows past a two dimensional geometry, one in the presence of a point vortex and the other in the presence of a vortex sheet. Very high values of lift coefficients were found compared to the usual lift on a thin wing. The predicted drag in this model is zero. In order to experimentally realize such high lift coefficents with large though not infinite lift to drag ratio, one must, however, make sure that the flow remains attached. This would be difficult to ensure because, as we noted earlier, an adverse pressure gradient exists for the potential flow on top of the flap and this is especially large near B and 0. Dr.

M. Gharib (personal communication) has suggested that by suitably tailoring the end B to have a curved segment with finite curvature that matches the curved streamline curvature close to the end of the straight segment, it may be possible to avoid the locally large adverse pressure gradient at B, while retaining the same flow features as the one calculated. Hurley and Ruglen (1958) used blowing to maintain an attached flow. Intense blowing however has the disadvantage of having to expend a lot of energy, besides inducing large drag, and earlier experience (Smith,1975) has shown that it is not very cost efficient. From the pressure profile, it seems that attached flow for moderately small β may be achieved provided the locally large gradient at O does not have a global separation effect, as it might have. Blowing or any such mechanism is unlikely to be of much help as far as flow separation near O is concerned since the the infinite pressure gradient is an artifact of Kutta condition at the trailing edge for nonzero β. Once the flow separates near O, it could have a tearing effect by which separation might occur far ahead of O. In the next chapter, we will deal with this separation problem by introducing a slightly modified geometry where the trailing edge is not a stagnation point and the pressure gradient is finite.

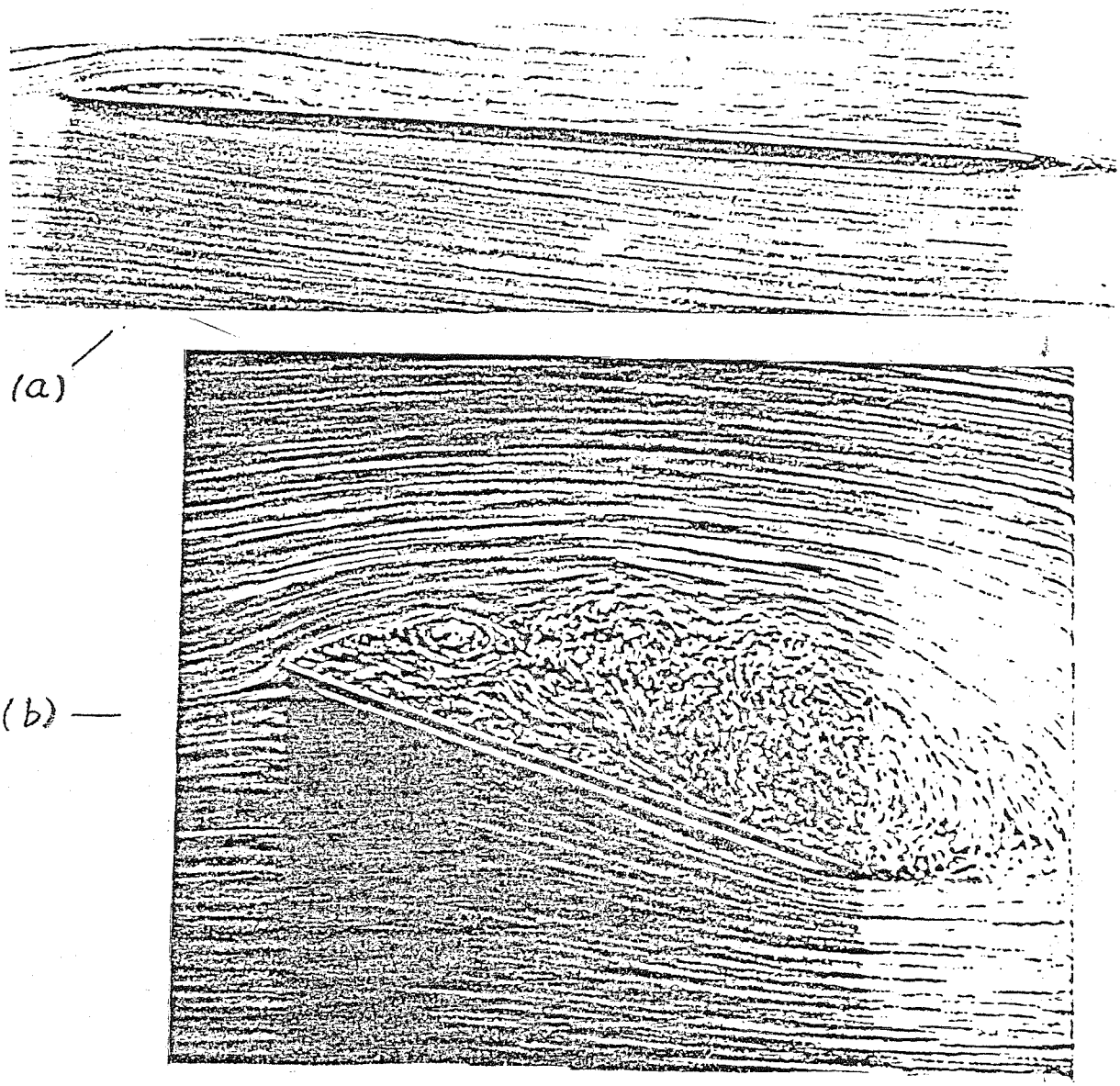

Fig.1.1: Films showing the boundary layer separation. In (a), a flat plate is held at $\alpha = 2.5°$. The laminar boundary layer separates and reattaches on the upper surface for Reynolds number equalling 10^4. In (b), the flow at angle of attack $\alpha = 20°$ is shown. Separation zone is far more extensive. ONERA photograph (Werle, 1974).

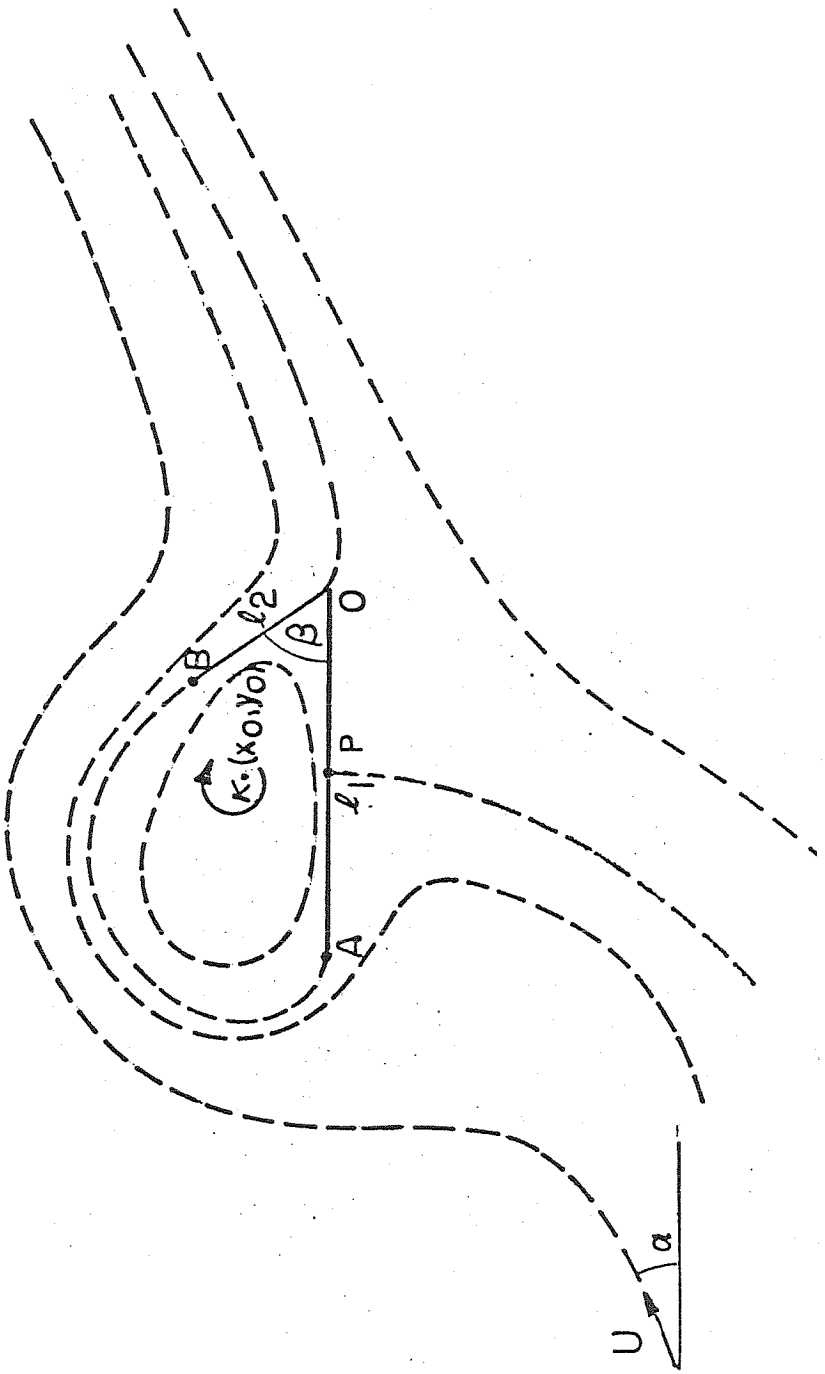

Fig.1.2a: Sketch of flow with point vortex.

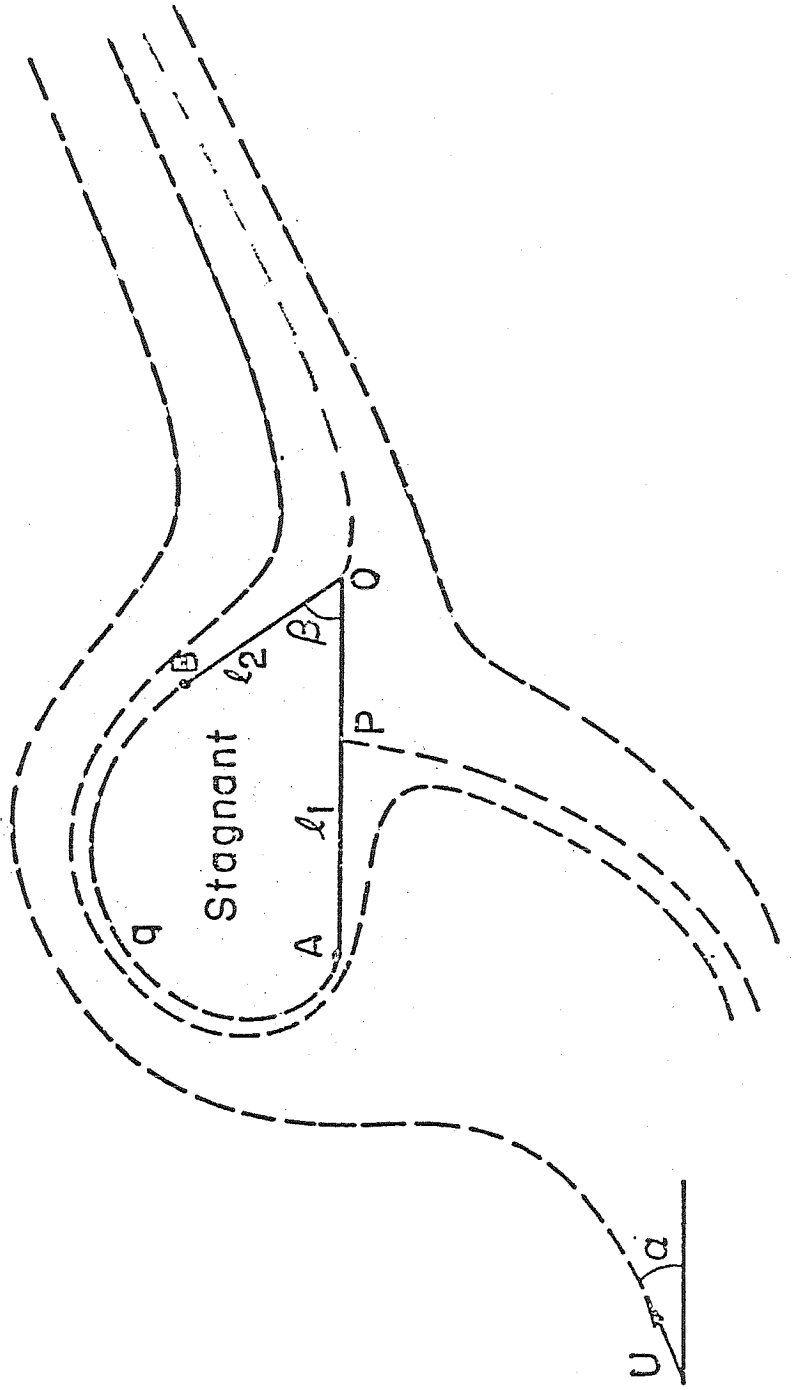

Fig.1.2b: Sketch of flow with vortex sheet.

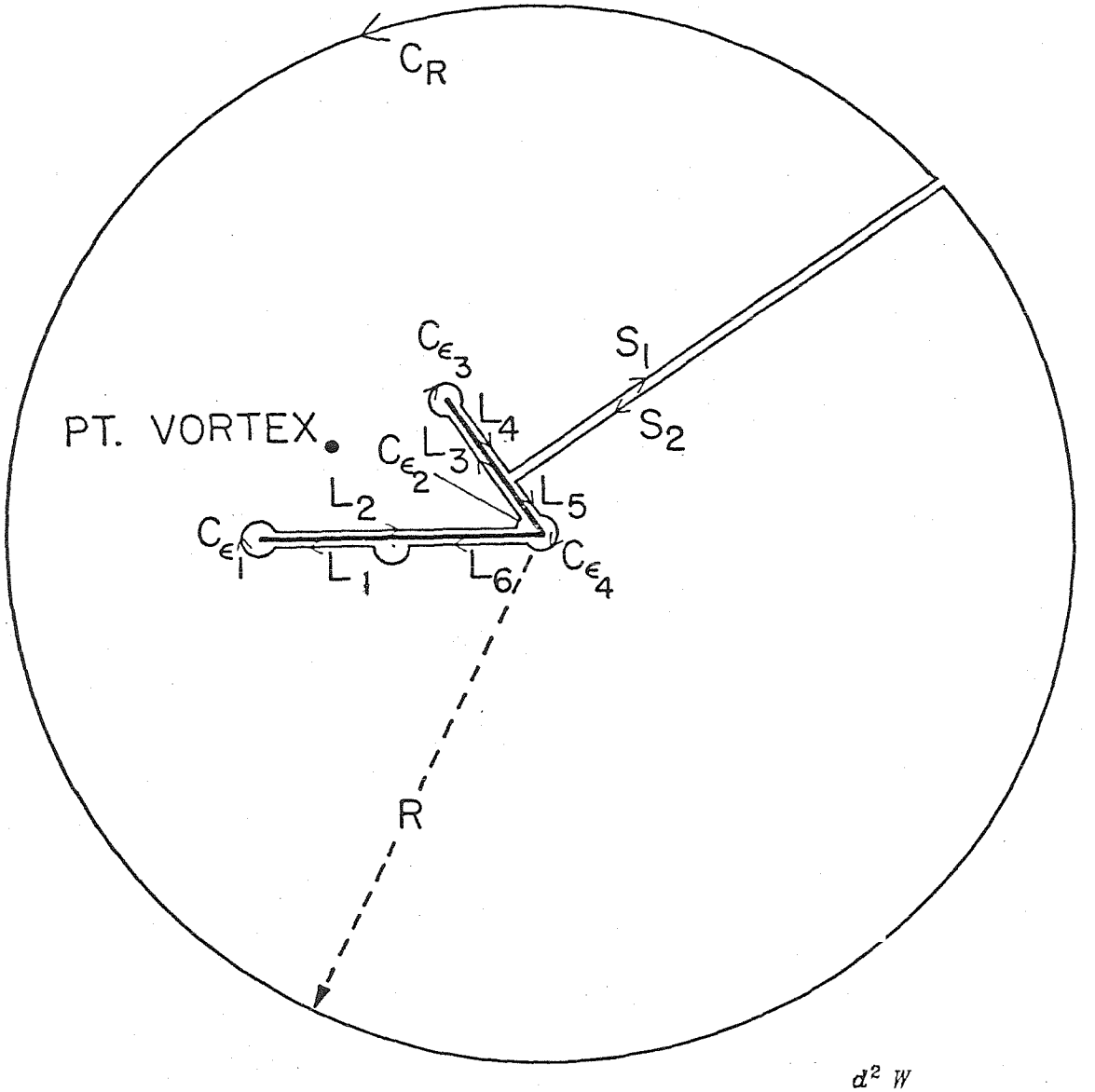

Fig.1.3: Closed contour C chosen for integration of $\frac{1}{2\pi i} \frac{\frac{d^2 W}{dz^2}}{\frac{dW}{dz}}$.

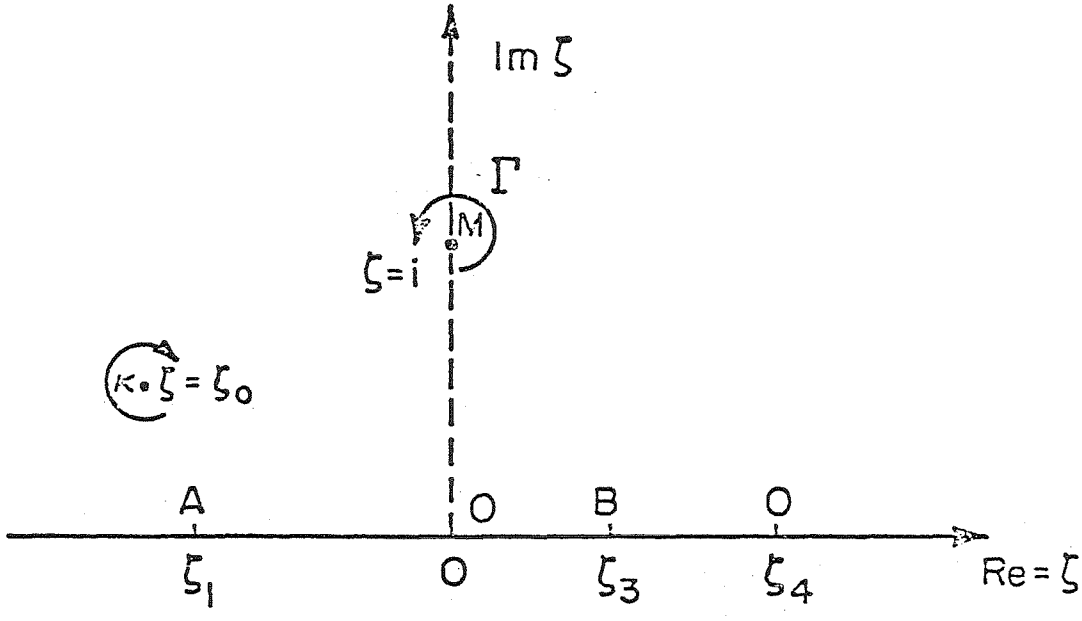

Fig.1.4: The upper half ζ-plane. There is a dipole of complex magnitude M and a counter clockwise circulation Γ at $\zeta = i$, while a point vortex with clock wise circulation κ sits at $\zeta = \zeta_o$. The real axis is a streamline.

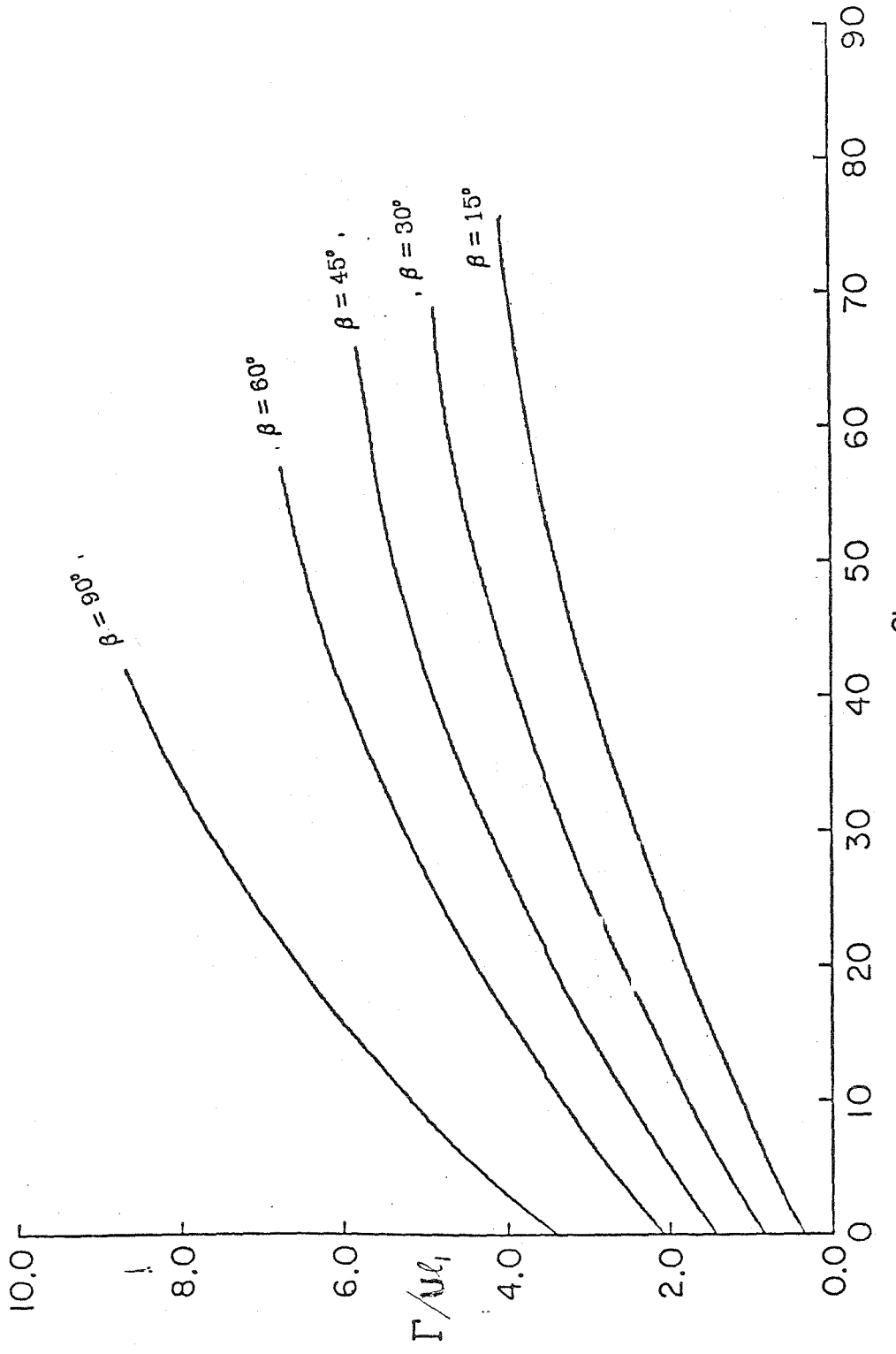

Fig 1.5: $\Gamma / U l_1$ vs. α (in degrees) for different β.

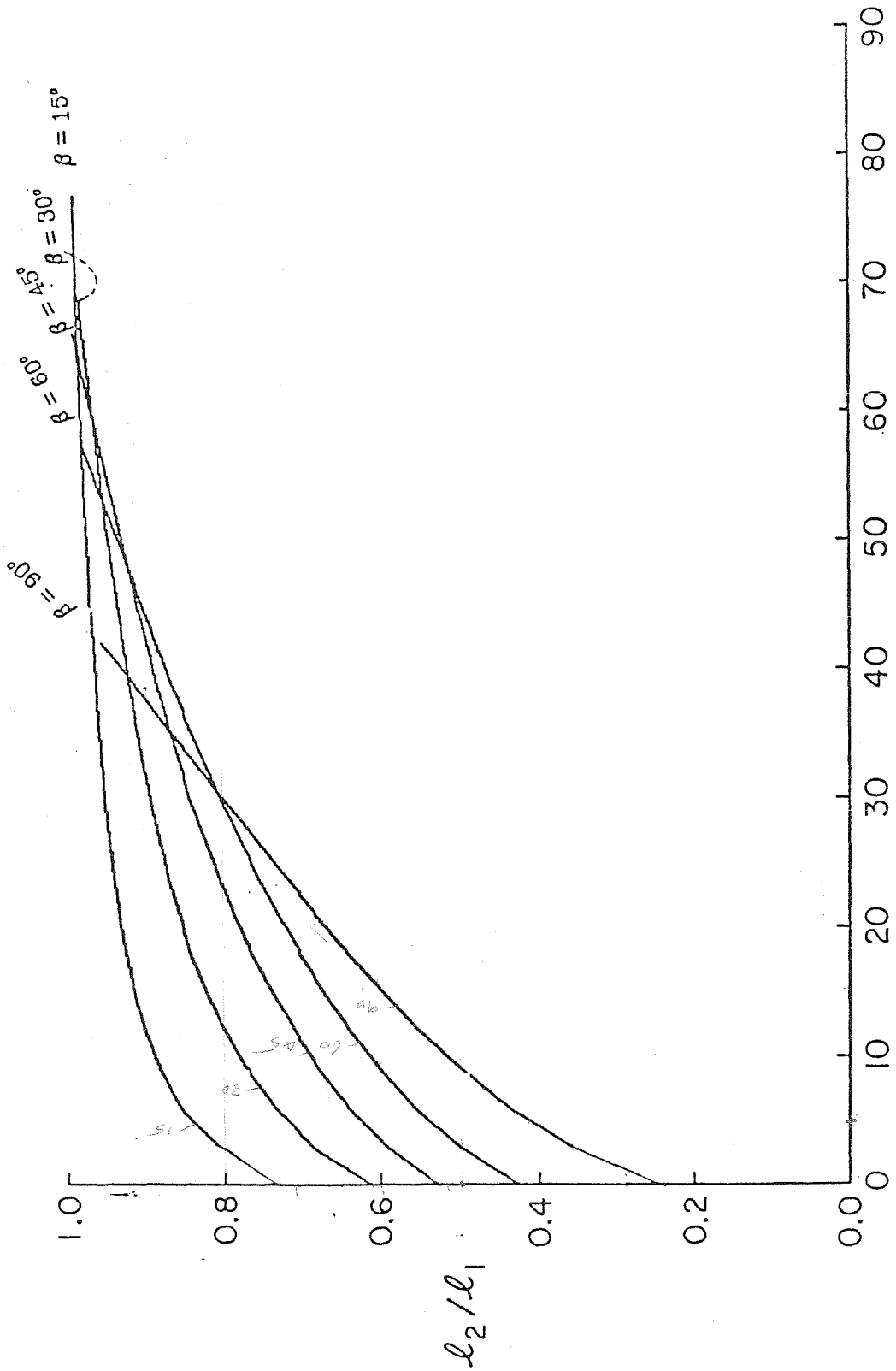

Fig.1.6: l_2/l_1 vs. α for different values or β.

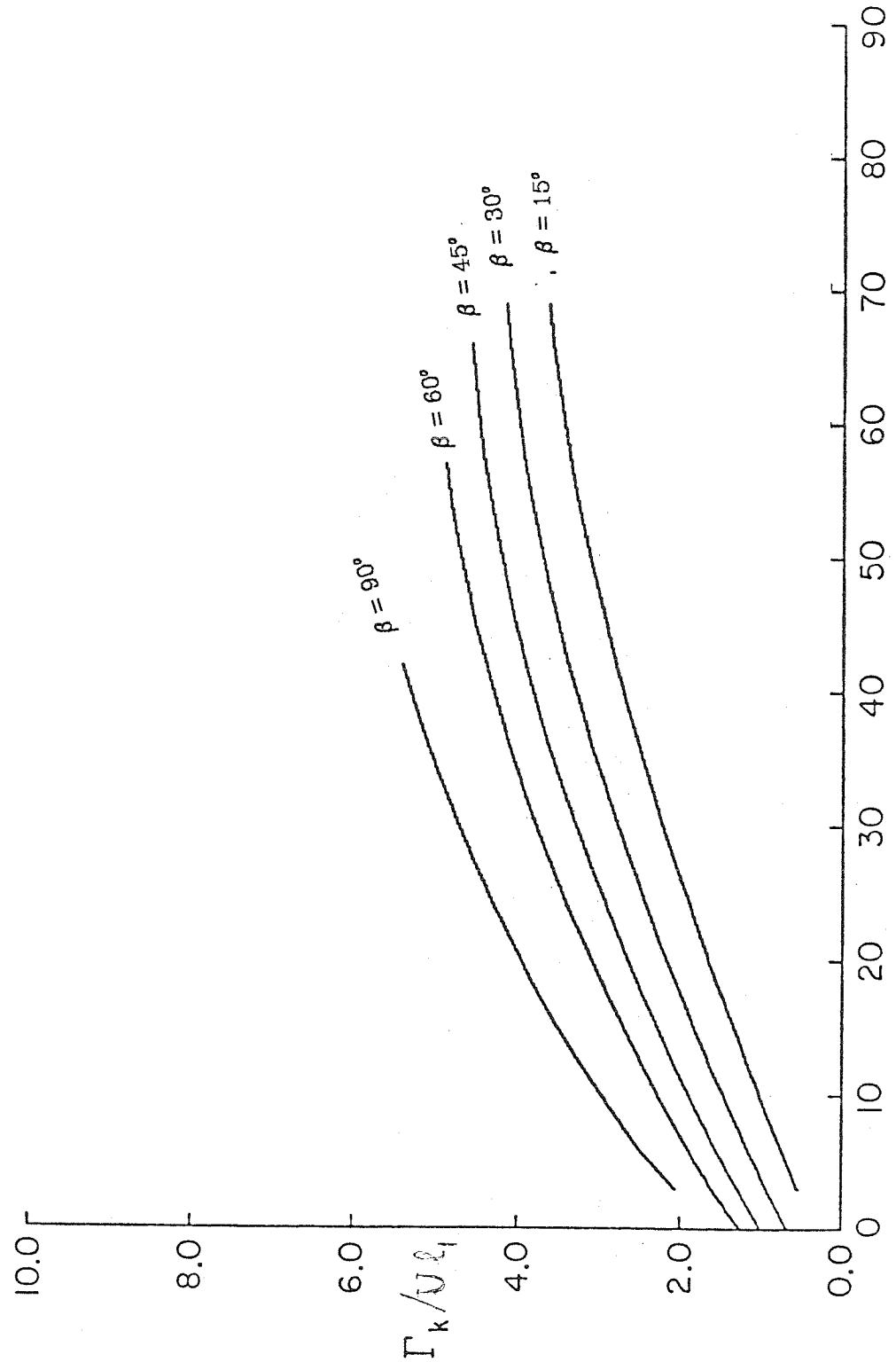

Fig.1.7: $\Gamma_k / U\ell_1$ vs. α for different β values, where Γ_k is the circulation induced at infinity for flow past our geometry in the absence of pt. vortex and with Kutta condition satisfied at trailing edge O.

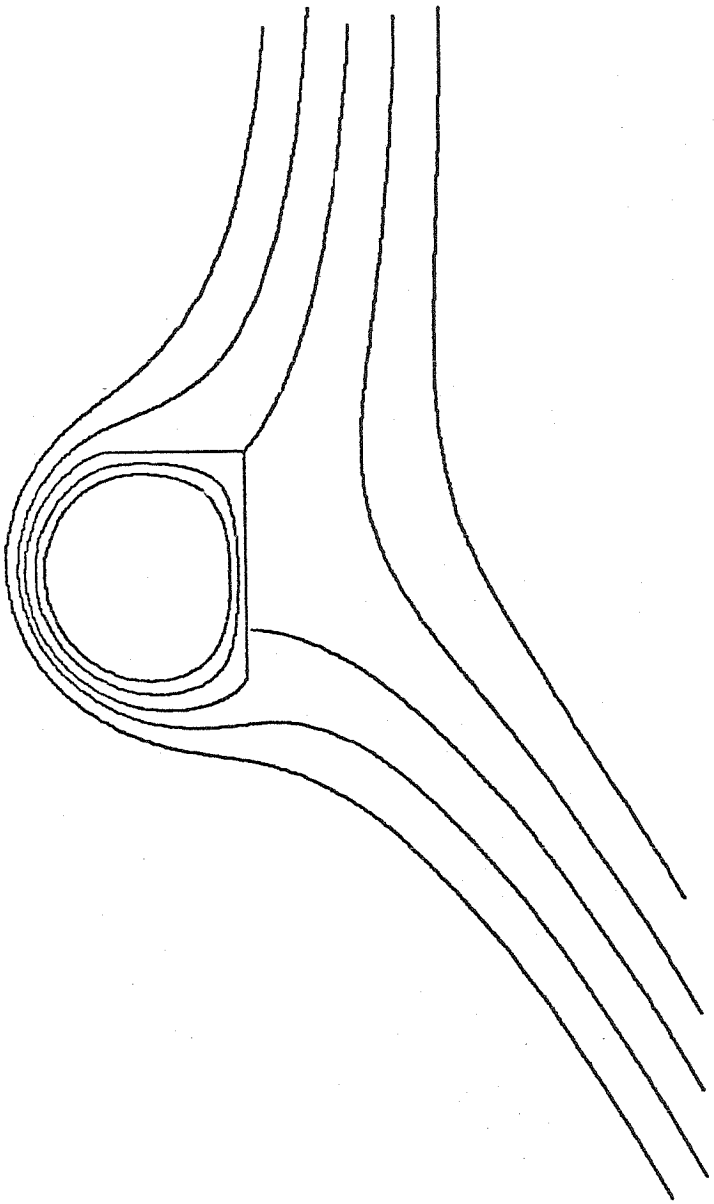

Fig.1.8: Streamlines for $\alpha = 15°$, $\beta = 90°$ for the point vortex case.

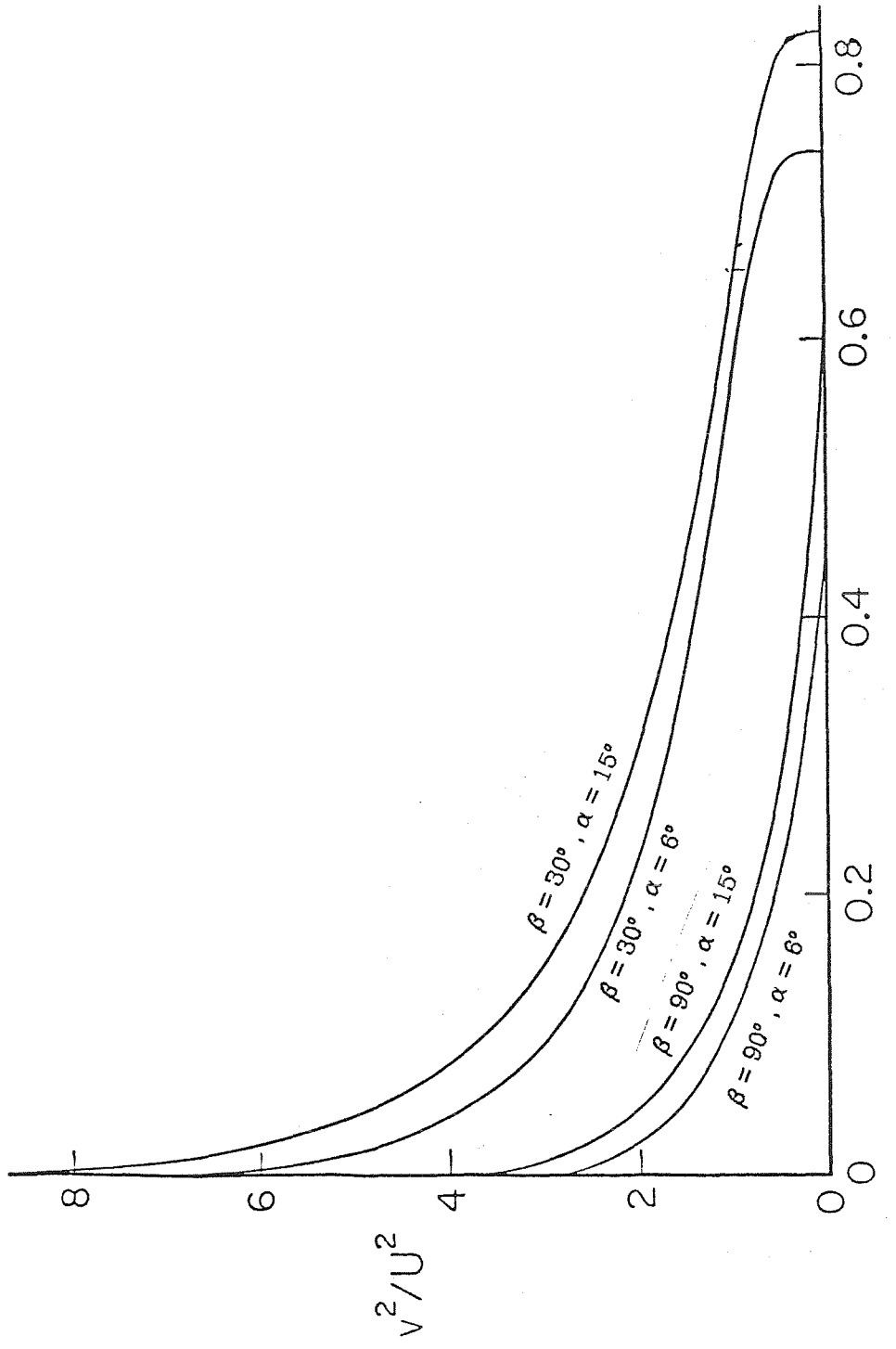

Fig.1.9: V^2 / U^2 vs. x/l_1 for four different combinations of α and β, where V equals velocity on top of the flap and x is the distance along the flap from B.

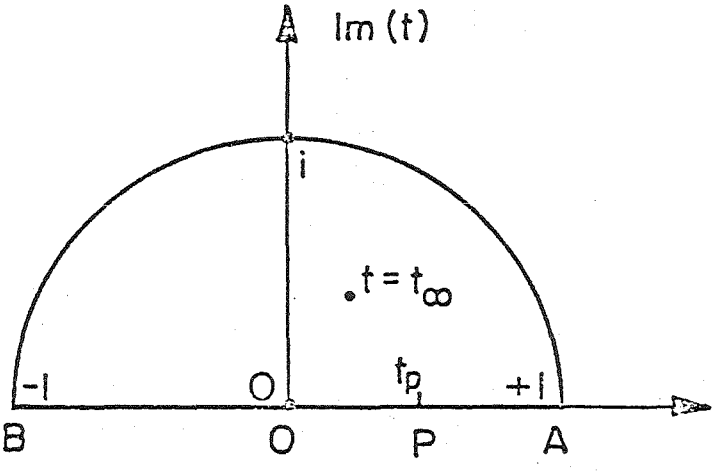

Fig.1.10: The t-plane.

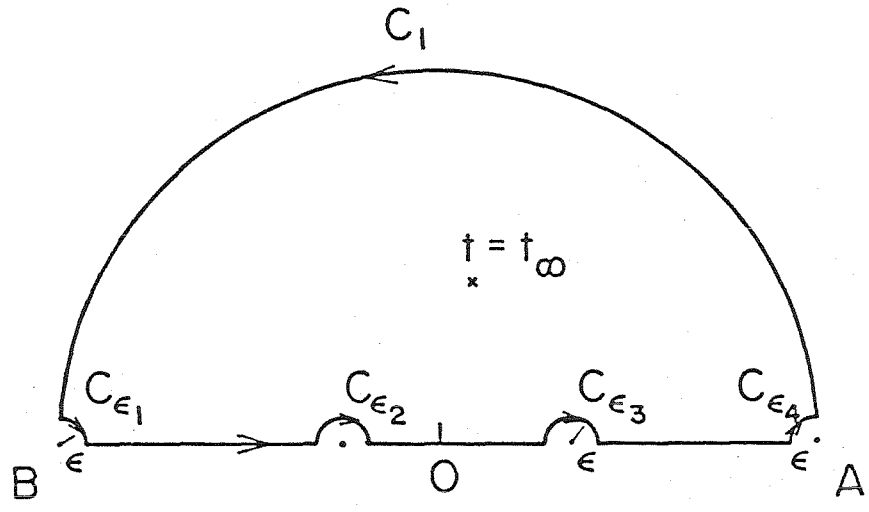

Fig.1.11: Closed contour C for inegrating $\frac{1}{2\pi i}\frac{\frac{d^2W}{dt^2}}{\frac{dW}{dt}}$. The contour coincides with the unit semi-circle except for small ε arc of a circle detours.

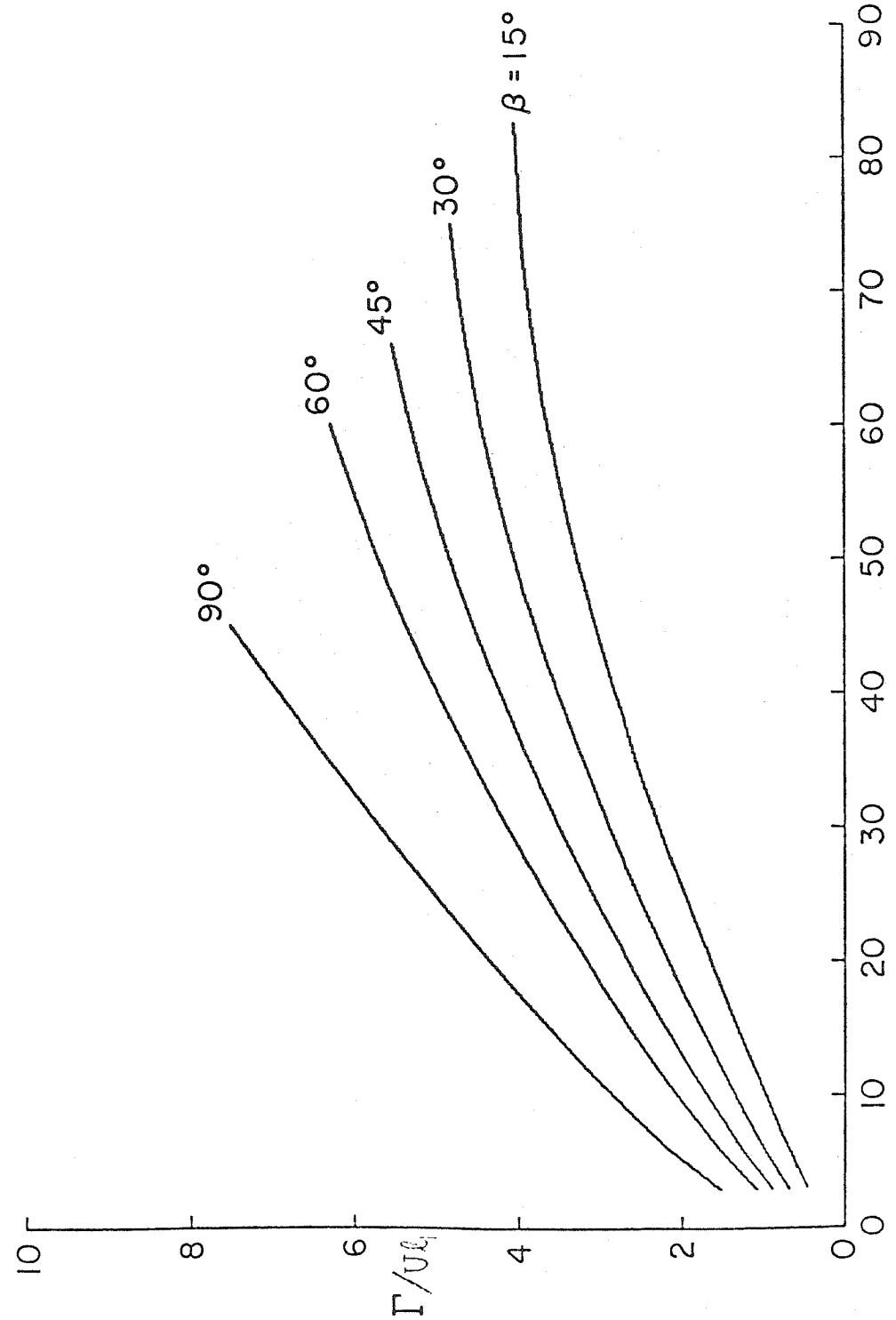

Fig.1.12: $\Gamma / U\ell_1$ vs. α for different β. (vortex sheet case)

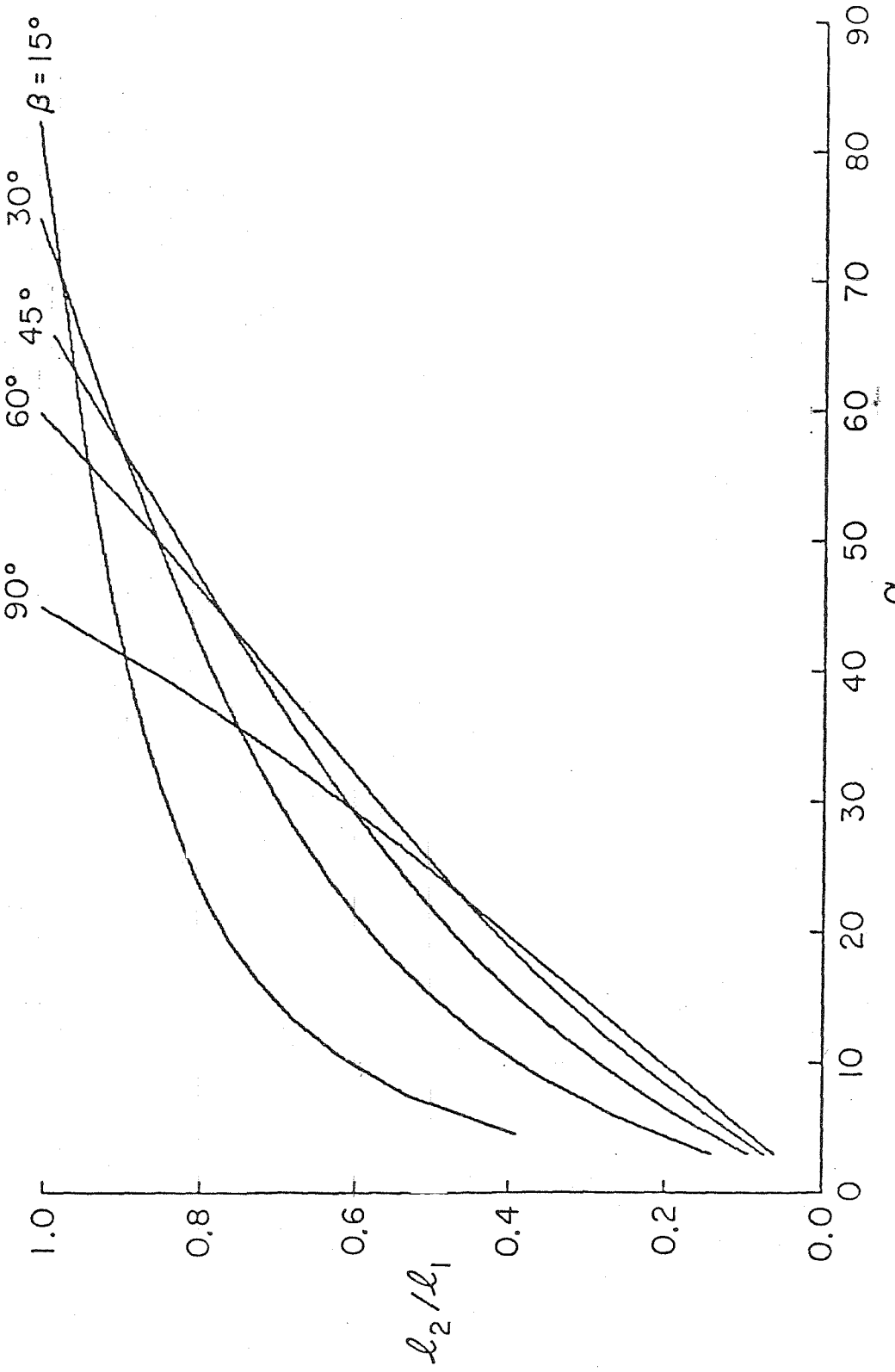

Fig.1.13: l_2/l_1 vs. α for different β (vortex sheet case)

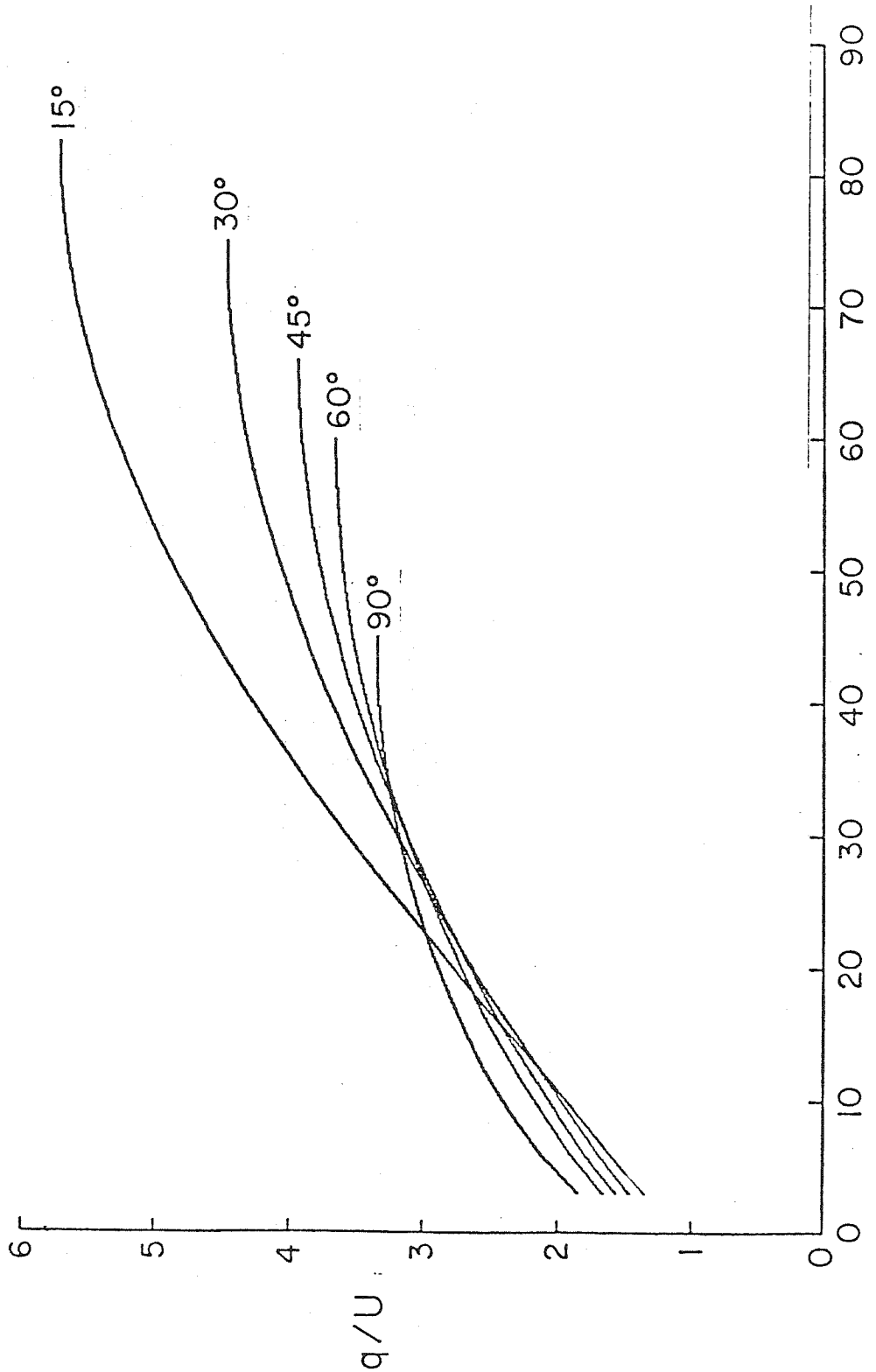

Fig.1.14: q/U vs. α for different β (vortex sheet case).

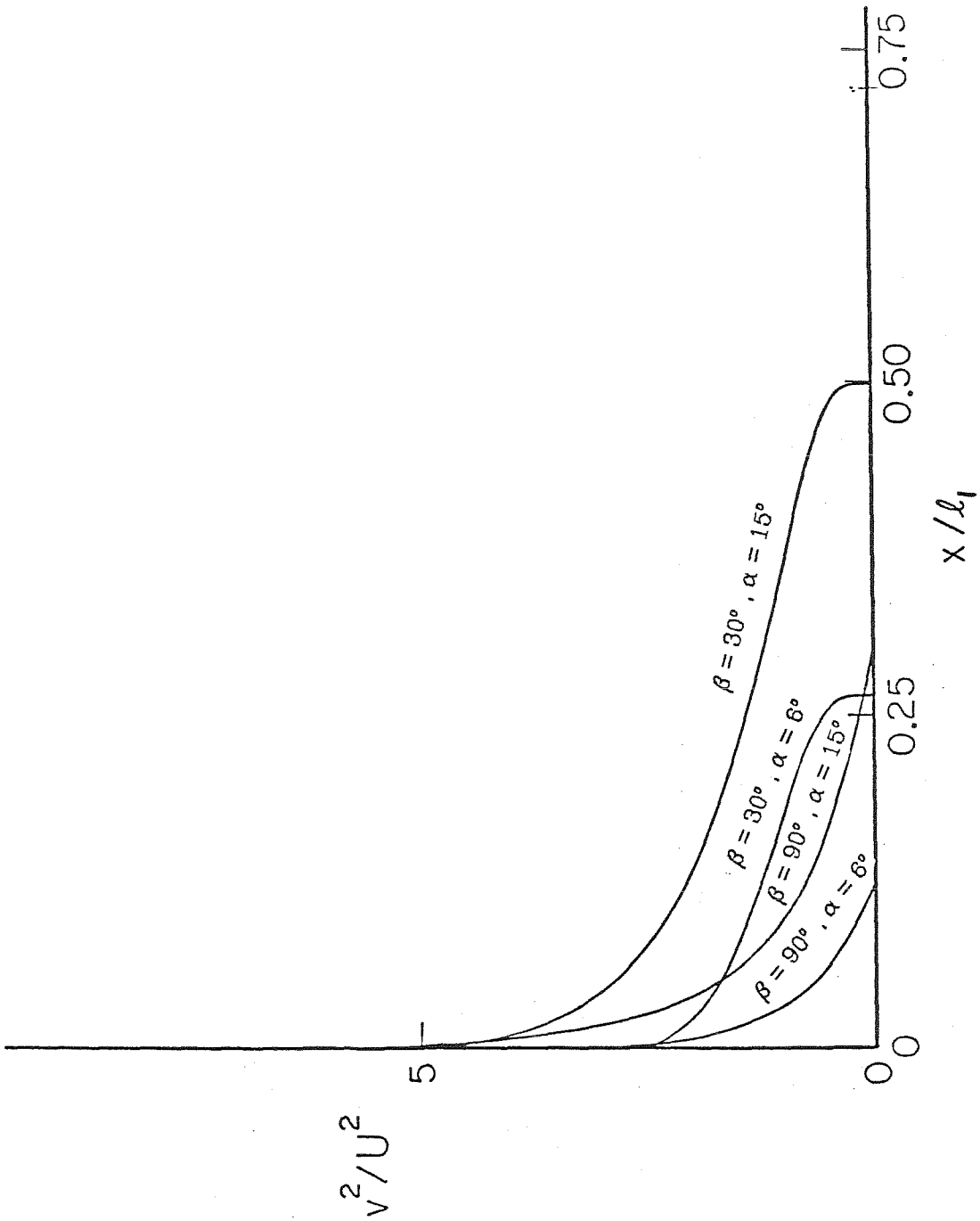

Fig.1.15: V^2 / U^2 vs. x/l_1 for four different combinations of α and β (vortex sheet case), where V equals velocity on top of the flap and x is the distance along the flap from B.

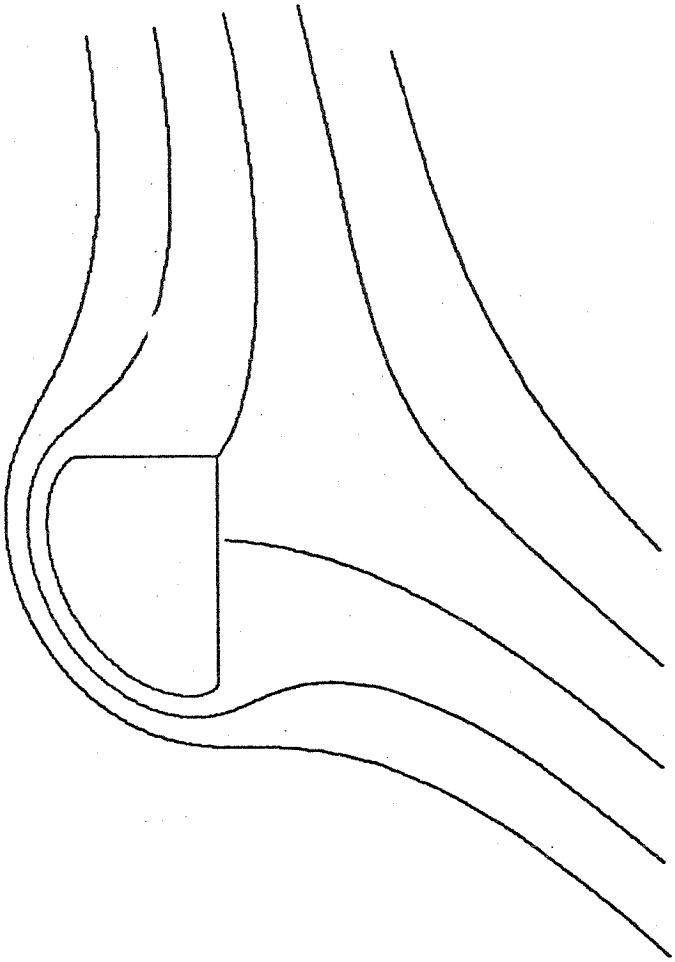

Fig.1.16: Streamlines for $\alpha = 15°$ and $\beta = 90°$

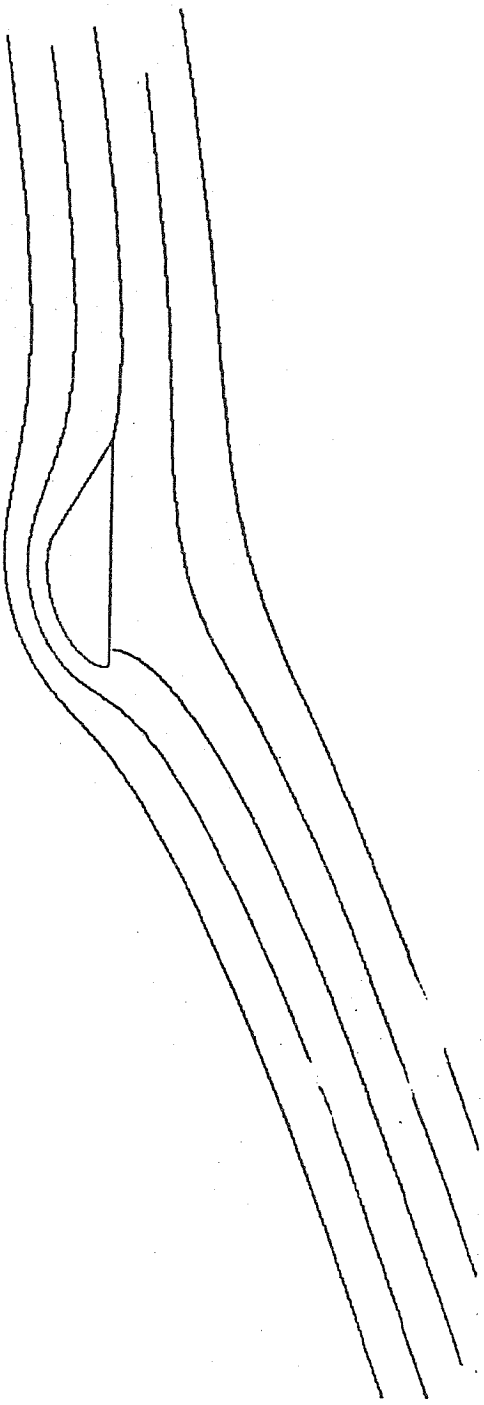

Fig.1.17: Streamlines for $\beta = 30°$ and $\alpha = 15°$.

Values of constants characterizing point vortex flow.									
	$\alpha = 6°$ $\beta = 30°$	$\alpha = 15°$ $\beta = 30°$	$\alpha = 30°$ $\beta = 30°$	$\alpha = 6°$ $\beta = 60°$	$\alpha = 15°$ $\beta = 60°$	$\alpha = 30°$ $\beta = 60°$	$\alpha = 6°$ $\beta = 90°$	$\alpha = 15°$ $\beta = 90°$	$\alpha = 30°$ $\beta = 90°$
Γ / Ul_1	1.415	2.176	3.273	2.840	3.859	5.259	4.530	5.886	7.659
l_2 / l_1	0.736	0.822	0.894	0.556	0.674	0.805	0.437	0.598	0.802
l_s / l_s	0.999	0.975	0.747	0.999	0.928	0.606	0.973	0.807	0.360
$\kappa / U l_1$	3.206	4.425	6.261	5.470	7.069	9.297	7.839	9.921	12.67
ξ	-0.0179	-0.0139	-0.0087	-0.0665	-0.0456	-0.0255	-0.1237	-0.0746	-0.0317
η	0.0696	0.0768	0.0806	0.1565	0.1581	0.1596	0.2386	0.2329	0.2310
Re z_0 / l_1	-0.703	-0.762	-0.805	-0.589	-0.639	-0.690	-0.521	-0.550	-0.590
Im z_0 / l_1	0.181	0.198	0.212	0.298	0.336	0.377	0.395	0.459	0.544
Re $M / U l_1$	-0.4469	-0.4579	-0.5219	-0.5981	-0.6248	-0.6827	-0.6452	-0.7051	-0.7895
Im $M / U l_1$	-0.3886	-0.4074	-0.3580	-0.1943	-0.2307	-0.1983	0.0025	-0.0615	-0.0564
ζ_1	-0.4852	-0.4127	-0.3615	-0.7439	-0.6336	-0.5430	-0.9909	-0.8106	-0.6687
ζ_3	0.1874	0.2203	0.2515	0.2688	0.3156	0.3683	0.3364	0.4112	0.4985
ζ_4^{-1}	0.2730	0.1764	0.1008	0.3959	0.2650	0.1456	0.4909	0.2996	0.1277
$\alpha \lvert\zeta_4\rvert^{1-\beta/\pi}$	2.033	2.185	2.299	1.857	2.098	2.329	1.646	1.991	2.346
ζ_3^{-1}	-2.061	-1.736	-0.998	-1.340	0.986	-0.572	-0.757	-0.562	-0.265

Table 1.1. Different quantities of interest for the point vortex case. l_s stands for the distance OP in the physical plane, while $\zeta = \zeta_s$ corresponds to P.

Values of constants characterizing point vortex flow.									
	$\alpha = 6°$ $\beta = 30°$	$\alpha = 15°$ $\beta = 30°$	$\alpha = 30°$ $\beta = 30°$	$\alpha = 6°$ $\beta = 60°$	$\alpha = 15°$ $\beta = 60°$	$\alpha = 30°$ $\beta = 60°$	$\alpha = 6°$ $\beta = 90°$	$\alpha = 15°$ $\beta = 90°$	$\alpha = 30°$ $\beta = 90°$
Γ / Ul_1	0.9947	1.7670	2.8787	1.5460	2.6273	4.1283	2.1499	3.6168	5.6760
l_2 / l_1	0.2648	0.4980	0.6971	0.1463	0.3309	0.5691	0.1223	0.3041	0.6139
l_s / l_1	0.9903	0.93078	0.7102	0.9756	0.8767	0.5789	0.9493	0.7876	0.3695
q / U	1.6874	2.3009	3.1925	1.8981	2.4573	3.1218	2.1192	2.6664	3.1797
t_p	0.7233	0.5079	0.3034	0.7089	0.5030	0.2875	0.6726	0.4503	0.2015
Re t_∞	0.1880	0.0977	0.0503	0.2908	0.1693	0.0864	0.3391	0.1980	0.0821
Im t_∞	0.3226	0.2985	0.2845	0.3796	0.3835	0.3803	0.4118	0.4370	0.4457
Re $M / q l_1$	-0.0934	-0.1667	-0.2242	-0.0830	-0.1531	-0.2231	-0.0835	-0.1578	-0.2450
Im $M / q l_1$	-0.3266	-0.3274	-0.2376	-0.1907	-0.2027	-0.1520	-0.1377	-0.1430	-0.0902

Table 1.2. Different quantities of interest for the vortex sheet case. l_s stands for the distance OP in the physical plane.

Chapter II

Lift on T-shaped wings and Kasper type wings

2.1. Introduction

In the last chapter, we demonstrated the theoretical possibility of high lift by the action of a free vortex and a vortex sheet located on top of a flat plate with a flap. In the conclusion, it was noted that near the trailing edge O there is a pronounced pressure gradient for moderately small β and that this problem is unlikely to be removed by installation of any boundary layer control mechanism since the Kutta condition translates into infinite pressure gradient at O for the geometry considered. This would then make separation inevitable. Here, we consider two classes of of airfoils where the flap is extended to include a tail. For these geometries, the Kutta condition at the trailing edge will imply a finite nonzero velocity with finite pressure gradient. The question remains whether such modified geometries continue to entertain the possibility of inviscid separated vortex flows found in chapter I. In this chapter, we answer this question in the affirmative for separated flows where the vorticity is confined to a vortex sheet and the region between the vortex sheet and the wing is stagnant. The existence of point vortex flows corresponding to case (a) of Chapter I is not addressed here and is therefore an open problem, though there seems to be little doubt that there exists such a flow.

Here, we propose to study the inviscid incompressible two dimensional potential flows past two classes of wings which are successive modifications of the geometry considered in the first chapter:

(a) T-shaped wings (fig.2.1a): A flat plate AO of length l_1 with a flap BQ attached to it at O such that $<BOA = \beta$, and the lengths $BO = l_2$ and $OQ = l_3$. A vortex sheet of strength q is located between A and B such that there is no flow on the inner side of the sheet. The Kutta condition is satisfied at Q and there is a stagnation point P on the plate AO. It may be shown using analytical arguments almost identical to those in 1.3.3 that if the Kutta condition is satisfied at Q,

then there is one and only one such stagnation point P. Since the flow is stagnant on the inner side of the vortex sheet, it follows from continuity of pressure across the vortex sheet and Bernoulli's equation that q is a constant.

(b) Kasper-type wings (fig 2.1b): A flat plate GO of length l_1 with two flaps GA and BQ attached at G and O and inclined at angles τ and β with respect to the flat plate GO. AG, BO and OQ are of lengths l_4 , l_2 and l_3 respectively. This geometry resembles the Kasper wing (Cox, 1973). As with (a), there is a vortex sheet of constant strength q leaving A and reattaching at B so that the flow on the inner side of the vortex sheet is stagnant. As in (a), the Kutta condition is satisfied at Q and there is one stagnation point P on the plate GO. The velocity at the leading edge G is infinite in general.

As in chapter I, since the flow is a two-dimensional potential flow we may introduce the complex velocity $W(z)$ as an analytic function of z, where $z = x + i\,y$, x and y being the physical coordinates as in figures 2.1a,b. The asymptotic behavior of the complex velocity potential at $z = \infty$, where $z = x + iy$, is given by

$$W(z) \to U\,z\,e^{-i\alpha} + i\Gamma \log z/(2\pi) \qquad (2.1)$$

where U is the free stream velocity, α is the angle of attack with respect to the x-axis and Γ the clockwise circulation induced at $z = \infty$ from the Kutta condition requirement at Q.

The results of this chapter show that these flows are not possible for arbitrary geometry. In the case of T-shaped wings, for given values of α, β and l_3/l_1 over a certain range, there exists a specific l_2/l_1 that would allow a flow of the type desired and that once the geometric constraint is satisfied, Γ/Ul_1, q/U and the location of the stagnation point P relative to the plate AO are all determined in terms of α, β and l_3/l_1. For the Kasper type wings, α, β, τ, l_3/l_1 and l_4/l_1 over a certain range determine l_2/l_1. Once the constraints are satisfied, a

flow exists for which Γ/Ul_1, and q/U are determined. In both cases, the lift coefficient C_L based on length l_1, which is $2\Gamma/Ul_1$, is an order of magnitude higher than the lift on a flat plate with the Kutta condition satisfied at the trailing edge. For the T-shaped case, C_L can be significantly larger than the Kutta lift on a bent wing formed by attaching OQ to plate AO (where OQ and OA are as shown in fig.2.1a) with identical values of α, β and l_3/l_1.

2.2. The method of solution

The method used in chapter I for case (b) needs only minor changes to accomodate flows past the geometries considered here. As in Chapter I, we consider the conformal map $t(z)$ that maps the region exterior of APOQBA in case (a) and AGPOQBA is case (b) in the physical z-plane into the interior of the semicircle such that the boundary point B is mapped to -1, O to 0 and A to +1. The arc of the semicircle in the t-plane corresponds to the vortex sheet between A and B, t_p corresponds to P and t_Q to Q and t_G to G (for case b), where $0 \le t_p < 1$, $-1 < t_Q \le 0$ and $t_p \le t_G < 1$. The values of t_p, t_Q and t_G are unknown apriori. By the Riemann mapping theorem, there exists a unique $t(z)$ as described. Now, consider the complex velocity $\frac{dW}{dz}$ as a function of t. Following the same arguments as in 1.3.2, we arrive at

$$\frac{dW}{dz} = q\ t^{\beta/\pi} \frac{(t_G - t)^\kappa}{(1 - tt_G)^\kappa} \frac{(t_p - t)}{(1 - tt_p)} \tag{2.2}$$

where $\kappa = 0,\ \tau/\pi - 1$ for cases (a) and (b) respectively and the arguments are chosen so that $-\pi \le arg\ \frac{dW}{dz} < \pi$, $-\pi \le arg\,(t_p - t) \le 0$, $-\pi \le arg\,(t_G - t) \le 0$, $-\pi < arg\,(1 - tt_p) \le 0$ and $-\pi < arg\,(1 - tt_G) \le 0$ for t in or on the semicircle. Further, if we consider W as a function of t, the arguments in 1.3.2 can be reproduced identically to obtain once again

$$\frac{dW}{dt} = \frac{(1-t^2)}{2}\left[\frac{4Mt_\infty^2}{(t-t_\infty)^2(1-tt_\infty)^2} + \frac{4\overline{M}\,\overline{t}_\infty^2}{(t-\overline{t}_\infty)^2(1-t\overline{t}_\infty)^2} \right.$$

$$- \frac{i\Gamma(t_\infty - \bar{t}_\infty)(1 - t_\infty \bar{t}_\infty)}{\pi(t - t_\infty)(t - \bar{t}_\infty)(1 - t t_\infty)(1 - t\bar{t}_\infty)} \Bigg] \tag{2.3}$$

Since $\frac{dz}{dt} = \frac{dW}{dt} / \frac{dW}{dz}$, it follows from (2.2) and (2.3) that

$$\frac{dz}{dt} = (1-t^2)t^{-\beta/\pi} \frac{(t_G - t)^{-\kappa}}{2q(1 - t t_G)^{-\kappa}} \frac{(1 - t t_p)}{(t_p - t)} \Bigg[\frac{4Mt_\infty^2}{(t - t_\infty)^2(1 - t t_\infty)^2} + \frac{4\bar{M}\,\bar{t}_\infty^2}{(t - \bar{t}_\infty)^2(1 - t\bar{t}_\infty)^2}$$

$$- \frac{i\Gamma(t_\infty - \bar{t}_\infty)(1 - t_\infty \bar{t}_\infty)}{\pi(t - t_\infty)(t - \bar{t}_\infty)(1 - t t_\infty)(1 - t\bar{t}_\infty)} \Bigg] \tag{2.4}$$

where t_∞ is the image of $z = \infty$ in the t-plane. Since $\frac{dW}{dt} = 0$ at $t = t_p$ and $t = t_Q$ because of stagnation point or Kutta condition, whatever the case may be, we have

$$\frac{4Mt_\infty^2}{(t_p - t_\infty)^2(1 - t_p t_\infty)^2} + \frac{4\bar{M}\,\bar{t}_\infty^2}{(t_p - \bar{t}_\infty)^2(1 - t_p \bar{t}_\infty)^2} = \frac{i\Gamma(t_\infty - \bar{t}_\infty)(1 - t_\infty \bar{t}_\infty)}{\pi(t_p - t_\infty)(t_p - \bar{t}_\infty)(1 - t_p t_\infty)(1 - t_p \bar{t}_\infty)} \tag{2.5}$$

$$\frac{4Mt_\infty^2}{(t_Q - t_\infty)^2(1 - t_Q t_\infty)^2} + \frac{4\bar{M}\,\bar{t}_\infty^2}{(t_Q - \bar{t}_\infty)^2(1 - t_Q \bar{t}_\infty)^2} = \frac{i\Gamma(t_\infty - \bar{t}_\infty)(1 - t_\infty \bar{t}_\infty)}{\pi(t_Q - t_\infty)(t_Q - \bar{t}_\infty)(1 - t_Q t_\infty)(1 - t_Q \bar{t}_\infty)} \tag{2.6}$$

Also the condition that the relation between z and t be 1-1 means that there should be no residue for $\frac{dz}{dt}$ at $t = t_\infty$. Using (2.4), this implies

$$\frac{i\Gamma}{2\pi} = \frac{2Mt_\infty^2}{1 - t_\infty^2} \Bigg[- \frac{\beta}{\pi t_\infty} - \frac{\kappa t_G}{(1 - t_G t_\infty)} + \frac{\kappa}{(t_G - t_\infty)} + \frac{1}{(t_p - t_\infty)} - \frac{t_p}{(1 - t_p\, t_\infty)} \Bigg] \tag{2.7}$$

Besides (2.7), for the T-shaped wing, geometrical conditions imply

$$\int_0^1 \frac{dz}{dt}\, dt = -l_1 \tag{2.8}$$

$$\int_{t_Q}^0 \frac{dz}{dt}\, dt = l_3\, e^{\,i(\pi - \beta)} \tag{2.9}$$

$$\int_{-1}^0 \frac{dz}{dt}\, dt = l_2\, e^{\,-i\beta} \tag{2.10}$$

For Kasper-type wings, the geometrical conditions are

$$\int_0^{t_G} \frac{dz}{dt}\, dt = -l_1 \tag{2.11}$$

$$\int_{t_G}^1 \frac{dz}{dt}\, dt = l_4 e^{i\tau} \tag{2.12}$$

$$\int_{t_Q}^0 \frac{dz}{dt}\, dt = l_3\, e^{\,i(\pi - \beta)} \tag{2.13}$$

$$\int_{-1}^0 \frac{dz}{dt}\, dt = l_2\, e^{\,-i\beta} \tag{2.14}$$

where $\frac{dz}{dt}$ is given by (2.4). From (2.2) and consideration of the velocity at $z = \infty$, we have

$$Ue^{-i\alpha} = qt_\infty^{\beta/\pi} \frac{(t_G - t_\infty)^\kappa}{(1 - t_G\, t_\infty)^\kappa} \frac{(t_p - t_\infty)}{(1 - t_p\, t_\infty)} \tag{2.15}$$

For the T-shaped wing case, (2.5), (2.6), (2.7), (2.8), (2.9), (2.10) and (2.15) constitute nine real relations to determine the nine real quantities Γ, q, t_p, t_Q, Re t_∞, Im t_∞, Re M, Im M and l_2, if l_1, l_3, U, β and α are treated as known. For the Kasper wing case, (2.5), (2.6), (2.7), (2.11), (2.12), (2.13), (2.14) and (2.15) determines ten real unknowns Γ, Q, t_p, t_Q, t_G, Re t_∞, Im t_∞, Re M, Im M and l_2, if l_1, l_3, l_4, β, U, α and τ are considered as known. Thus the flow is completely determined if these equations can be solved. We were unable to prove rigorously that solutions exist for these systems of equations, but numerical procedures, employed as described in the next section, solved the above equations to determine all the unknowns that characterize each of the flow in (a) and (b).

As in the vortex sheet case of Chapter I, it is not clear that the function $z(t)$ defined by (2.12) has indeed the required properties for it to map the t plane into the z plane as desired. However, almost the same arguments as in the last chapter can be made to argue that (2.12) indeed defines the correct mapping function.

2.3. Numerical procedure

Since each of l_1 and U scales the dimensional variables linearly, they were set equal to unity without any loss of generality. For case (a), it was convenient for the numerical calculations to consider t_p rather than l_3 together with the angles β and α as known. Equations (2.5), (2.6) and (2.15) contain four real equations for the four real unknowns t_Q, q/U, Re t_∞ and Im t_∞ where M/Γ is eliminated by using (2.7). These are just algebraic equations and were conveniently solved by Newton iteration. Once t_Q, q/U and t_∞ are determined,

equation (2.7) then determines M/Γ. One numerical integration in (2.8) determines Γ/Ul_1. The lengths l_2 and l_3 are determined in terms of l_1 from the integrations in (2.9) and (2.10).

For case (b), once again we considered t_p rather than l_3 together with β, α, τ and l_4 as known. In addition to (2.5), (2.6) and (2.15), the following equation obtained from (2.11) and (2.12)

$$\frac{l_4}{\Gamma}\int_0^{t_G}\left|\frac{dz}{dt}\right| dt = \frac{1}{\Gamma}\int_{t_G}^{1}\left|\frac{dz}{dt}\right| dt \qquad (2.16)$$

determines the five real unknowns t_Q, t_G, q/U, Re t_∞ and Im t_∞, where M/Γ is again determined from (2.7). Integration in (2.11), (2.13) and (2.14) determines the remaining unknowns Γ/Ul_1, l_2/l_1 and l_3/l_1.

2.4. Results for the T-shaped wing

Numerical solutions were found for a wide range of geometries and angles of attack. For $t_Q = 0$, i.e.$l_3 = 0$ the results of Hurley and Skeat were reproduced which provided a check on the code. No convergence in the iteration scheme could be obtained for $\alpha \leq 0$ suggesting that solutions do not exist in that range. The continuous curves in figures (2.2), (2.3) and (2.4) show the values of the the lift coefficient $C_L = 2\Gamma/Ul_1$ vs l_3/l_1 for different α and β values. There is a steep rise in C_L at the left end of each of the curves which is not visible in the scale used in each of the plots. The right end of each of the curves in these figures correspond to the maximum value of l_3/l_1 for which the flow sketched in fig.2.1a exists. It corresponds to the stagnation point P coinciding with O. No efforts were made to study solutions for which the stagnation point P was located on the tail OQ. The broken lines in each of figures (2.2), (2.3), (2.4) shows the Kutta lift coefficient on a bent wing formed by attaching OQ to OA where their lengths are l_3 and l_1. The C_L for the T-shaped wing is considerably larger than the the lift on this bent wing for large values of β. Figures (2.5), (2.6) and

(2.7) show plots of l_2/l_1 against l_3/l_1 again for different α and β values. Figures (2.8), (2.9) and (2.10) show the corresponding values of q/U and the ratio of magnitude of trailing edge to main stream velocity, $|\zeta_Q|/U$ (in broken lines). Figure (2.11) is a plot of the actual streamlines when $l_3/l_1 = 0.2027$, $\beta = 60$ and $\alpha = 15$ degrees. For this case, the values of Γ/Ul_1, l_2/l_1 and q/U are 3.919, 0.3747 and 2.977 respectively while the stagnation point P is located where the length OP equals 0.6979 l_1. The magnitude of the velocity at the trailing edge Q was 0.1546 q. The square of the ratio of velocity on the flap to the free stream velocity at infinity is plotted against the distance from B as a fraction of l_1 in fig.2.12. From Bernoulli's principle, these plots may be interpreted as pressure plots. The pressure gradient is infinite at B as for the geometry of Chapter I. However, trailing edge Q has a finite velocity and a relatively small pressure gradient. Comparing fig.2.12 with fig.1.15, we find that the shape of the pressure profile is only locally affected near the trailing edge and that the average pressure gradient is not affected significantly by the addition of the tail.

2.5. Results for the Kasper-type wings

Solutions were found for a range of values of α, β , τ, l_3/l_1 and l_4/l_1. This is a five parameter family of solutions. Here, we only present solutions for the case $\beta = 30°$, $\tau = 75°$ and $l_4/l_1 = 0.14$. Figure (2.13) shows the values of lift coefficients C_L as a function of l_3/l_1 for three different angles of attack. As with the T-shaped wing case, no solution could be found for $\alpha \leq 0$. The right end of each of the curves corresponds to t_p equalling zero, i.e. stagnation point P and O coincides for those cases. Figures (2.14) and (2.15) shows corresponding values of l_2/l_1 and q/U against l_3/l_1 for different α. Comparing figures (2.13), (2.14) and (2.15) with figures (2.2), (2.5) and (2.8) shows that the flow is relatively insensitive to the leading edge flap for small l_4/l_1. Figure (2.16) is a plot of the actual streamlines for the case $\beta = 60°$, $\alpha = 15°$, $\tau = 75°$, $l_4/l_1 = 0.14$ and

$l_3/l_1 = 0.2253$. The corresponding values of Γ/Ul_1, l_2/l_1 and q/U were 3.881, 0.3723 and 3.027 respecitvely. The large values for the lift coefficients provides a theoretical basis for Kasper's claim that by designing a wing as suggested, one could indeed obtain very high lift.

2.6. Conclusion

Exact solutions have been obtained for two dimensional inviscid incompressible flows past T-shaped wings and Kasper type wings which may be of relevance to the actual high Reynolds number subsonic flows past these geometries. The addition of the tail improves the lift coefficent dramatically besides getting rid of the infinite pressure gradient at the trailing edge. Comparison with the pressure profile for the zero tail case of chapter I reveals however that the nonzero velocity at the trailing edge has only a local effect on the pressure profile. The pressure gradient continues to be infinite at B and the average pressure gradient over the plate BQ is not changed significantly. Nonetheless, the removal of locally large pressure gradient at the trailing edge makes it easier for the flow to be experimentally realized for moderately small β since suitable tailoring of the flap end B as mentioned in chapter I combined with blowing on the upper surface of BQ may wipe out large adverse pressure gradient regions near B. Thus, it may very well be possible to install some effective mechanism so as to avoid the separation problem. Indeed, the separating streamline can be expected to become a turbulent mixing layer and suction may have to be applied at B to produce smooth reattachment, which could be combined with blowing over the upper surface. It should be noted that the shear layer is convex to the high velocity side and may therefore be expected to be relatively stable.

Professor E.O. Tuck (communication with Prof. P.G. Saffman) has commented that the solutions are akin to constant pressure airfoils investigated many years ago in attempts to delay the boundary layer separation (see, e.g.

Thwaites 1960). The free streamline can in the content of inviscid theory be replaced by a solid boundary and our solutions can therefore be regarded as providing a class of thick airfoils on which the pressure gradient is zero over a significant part of the upper surface.

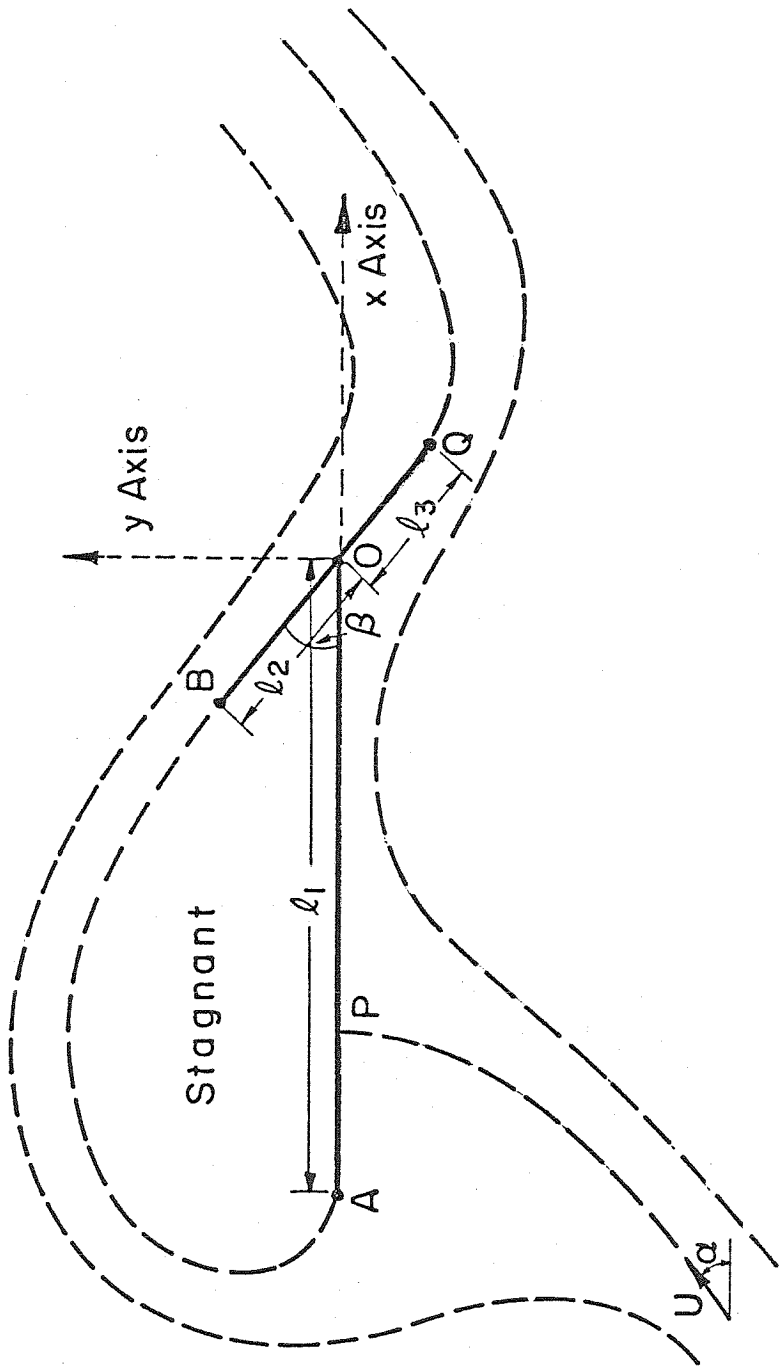

Fig.2.1a: Sketch of flow past a T-shaped wing.

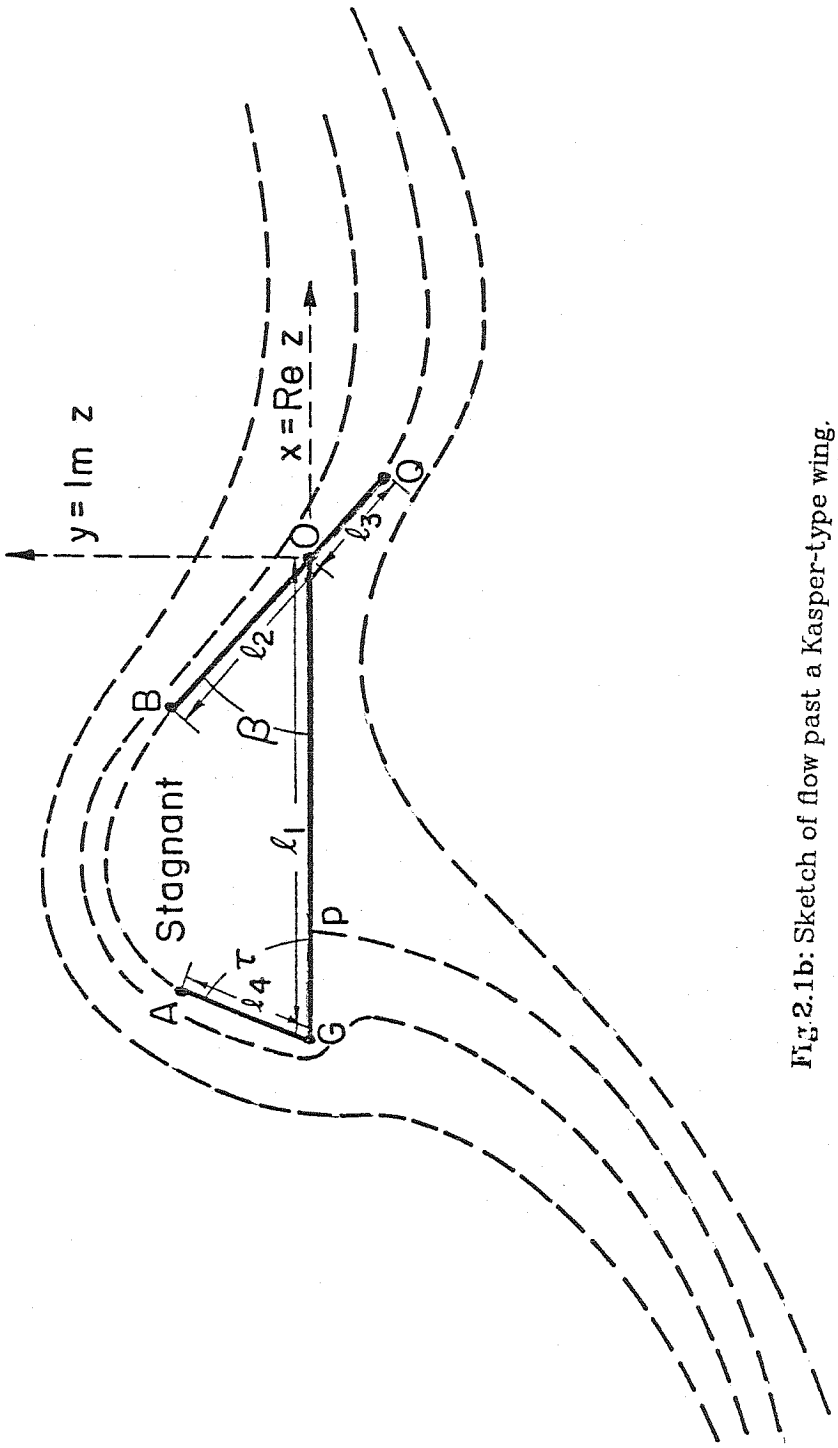

Fig.2.1b: Sketch of flow past a Kasper-type wing.

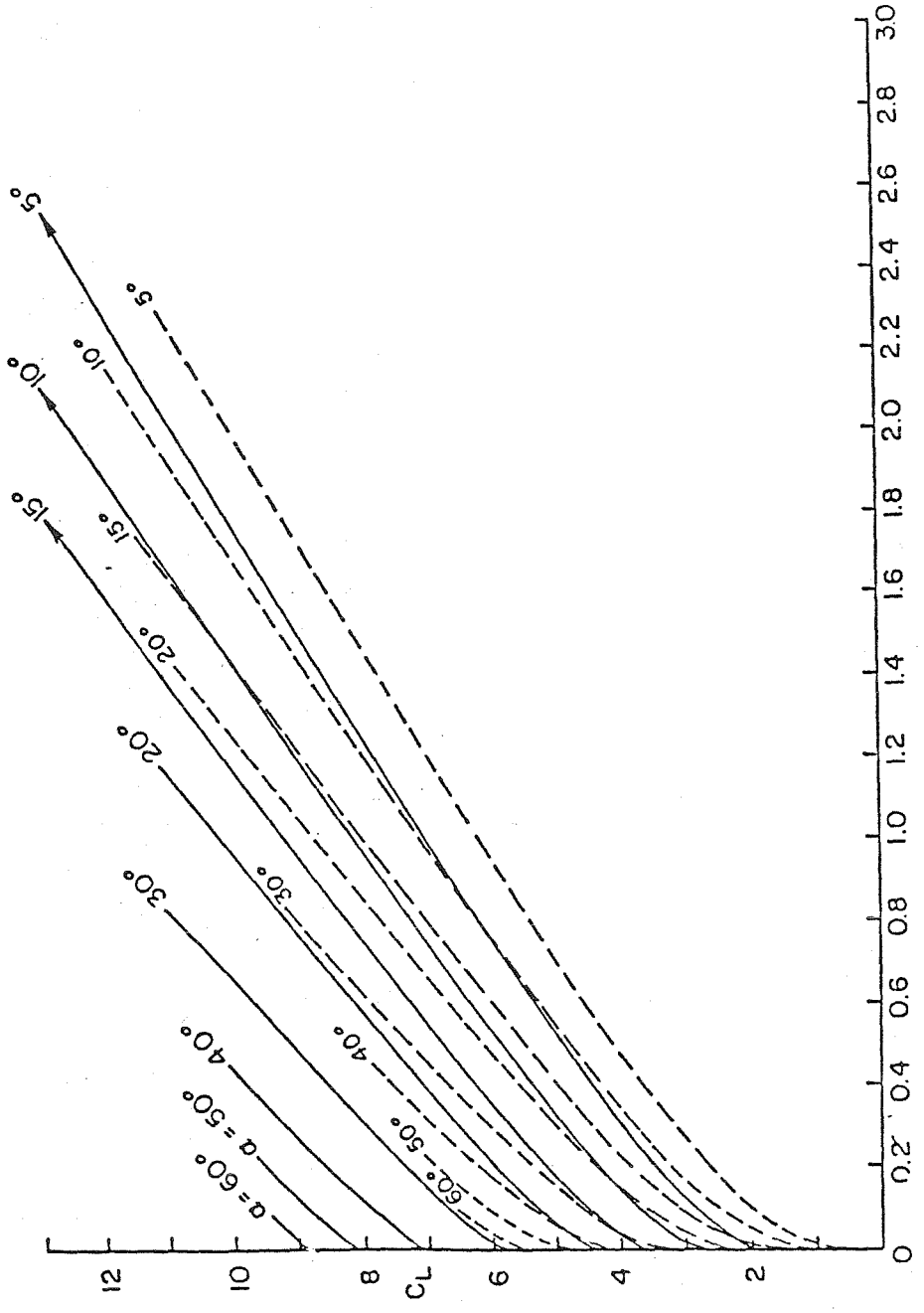

Fig.2.2: Solid lines are the lift coefficient C_L vs. l_3/l_1 for α as marked and β=30°. The right end of each of the curves (except the ones marked by arrows) indicate the limiting case with stagnation points P and O coinciding. For cases with arrows, the curve continues beyond the scale given and the values of l_3/l_1 corresponding to O and P coinciding may be found in fig.2.5. Broken lines show the Kutta lift coefficients for a bent wing formed by joining QO to OA.

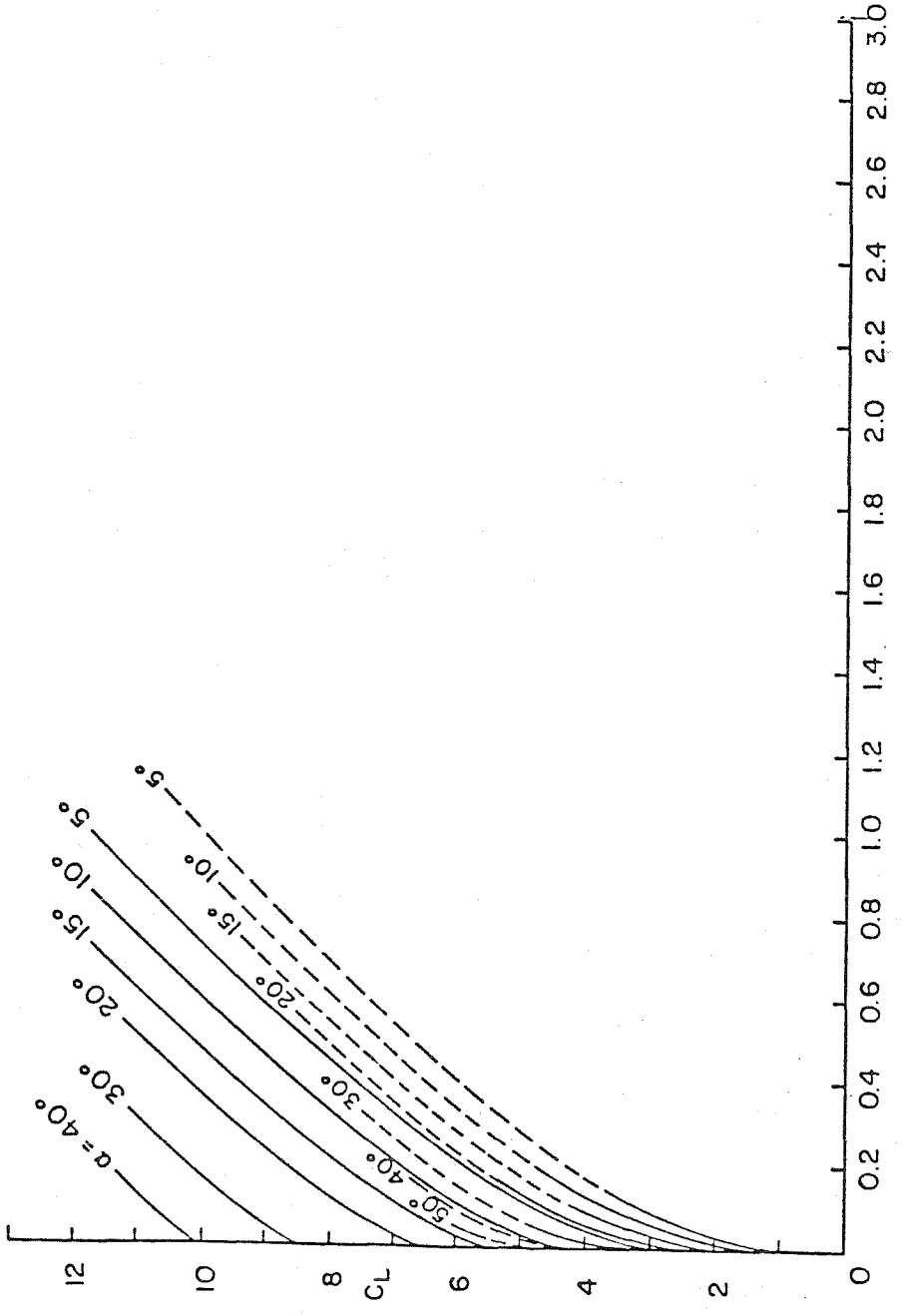

Fig.2.3: C_L against l_3/l_1 for different α and for $\beta = 60°$. The right ends correspond to coincident P and O. The broken lines indicate Kutta lift coefficient on a bent wings for identical values of α and β.

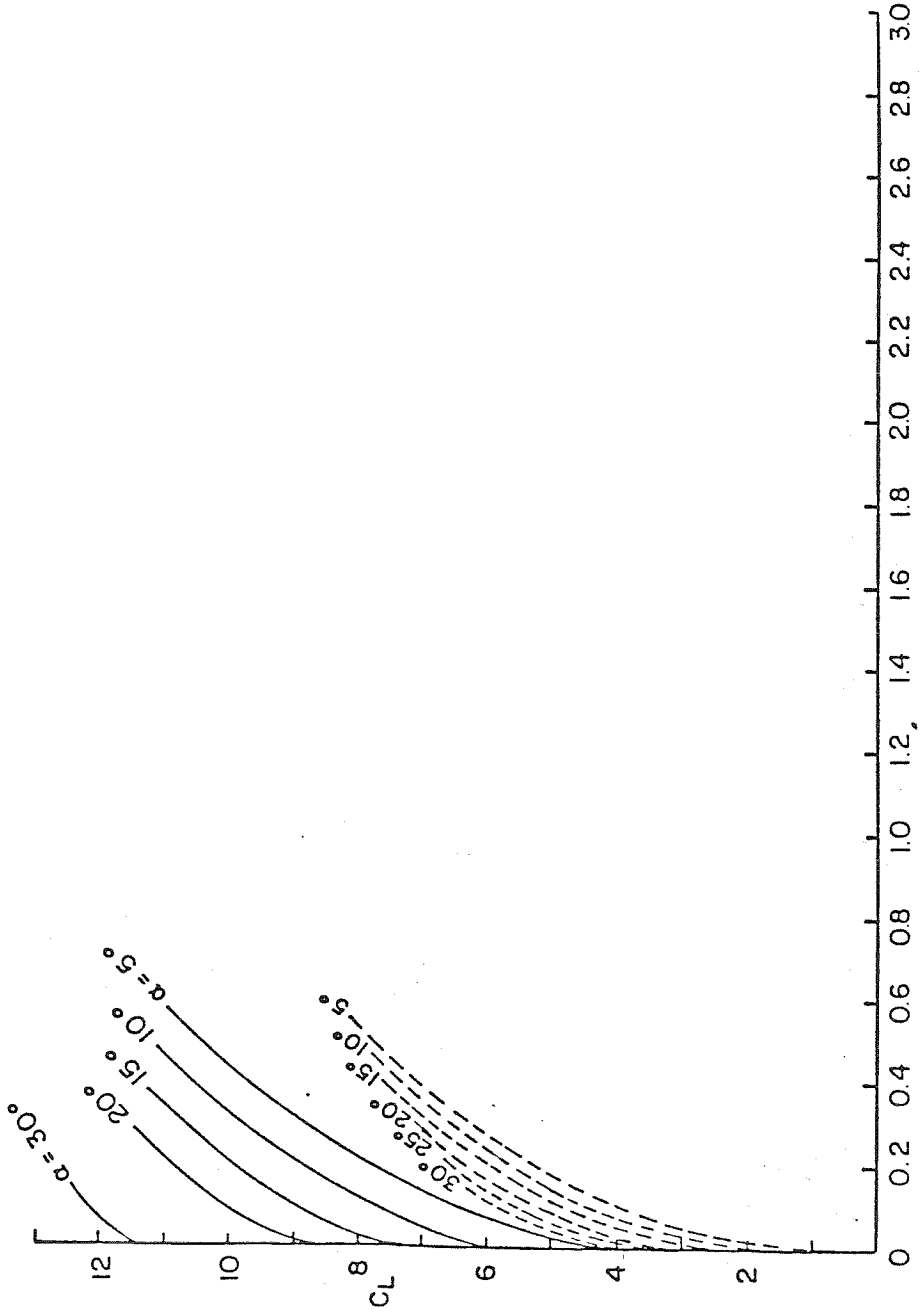

Fig.2.4: C_L against l_3/l_1 for different α and for $\beta = 90°$. The right ends correspond to coincident P and O. The broken lines are once again corresponding Kutta lift coefficients on a bent wing.

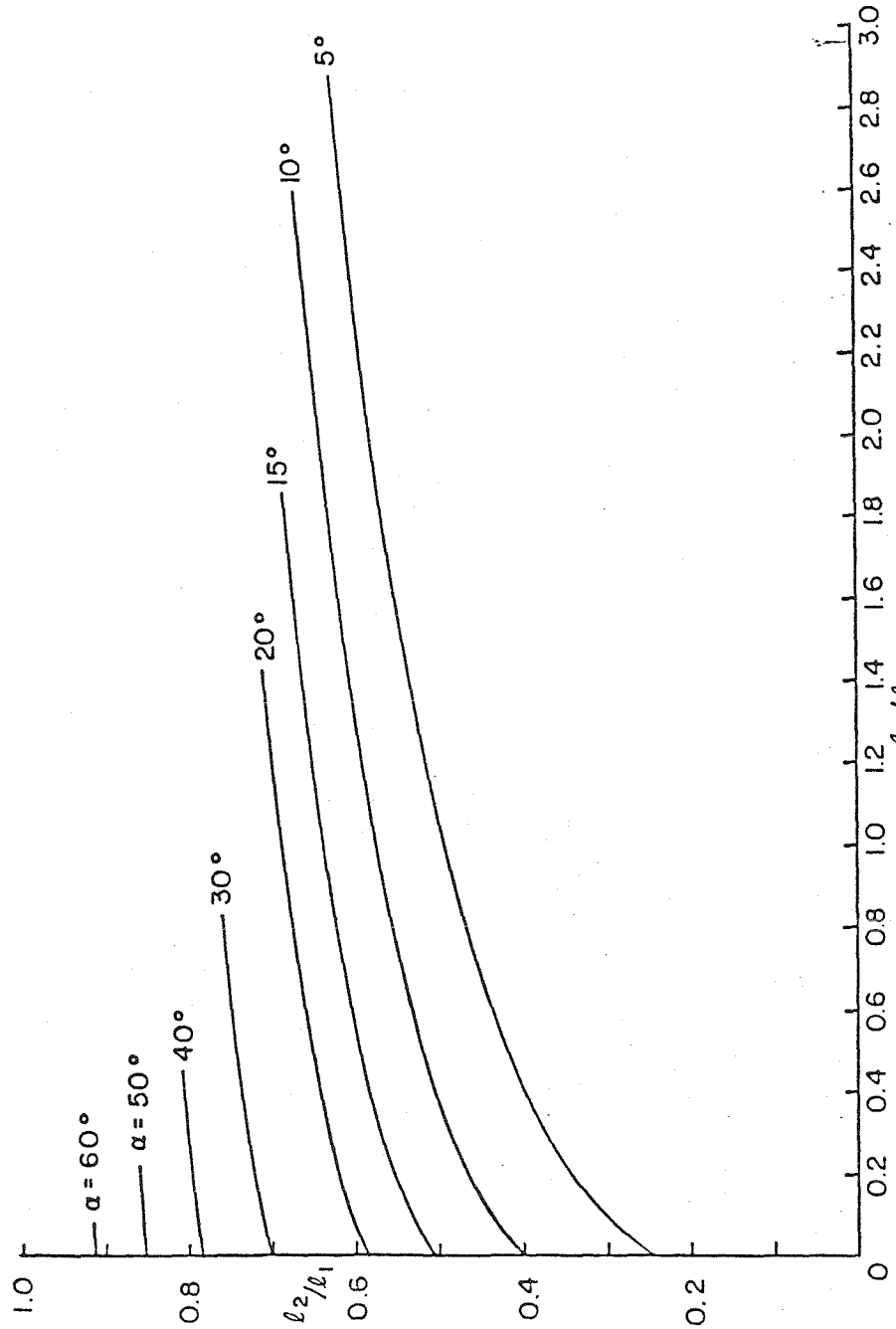

Fig.2.5: l_2 / l_1 vs. l_3 / l_1 for different α as marked and $\beta = 30°$.

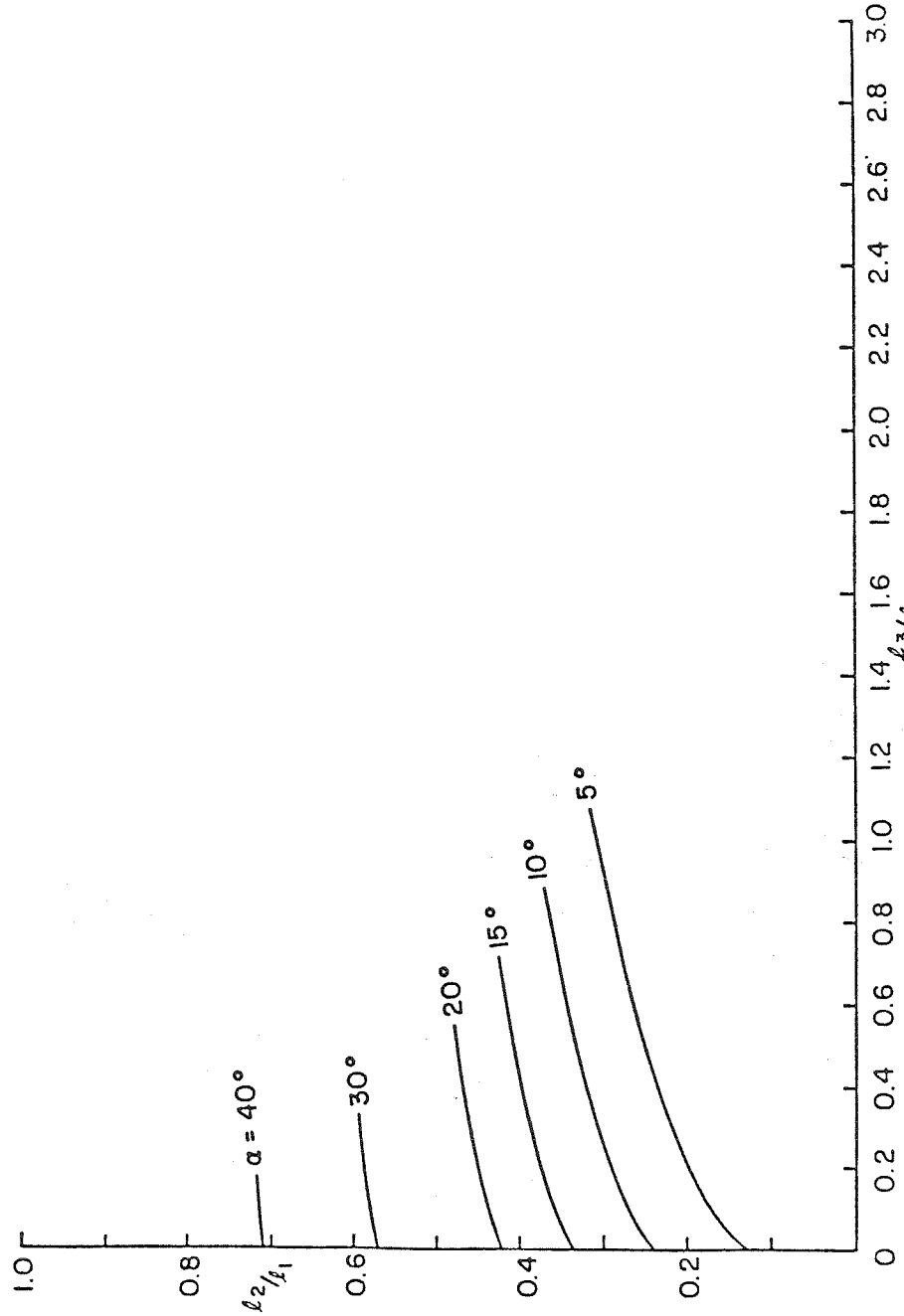

Fig.2.6: l_2 / l_1 vs. l_3 / l_1 for different α as marked and $\beta = 60°$.

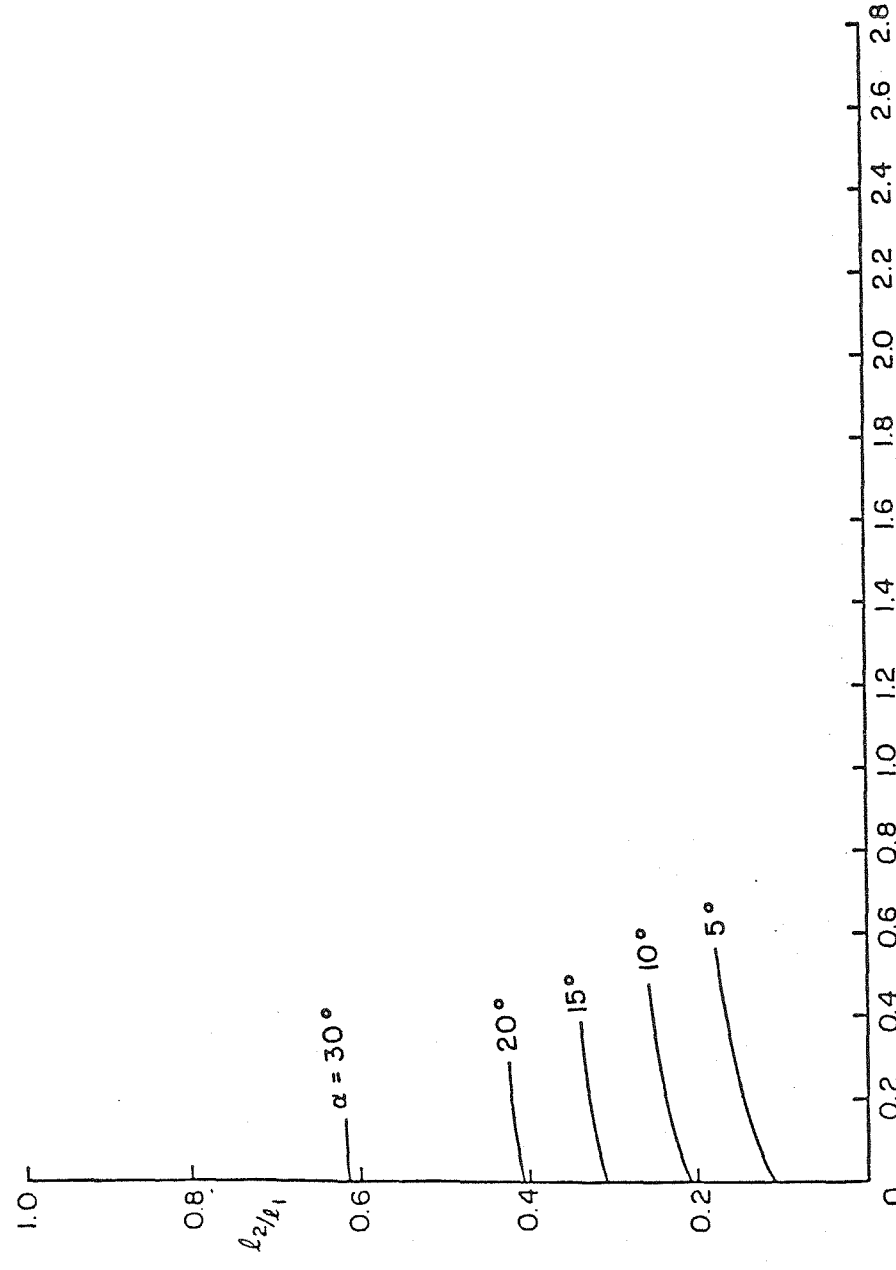

Fig.2.7: l_2 / l_1 vs. l_3 / l_1 for different α as marked and $\beta = 90°$.

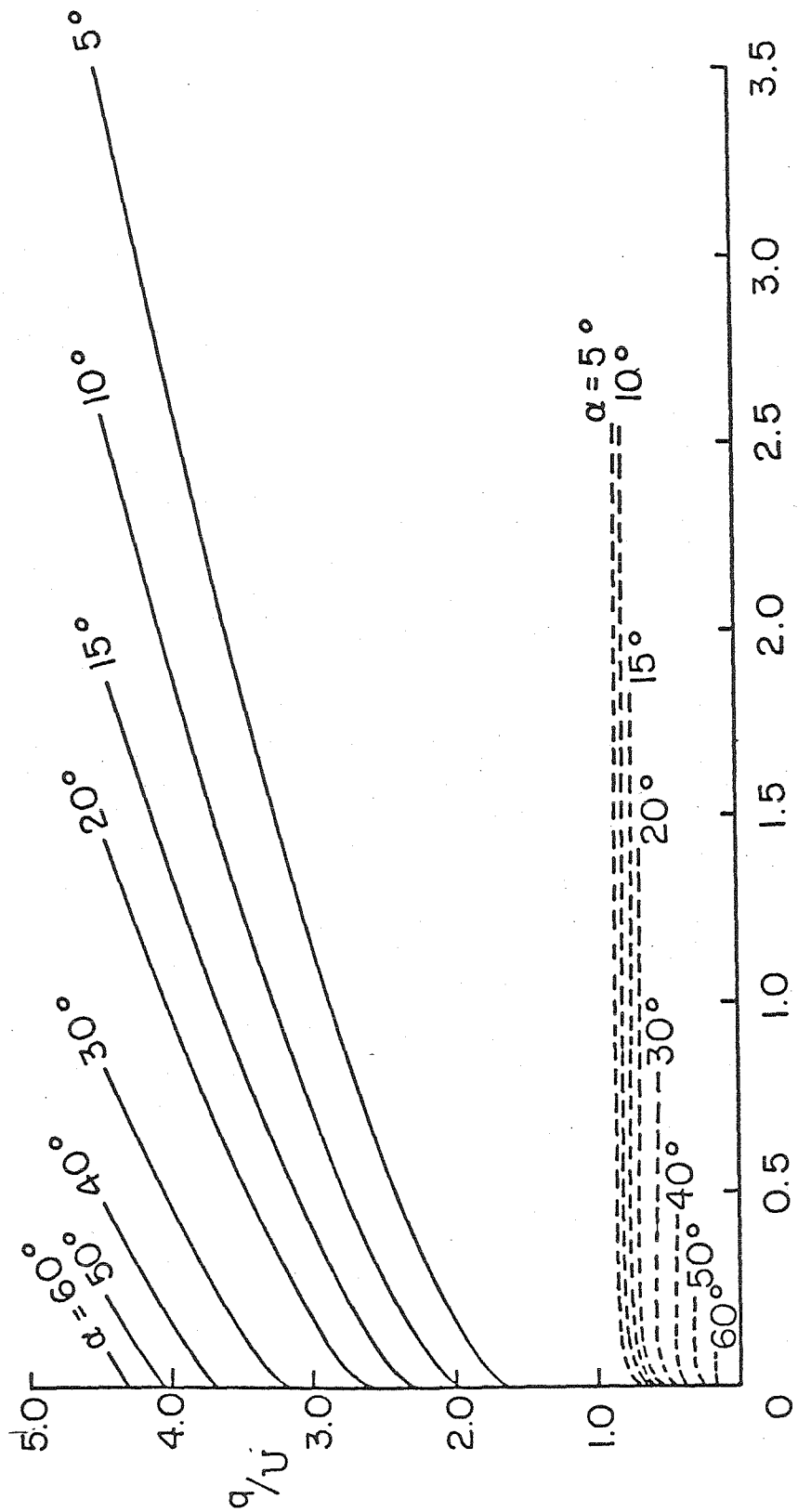

Fig.2.8: Solid lines are values of q/U vs. l_3/l_1 for $\beta = 30°$. Broken lines show corresponding value of the ratio of velocity at trailing edge to the free stream velocity U.

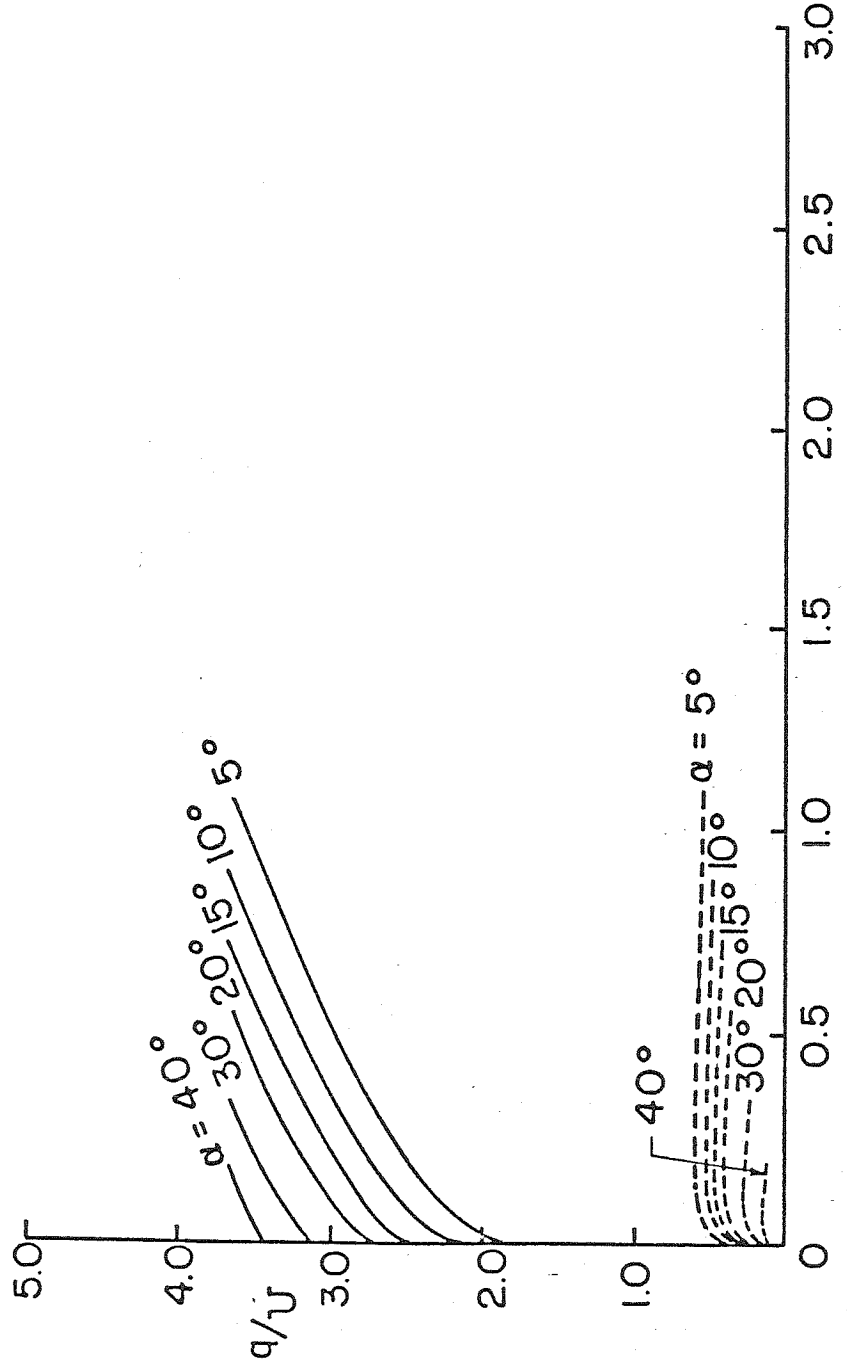

Fig.2.9: Solid lines are values of q/U vs. l_s/l_1 for $\beta = 60°$. Broken lines show corresponding value of the ratio of velocity at trailing edge to the free stream velocity U.

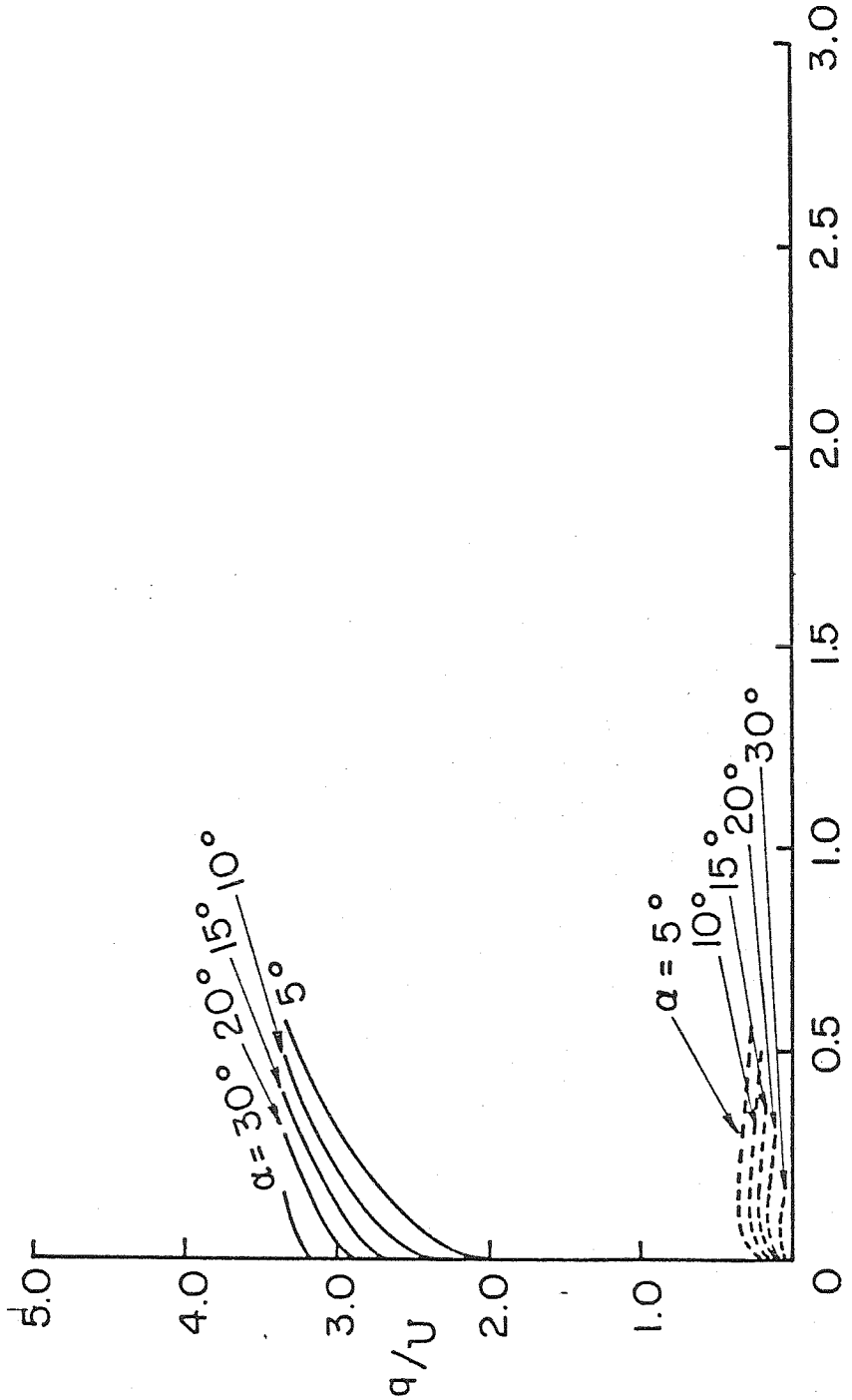

Fig.2.10: Solid lines are values of q/U vs. l_3/l_1 for $\beta = 90°$. Broken lines show corresponding value of the ratio of velocity at trailing edge to the free stream velocity U.

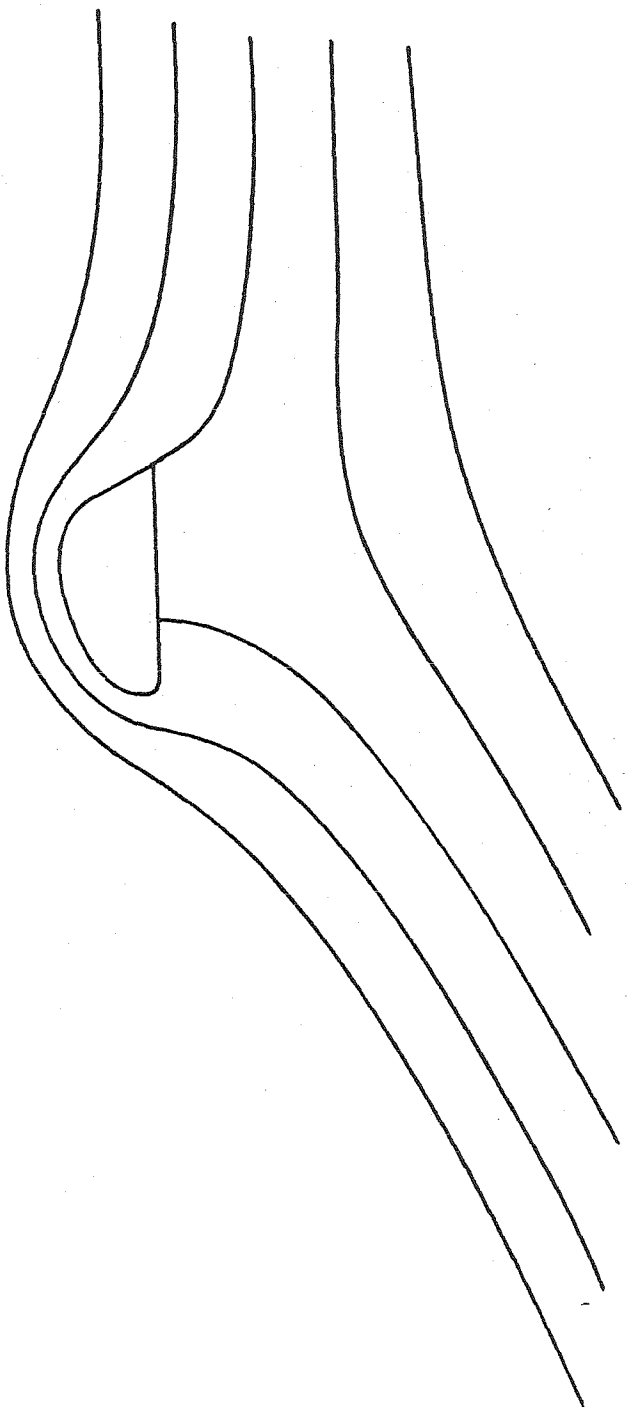

Fig.2.11: Streamline plot for T-shaped wing with $\beta = 60°$, $\alpha = 15°$ and $l_3 / l_1 = 0.2027$.

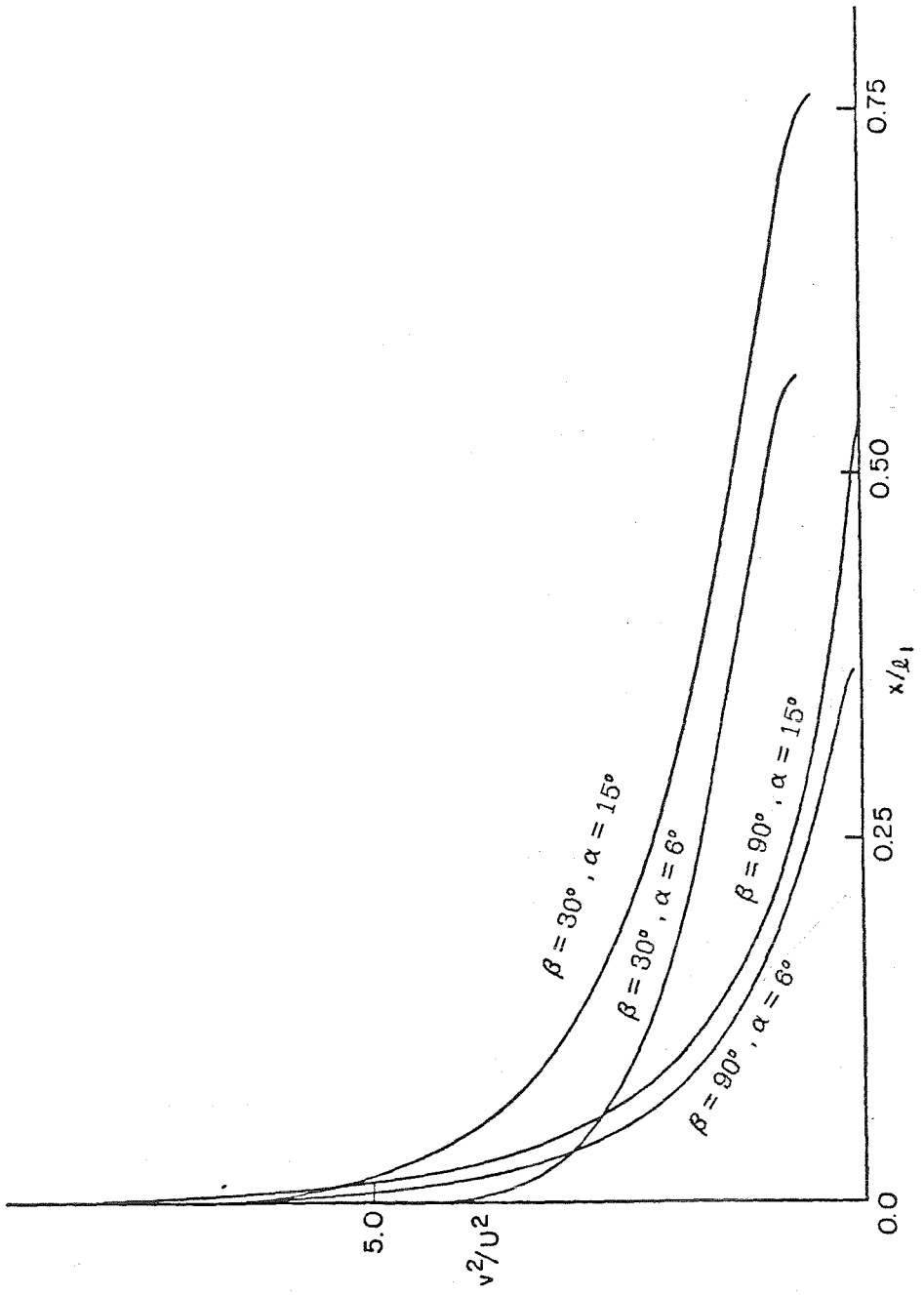

Fig.2.12: V^2 / U^2 vs. x/l_1 for four different combinations of α and β with l_3/l_1 set equal to 0.2. V is once again the velocity of top of the flap and x is the distance along the flap from B.

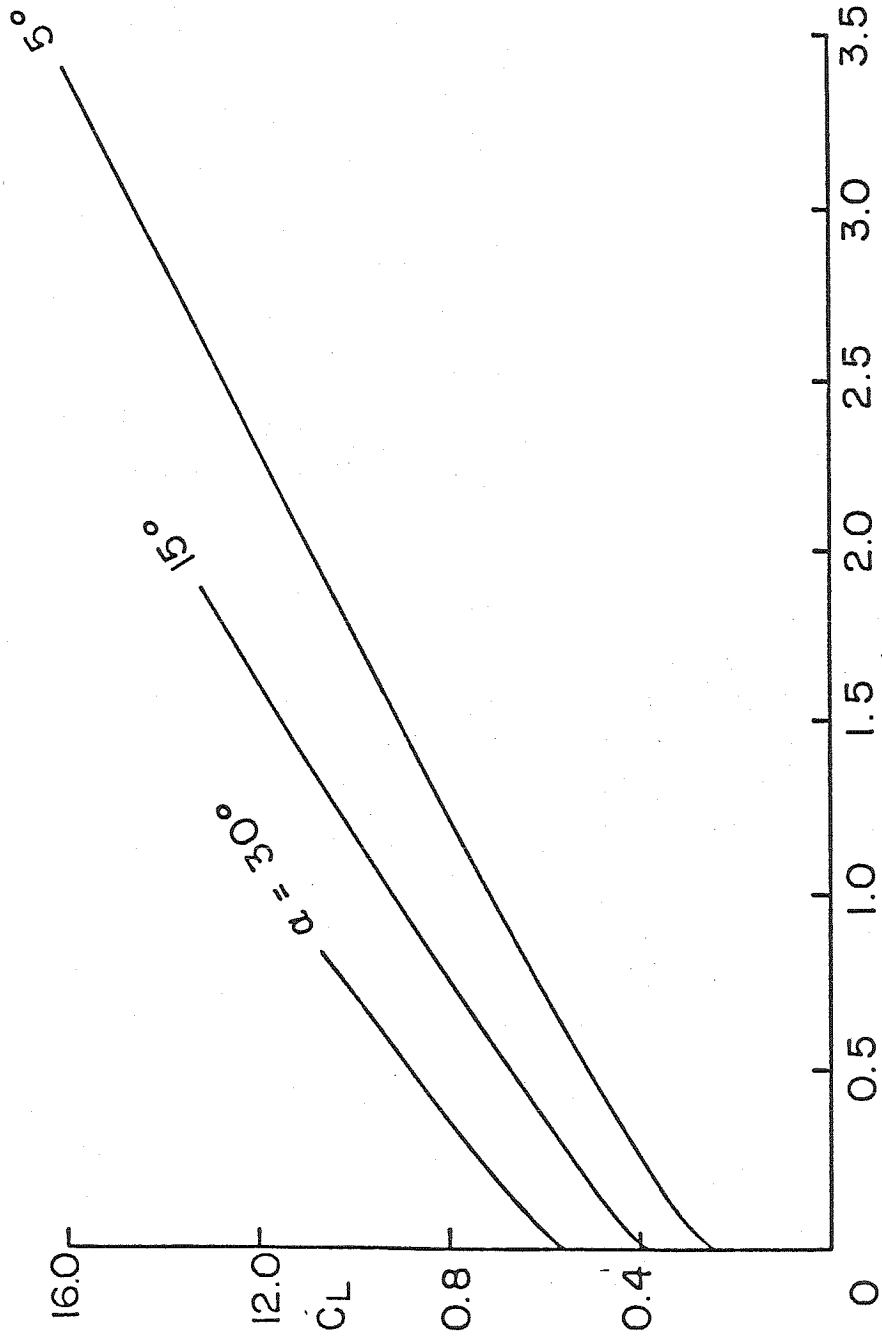

Fig.2.13: Lift coefficient C_L for Kasper type wings as a function of l_3 / l_1 for different values of α. β, τ and l_4 / l_1 were all fixed and had values 30°, 75° and 0.14 respectively.

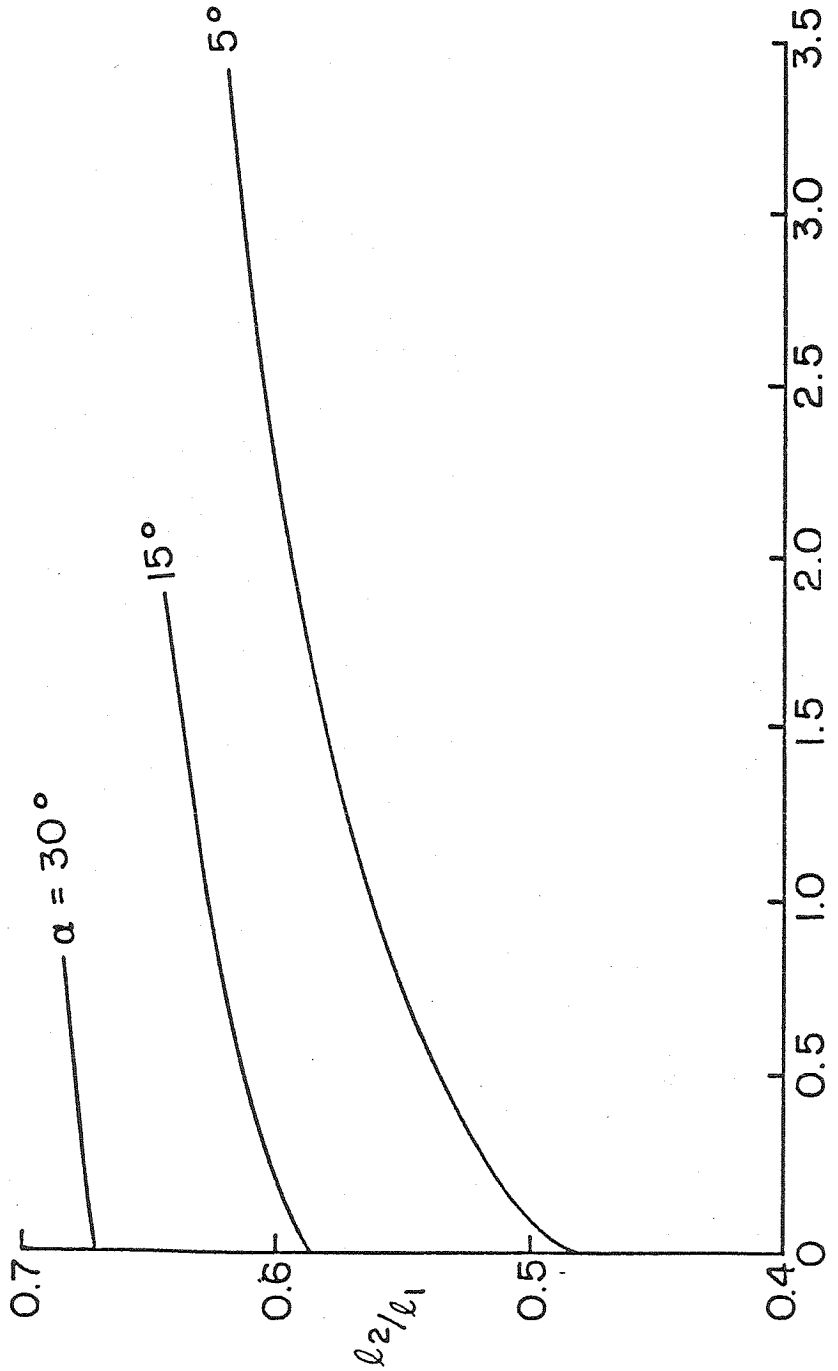

Fig.2.14: l_2 / l_1 for Kasper type wings as a function of l_3 / l_1 for different values of α. β, τ and l_4/l_1 were all fixed and had values 30°, 75° and 0.14 respectively.

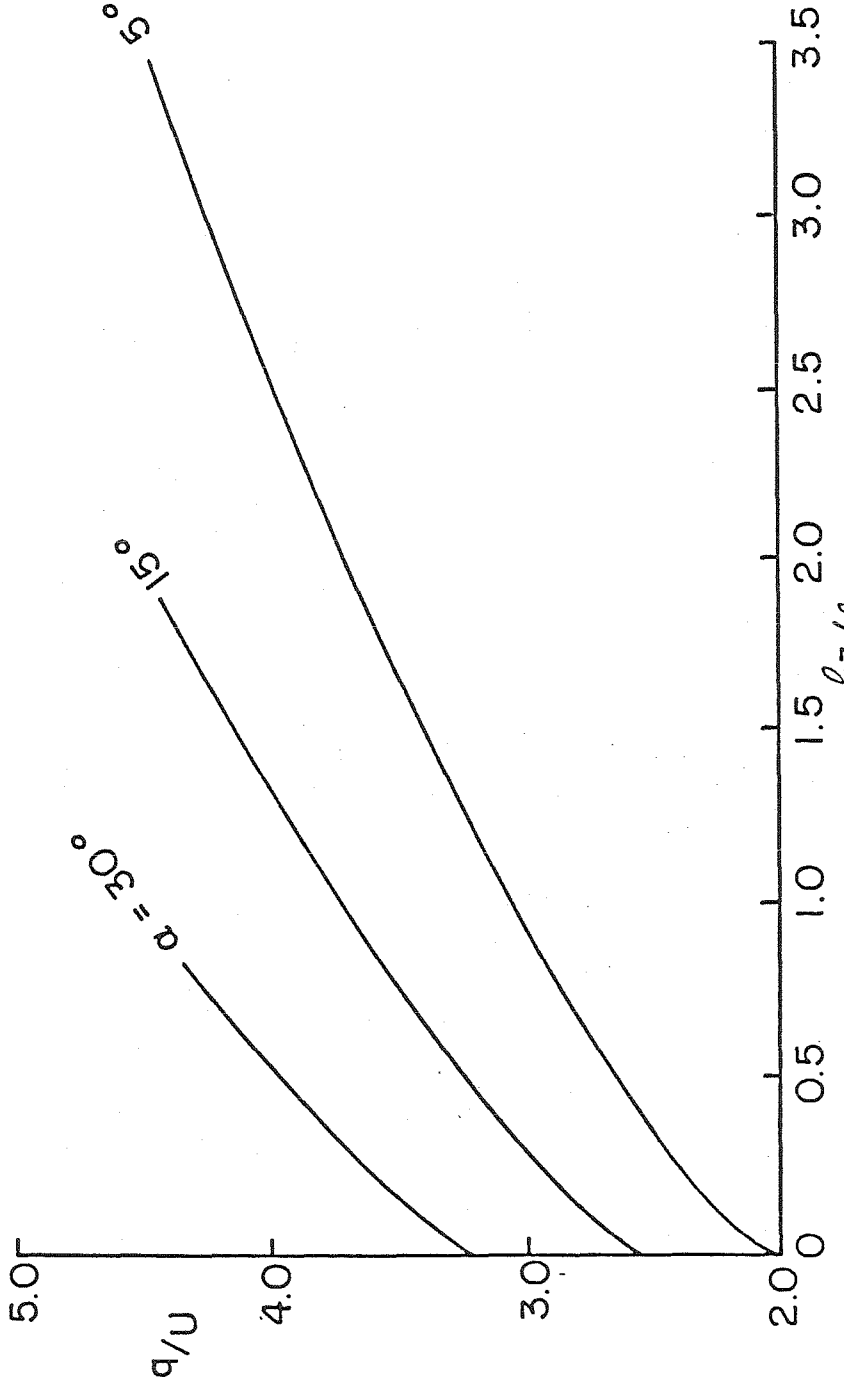

Fig.2.15: q / U for Kasper type wings as a function of l_3/l_1 for different values of α. β, τ and l_4/l_1 were all fixed and had values 30°, 75° and 0.14 respectively.

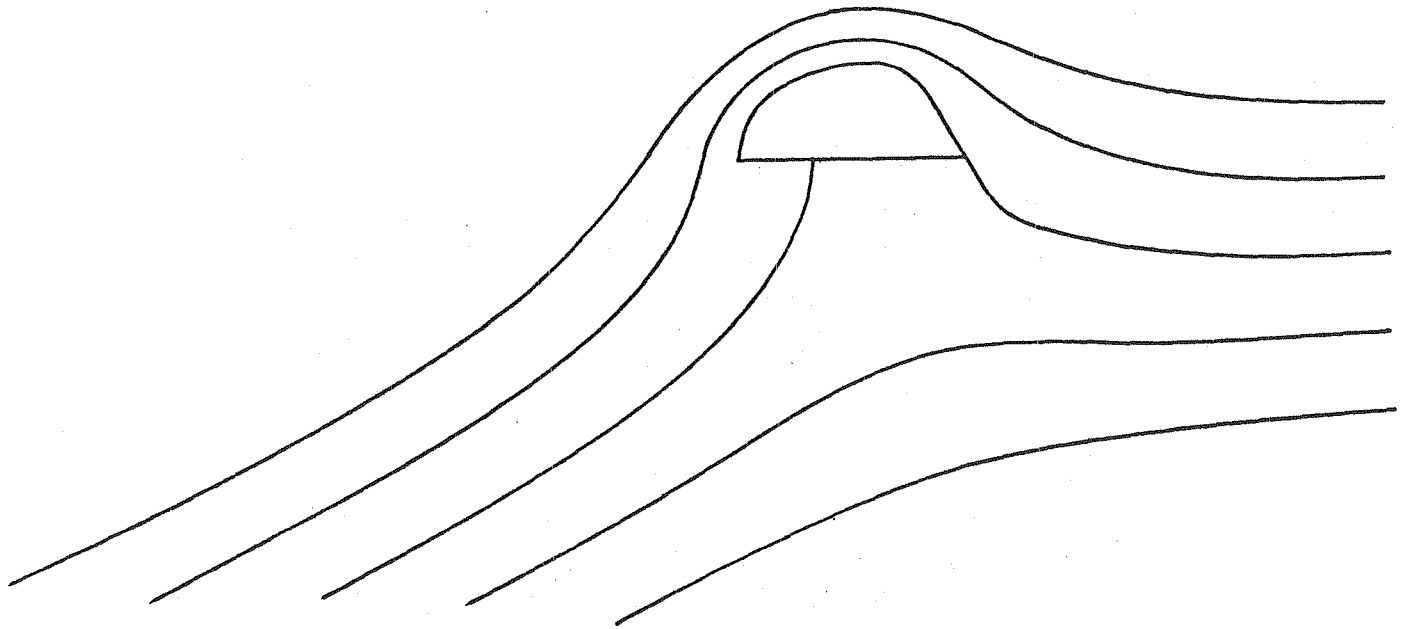

Fig.2.16: Streamlines for Kasper wings for $\beta = 60°$, $\alpha = 15°$, $\tau = 75°$, $l_4 / l_1 = 0.14$ and $l_3 / l_1 = 0.2253$ respectively.

Chapter III

Prandtl-Batchelor Flow past a flat plate with a forward facing flap

3.1. Introduction

In the last two chapters, we presented two dimensional potential flows past airfoils for which the vorticity was confined to a point vortex or a vortex sheet. For flows with a vortex sheet, the region between the vortex sheet and the airfoil was assumed stagnant. In an actual flow, we expect such a region to contain recirculating fluid. Such a recirculation not only changes the interior flow but affects the exterior flow as well since the vortex sheet location is determined from the continuity of pressure and this involves velocities on either side of the vortex sheet. In an attempt to refine the flow model considered in chapter I for the infinite Reynolds number limit of a separated flow that reattaches on a suitably placed flap, we introduce constant nonzero vorticity ω in the region previously assumed stagnant.

The flow model, therefore, consists of an exterior potential flow, as in Chapter I and II, and an inviscid but rotational region with constant vorticity ω between the vortex sheet and the airfoil, where the vortex sheet location is determined from continuity of pressure. Such flows, in general, have been called Prandtl-Batchelor flows since the the Prandtl-Batchelor theorem (Batchelor,1956a) about the uniformity of vorticity in a region with steady closed streamlines in the limit of zero viscosity applies. Batchelor (1956b) suggested a closed wake model of boundary layer separation involving such a flow with two counter rotating eddies in the wake. Since then, there has been a number of attempts at calculating inviscid two dimensional flows past bodies with one or two standing eddies of uniform vorticity separated from the exterior irrotational flow by vortex sheets. However, success to date has been somewhat limited.

Dzugaev (1982) presents an approximate calculation of Prandtl-Batchelor flow past a normal flat plate in a channel based on the assumption that the vor-

tex sheet strength is a constant, but the details are sketchy and it is not clear to us that the solution is consistent. Also, D.I. Pullin (personal communication with Prof.Saffman) reported failure to calculate such a flow past a finite flat plate placed normal to a uniform unbounded stream. Herwig (1982) discusses Prandtl-Batchelor flow over a cavity using asymptotic methods, but arrives at no definite conclusions about the existence of such a flow. The procedure that has been used for numerical calculations is to solve two nonlinear coupled integro-differential equations for the two unknown functions, the vortex sheet strength and the location of the streamline separating the rotational from the exterior irrotational flow. There are however difficulties with such an approach. Very little can be derived analytically about the nature of singularities of the separating streamline curve at the separation and reattachment points or the local behavior of the vortex sheet strength in those neighborhoods. Besides, there are problems associated with numerically integrating singular integrands efficiently. Failure to obtain solutions does not therefore mean that solutions do not exist and the existence of Prandtl-Batchelor flows in the presence of bodies has remained an important open question in high Reynolds number incompressible flows (see Saffman (1981) for example). It is worth noting that there have been successful calculations of Prandtl-Batchelor flows in the absence of physical bodies. For instance, Sadovskii (1971) considers vortex regions in a potential stream with a vortex sheet on the boundary and finds a one-parameter family of solutions for different jumps of the Bernoulli's constant across the vortex sheet. Deem and Zabusky (1978) and Pierrehumbert (1980) have calculated steady motion past pairs of uniform vortex regions of equal and opposite vorticity with no vortex sheet imbedded in an irrotational flow.

Therefore, our calculations in this chapter not only provide a more realistic model for large Reynolds number flow past an airfoil considered earlier in

chapter I, but also address the question of existence of Prandtl-Batchelor flows. Figure 3.1 illustrates the flow being considered. The separating streamline and hence the vortex sheet goes from A to B dividing the fluid flow region into an outer irrotational one (region I) and an inner inviscid but rotational region (region II) with vorticity ω . Our method of calculation is very different from the integral equation approach and is an extension of the function theoretic approach of complex variables which has been used successfully in problems where the velocity on the separating streamline is a constant. Our numerical evidence suggests strongly that Prandtl-Batchelor flows indeed exist, at least for asymmetrical geometries of the type considered here up to some critical value of the vorticity ω . The existence of symmetrical Prandtl-Batchelor flows with two counter rotating eddies remains an open question and the possibility of generalizing the method used here to such flows is presently under consideration. It is also found that exterior flow is only affected in a small way by the recirculation. This justifies the use of free-streamline solutions for determination of lift on airfoils as considered in chapters I and II.

3.2. Mathematical Formulation.

In region I, the flow is irrotational and therefore, as before, we may introduce the complex velocity potential $W(z) = \Phi + i\Psi$, where Φ is the velocity potential, Ψ is the stream function and $z = x + iy$, with x and y as shown in Fig 3.1. Once again as $z \to \infty$

$$W(z) \to U\, z\, e^{-i\alpha} + i\Gamma \log z / (2\pi) \qquad (3.1)$$

U, α, Γ being respectively the magnitude of free stream velocity, the angle of attack with respect to plate OA and the clockwise circulation induced at infinity by the requirement of finite velocity (Kutta condition) at O. There is a stagnation point of the exterior irrotational flow at P on the plate OA and it can be shown as in chapter I, that there are no other stagnation points besides P and O. ABOA

is a streamline on which $Im\ W = 0$ without any loss of generality. In region II the streamfunction satisfies

$$\nabla^2\Psi = \omega \tag{3.2a}$$

and on the boundary AOBA

$$\Psi = 0 \tag{3.2b}$$

The location of the vortex sheet AB is determined by the pressure condition

$$\left|\frac{dW}{dz}\right|^2 - (\nabla\Psi)^2 = q^2 \tag{3.3}$$

where $\frac{dW}{dz}$ and $\nabla\Psi$ are evaluated on the vortex sheet from the outside and the inside respectively. q^2 is a constant which is twice the jump in the Bernoulli's constant across the boundary between region I and II.

As before, consider the conformal map $t(z)$ of the exterior region I into the interior of the unit semicircle. A, B, O and P in the z-plane correspond to 1, -1, 0 and t_p in the t plane, where t_p is an unknown to be determined. We regard $\frac{dW}{dz}$ as a function of t and introduce the analytic function $\Omega(t)$ defined by

$$\frac{dW}{dz} = qt^{\beta/\pi}\frac{(t_p - t)}{(1 - tt_p)}\, e^{\Omega} \tag{3.4}$$

where $0 \leq arg\,(t) \leq \pi$, $-\pi \leq arg\,(t_p - t) \leq 0$ and $-\pi < arg\,(1 - t_p\ t) \leq 0$ for t in or on the unit semicircle. The arguments of 1.3.2 in chapter I may be duplicated to show that

$$\Omega(t) = a_0 + a_1\, t + a_2\, t^2 + \cdots \tag{3.5}$$

with $a_0, a_1, \ldots$ all real and Ω analytic in the interior of the unit circle and continuous upto the boundary. Unlike the vortex sheet case of chapter I, however, $\Omega(t)$ is no longer a constant. Now, if we consider W as a function of t, the relevant arguments of 1.3.2 can be repeated once again to give

$$\frac{dW}{dt} = \frac{(1-t^2)}{2}\left[\frac{4Mt_\infty^2}{(t-t_\infty)^2(1-tt_\infty)^2} + \frac{4\bar{M}\,\bar{t}_\infty^2}{(t-\bar{t}_\infty)^2(1-t\bar{t}_\infty)^2} - \frac{i\Gamma(t_\infty-\bar{t}_\infty)(1-t_\infty\bar{t}_\infty)}{\pi(t-t_\infty)(t-\bar{t}_\infty)(1-tt_\infty)(1-t\bar{t}_\infty)}\right] \tag{3.6}$$

where $t = t_\infty$ is as before the image of $z = \infty$. From (3.4) and (3.6) we obtain

$$\frac{dz}{dt} = e^{-\Omega}(1-t^2)t^{-\beta/\pi}\frac{(1-tt_p)}{2q(t_p-t)}\left[\frac{4Mt_\infty^2}{(t-t_\infty)^2(1-tt_\infty)^2}+\frac{4\bar{M}\,\bar{t}_\infty^2}{(t-\bar{t}_\infty)^2(1-t\bar{t}_\infty)^2}\right.$$
$$\left.-\frac{i\Gamma(t_\infty-\bar{t}_\infty)(1-t_\infty\bar{t}_\infty)}{\pi(t-t_\infty)(t-\bar{t}_\infty)(1-tt_\infty)(1-t\bar{t}_\infty)}\right] \tag{3.7}$$

From the knowledge of the velocity at infinity , we have the condition

$$U\,e^{-i\alpha} = qt_\infty^{\beta/\pi}\frac{(t_p-t_\infty)}{(1-t_pt_\infty)}\,e^{\,\Omega(t_\infty)} \tag{3.8}$$

Also, from the requirement that $\frac{dz}{dt}$ has no residue at $t=t_\infty$,which is necessary for the $z-t$ mapping to be one to one,we have

$$\frac{i\Gamma}{2\pi} = \frac{2Mt_\infty^2}{1-t_\infty^2}\left[-\frac{\beta}{\pi t_\infty}-\frac{t_p}{(1-t_pt_\infty)}+\frac{1}{(t_p-t_\infty)}-\Omega'(t_\infty)\right] \tag{3.9}$$

The geometric constraints are

$$\int_0^1 \frac{dz}{dt}\,dt = -l_1 \tag{3.10}$$

$$\int_{-1}^0 \frac{dz}{dt}\,dt = l_2\,e^{-i\beta} \tag{3.11}$$

where $\frac{dz}{dt}$ is given by equation (3.7). Further, as in chapter I, the stagnation points at P and O imply that $\frac{dW}{dt} = 0$ at $t = t_p$ and $t = 0$. This means that

$$\frac{4Mt_\infty^2}{(t_p-t_\infty)^2(1-t_pt_\infty)^2}+\frac{4\bar{M}\,\bar{t}_\infty^2}{(t_p-\bar{t}_\infty)^2(1-t_p\bar{t}_\infty)^2} = \frac{i\Gamma(t_\infty-\bar{t}_\infty)(1-t_\infty\bar{t}_\infty)}{\pi(t_p-t_\infty)(t_p-\bar{t}_\infty)(1-t_pt_\infty)(1-t_p\bar{t}_\infty)} \tag{3.12}$$

$$4M+4\bar{M} = \frac{i\Gamma(t_\infty-\bar{t}_\infty)(1-t_\infty\bar{t}_\infty)}{\pi t_\infty\bar{t}_\infty} \tag{3.13}$$

If $\Omega(t)$ were known inside the unit semicircle, then equations (3.8) through (3.13) would constitute eight real relations between the twelve real quantities Γ, q, t_p, Re t_∞, Im t_∞, Re M, Im M, l_2, l_1, β, U and α . If we nondimensionalise all our variables using U and l_1, we are left with ten nondimensional unknowns and eight real equations. There would then be a two parameter family of solutions for the flow in the region I and its boundary and specification of those parameters completely determines the flow for given Ω. It may be noted at this

point that $z(t)$ defined by (3.7) indeed has all the requisite properties for it to map the interior of the unit circle into the exterior z-plane as sketched in figure 4.1. The proof of this statement goes along the same lines as the one sketched in chapter I, section 1.3.2 since the presence of nonzero Ω in (3.7) does not alter any of the arguments presented before. However, $\Omega(t)$ cannot be specified at will but has to be determined so that the interior flow in region II satisfies (3.3) on the vortex sheet. It will be seen later that the magnitude of the constant vorticity ω , provided it is not too large, together with two of the parameters, say α and β, determine $\Omega(t)$ and all the other constants.

The case $\omega = 0$ corresponds to the free streamline case of chapter I since (3.3) reduces to constancy of velocity on the vortex sheet. As we have seen in chapter I, $\Omega = 0$ for this case and the problem is completely determined by specification of the parameters α and β .

For the general case with $\omega \neq 0$, the determination of $\Omega(t)$ is more complicated since the velocity in region II has to be taken into account in the pressure condition (3.3). For a vortex sheet location corresponding to $t = e^{i\theta}$ for $\theta \in [0,\pi]$, (3.3), (3.4) and (3.5) imply

$$a_0 + a_1 \cos\theta + a_2 \cos 2\theta + \cdots = \frac{1}{2} \ln\left(1 + (\nabla\Psi)^2/q^2\right) \qquad (3.14)$$

The problem now reduces to determining the right hand side of (3.14) and its Fourier cosine expansion with respect to θ in terms of $a_0, a_1, \cdots$ and the parameters. In the next section, we describe how the inner velocity and hence the right hand side of (3.14) is determined for given $a_0, a_1, \ldots$ and $\Gamma, q, t_p, t_\infty, M$ and l_2.

3.3. Determination of the velocity in region II on the vortex sheet

For given $a_0, a_1, \cdots$ and $\Gamma, q, t_p, t_\infty, M, l_2$, we integrate (3.7) , using $z(1) = -l_1$, to determine $z(e^{i\theta})$, the location of the vortex sheet, and therefore

the boundary of region II. We are then left with the problem of computing the velocity $|\nabla\Psi|$ on the free streamline , where Ψ satisfies equations (3.2a) and (3.2b). Since determination of the velocity on the vortex sheet boundary of region II by the usual finite difference or finite element schemes in the physical plane is likely to be inaccurate in view of the infinite curvature expected at A and B , we employ conformal mapping of region II into a more suitable region. It is convenient to separate Ψ into a particular solution Ψ_p and a harmonic function Ψ_h . Since ω is a constant, this can be easily done. Ψ_h remains a harmonic function in the conformally transformed plane. Then the problem is reduced to determining the normal derivative of a harmonic function from given boundary data in a 'nice' domain. For the purpose of mapping, we introduce the complex variable $z_i = -x + iy$ (see footnote) defined in region II of the physical plane. It is convenient to take the particular solution Ψ_p defined by

$$\omega^{-1}\Psi_p = \frac{1}{2}(Imz_i)^2 - \frac{1}{2}(Imz_i)(Rez_i)\tan\beta \qquad (3.15)$$

since this vanishes on the solid boundaries. The harmonic function Ψ_h in the decomposition $\Psi = \Psi_h + \Psi_p$ satisfies $\Psi_h = -\Psi_p$ on the boundary.

Consider the conformal map $Q(z_i)$ that maps the z_i plane interior of the boundaries AOBA into the unit semi-circle (Fig.3.2), such that B is mapped to -1, A is mapped to +1 and O to Q_0 on the real axis. The value of Q_0 is fixed automatically in the numerical conformal mapping procedure to be described later. The vortex sheet AB is mapped to the semi-circular boundary. The details of the mapping $z_i(Q)$ will be dicussed in the next section. We now consider Ψ_h as a harmonic function in the Q plane which satisfies boundary conditions as follows:

$$\Psi_h(e^{i\varphi}) = -\Psi_p(z_i(e^{i\varphi})) \qquad (3.16)$$

where $\varphi \in [0,\pi]$ and $Q = \rho\, e^{i\varphi}$ in the Q plane . From (3.15) , Ψ_p is zero on the

This unconventional choice of complex variable allows region II to be mapped to the interior of the semicircle of fig.3.2

real diameter and so for $Q \varepsilon [-1,1]$ we have

$$\Psi_h(Q) = 0 \tag{3.17}$$

Using the Schwarz reflection principle , we extend the domain of existence of Ψ_h to the entire unit Q-circle with boundary condition (3.16) applied to $\varphi\varepsilon[0,\pi]$, while

$$\Psi_h(e^{i\varphi}) = -\Psi_h(e^{-i\varphi}) \tag{3.18}$$

extends the boundary data to the lower half segment of the circumference where $\varphi \varepsilon [-\pi,0]$. On the vortex sheet , the velocity $|\nabla\Psi|$ equals the normal derivative of Ψ in the z_i plane. Now, the outward normal direction on the vortex sheet in the z_i plane corresponds to the radially outward direction on the circumference of the unit semicircle in the Q plane . Therefore, on $Q=e^{i\varphi}$, the magnitude of the velocity is given by

$$\begin{aligned}
|\nabla\Psi| &= \left|\frac{dQ}{dz_i}\right|\left(\frac{\partial\Psi_p}{\partial\rho} + \frac{\partial\Psi_h}{\partial\rho}\right) \\
&= \mathrm{Im}z_i \frac{\mathrm{Im}\left(Q\frac{dz_i}{dQ}\right)}{\left|\frac{dz_i}{dQ}\right|} - \frac{1}{2}\tan\beta \frac{\mathrm{Re}\left(Q\frac{dz_i}{dQ}\right)}{\left|\frac{dz_i}{dQ}\right|}\mathrm{Im}z_i \\
&+ \left|\frac{dz_i}{dQ}\right|^{-1}\frac{\partial\Psi_h}{\partial\rho} - \frac{1}{2}\tan\beta\,\mathrm{Re}z_i \frac{\mathrm{Im}\left(Q\frac{dz_i}{dQ}\right)}{\left|\frac{dz_i}{dQ}\right|}
\end{aligned} \tag{3.19}$$

Now, (3.16) and (3.18) determine the harmonic function Ψ_h on the boundary of the unit circle from which the Fourier coefficients of the following expansion are determined

$$\Psi_h(e^{i\varphi}) = \sum_{-\infty}^{+\infty}\psi_k\, e^{\,ik\varphi} \tag{3.20}$$

It is easily seen that the normal derivative

$$\frac{\partial\Psi_h}{\partial\rho}(e^{i\varphi}) = \sum_{-\infty}^{+\infty}|k|\,\psi_k\, e^{\,ik\varphi} \tag{3.21}$$

Using $z_i(Q)$ and $\left|\frac{dz_i}{dQ}\right|$ as determined in the following section, (3.21) provides a

complete determination of $|\nabla\Psi|$ in (3.19) in terms of φ . The apparent singularities at φ=0 and π are actually removable since Ψ and therefore $\frac{\partial\Psi}{\partial\rho}$ are odd 2π-periodic functions of φ and hence vanish at 0 and π . It is to be noted that in (3.14) we need $|(\nabla\Psi)|^2$ as a function of θ and not φ, as given by (3.19). However, for each θ , (3.7) locates $(x(\theta),y(\theta))$ on the physical vortex sheet and therefore the corresponding position in the z_i plane. The conformal map $Q(z_i)$ provides the relation $\varphi(z_i(\theta))$ needed to determine the velocity as a function of θ. The details of this correspondence and its usage are discussed in section 3.6.

3.4. Mapping into a semicirle in the Q-plane

As mentioned before, we wish to find $Q(z_i)$ that maps the z_i plane into a semicircle with A mapped to +1, B to -1 and O to some suitable point Q_0 on the real diameter of the Q plane. Initially , we carry out a series of explicit transformations starting with the z_i plane and finally ending up with a geometry which is close to a semicircle. With choice of appropriate branches , the transformations are

$$W_1(z_i) = (z_i^{\pi/\beta} - s_1)/E \tag{3.22}$$

$$W_2(W_1) = -1 - \frac{2i}{\pi}\log(-W_1 + i(1 - W_1^2)^{\frac{1}{2}}) \tag{3.23}$$

$$W_3(W_2) = \frac{(r\,\sin\frac{\delta}{2} + W_2)^{\pi/\delta} - (r\,\sin\frac{\delta}{2} - W_2)^{\pi/\delta}}{(r\,\sin\frac{\delta}{2} + W_2)^{\pi/\delta} + (r\,\sin\frac{\delta}{2} - W_2)^{\pi/\delta}} \tag{3.24}$$

where $s_1 = \frac{1}{2}(1 - l_2^{\pi/\beta})$, $E = \frac{1}{2}(1 + l_2^{\pi/\beta})$. r is chosen to be the radius of the circular arc shown in dotted line in Fig 3.3b , which together with the real axis encloses our region of interest in the W_2 plane. The angle between the circular arc and the real axis is $\delta/2$. Figures 3.3 a, b & c shows the approximate shapes of the region of interest after each of the transforms (3.22) through (3.24). The transformation (3.24) converts the circular arc and the real axis of Fig.3.3b into a unit semi circular boundary . If $r\,\sin(\delta/2)$ is chosen close to 1, the transfor-

mation (3.24) gets rid of the large curvature of the boundary of the region of interest in the W_2 plane near the real axis. The choice of r and δ is made so as to make the shape of the boundary in the W_3 plane as nearly semicircular as possible.

Consider now function $W_3(Q)$ that maps a semicircle into this nearly semicircular region with the origin 0 of the Q plane mapped to 0 in the W_3 plane , -1 to -1 and +1 to +1 . We realize that $W_3(Q)$ also maps the unit circle about the origin in the Q plane into the nearly circular geometry of the W_3 plane formed by extending the original nearly semicircular region through reflection on the real axis . Henceforth , the nearly circular region of the W_3 plane will be called the extended W_3 region. If $W_3=R_w\, e^{i\nu}$ and $Q=e^{i\varphi}$, $-\pi \leq \nu$, $\varphi \leq \pi$, characterize corresponding points on the boundary of the extended W_3 region and the unit circle respectively, then the integral equation satisfied by $\nu(\varphi)$ is

$$\nu(\varphi) - \varphi = \frac{1}{2\pi} \int_{-\pi}^{\pi} \cot\left(\frac{\varphi - \varphi'}{2}\right) \log(R_w\ (\nu(\varphi'))) \, d\varphi' \,, \tag{3.25}$$

where the integral is in the principal value sense. This equation , commonly known as Theodersen's integral equation , is very easily solved numerically in Fourier space by an iterative technique as discussed by Henrici (1979). It requires two Fourier transforms and one R_w evaluation per iteration. Once the iterations converge, we obtain the complex Fourier series for $\log(R_w\ (\nu(\varphi)))$ which allows us to find the coefficients of the Fourier cosine series in φ as well, since it is an even periodic function. Thus , we can write

$$\log(R_w\ (\nu(\varphi))) = \sum_{0}^{\infty} b_n \cos n\varphi \,, \tag{3.26}$$

from which it follows that

$$\log\left(\frac{W_3}{Q}\right) = \sum_{0}^{\infty} b_n Q^n \tag{3.27}$$

since the left hand side of (3.26) is the real part of the analytic function $\log\left(\frac{W_3}{Q}\right)$ evaluated at the boundary of the unit circle. Thus we have arrived at a

power series expression to describe the mapping function $W_3(Q)$ that maps the circle in the Q plane to the extended W_3 region and therefore the semi-circle into the original near semi-circular region of the W_3 plane. Inverting the relations in the equations (3.22) through (3.24), and using (3.27) we arrive at $z_i(Q)$ from which $Q(z_i)$ is known in principle . The velocity is therefore determined from the inside of the vortex sheet for a given vortex sheet location. Equating the coefficients of $\cos n\theta$ in (3.14) the coefficients a_0, a_1,... are determined.

Here, we justify the mapping of region II into a semicircle to determine the velocity on the vortex sheet. We remarked in the introduction about problems in the calculation of Prandtl-Batchelor flows due to singularities of the separating streamline curve at the separation and reattachment points. In general, the separating streamline curvature at the separation and reattachment points is infinite. Infinite curvature causes infinite velocity gradients at those points leading to numerical inaccuracies if a direct scheme (such as finite differences) is used to calculate the flow in region II on the vortex sheet boundary. The commonly used technique of conformal mapping into a circle does not get rid of the problem either, because the boundary data assumed by the harmonic decomposition Ψ_h, as introduced in section 3.3, is not a smooth function of the angle on the circle. Mapping into a semicircle with the separation and reattachment points at the two ends of the real diameter, as we have done, gets rid of the problem of accurately calculating the velocity close to the separation and reattachment points. Infinite velocity gradients in the physical plane present no obstacles since the numerically calculated velocities seem to be smooth functions of both φ and θ in $[0,\pi]$. This smoothness can be expected from further arguments in the following section. Thus, the numerical calculation of velocity in region II is easily facilitated even in the neighborhood of A and B by using the conformal mapping into the Q-plane as described.

Further, from plausibility arguments in the following section supported later by numerical evidence, Ω is analytic for t in or on the unit circle and thus we find that our function theoretic approach for determination of the exterior flow is quite suitable even when the free streamline boundary in the physical plane has infinite curvature.

3.5. Smoothness of function $\Omega(t)$ and $\varphi(\theta)$

Here we present plausibility arguments to show that the solution $\Omega(t)$ to the flow problem posed is an analytic function of t for $|t| \leq 1$ a consequence of which is that φ is a smooth infinitely differentiable function of θ. We proceed by presenting a conjecture which we were unable to prove rigorously; nonetheless, we believe it to be true and present reasons for doing so. It will be followed by a few lemmas and a theorem which are proved. Based on the assumption that the conjecture is true, we use the lemmas and the theorem to arrive at our conclusion.

Conjecture 1 :

Let $(x, y(x))$ be a point on the vortex sheet. Define analytic function $f(Q)$ by the relation

$$\frac{dz_i}{dQ} = (1 - Q^2)(Q - Q_o)^{\beta/\pi - 1} f(Q). \tag{3.28}$$

(i) If $y(x)$ is an analytic function of $(-x - l_1)^{\frac{1}{2}}$ in the neighborhood of A and has the form

$$y = (-x - l_1)^{3/2} [\, c_0 + c_1 (-x - l_1)^{\frac{1}{2}} + c_2 (-x - l_1) + \cdots], \tag{3.29}$$

then f is analytic at $Q = 1$.

(ii) If an expansion similar to (3.29) holds near B with $(-x - l_1)$ and y replaced by the distances from B along OB and direction perpendicular to OB respectively, then f is analytic at $Q = -1$.

Arguments supporting conjecture :

We will only present arguments in support of (i) since arguments to support (ii) follow exactly along similar lines. If we assume f to be analytic at $Q = 1$ and expand the right hand side of equation (3.28) in powers of $(Q - 1)$, integrate the expansion and take the real and imaginary parts of the resulting expression for $Q = e^{i\varphi}$, then elimination of φ results in (3.29). For arbitrary c_0, c_1, ..., it seems to be possible to find the corresponding f_0, f_1, etc. in the assumed analytic expansion

$$f(Q) = f_0 + f_1(Q - 1) + \cdots \tag{3.30}$$

around $Q = 1$ with f_0 nonzero. However, we were unable to show that (3.30) is the only allowable form of $f(Q)$ in the neighborhood of $Q = 1$ in order that (3.29) is valid around A. We could not think of any kind of nonanalyticity of f at $Q = 1$ for which (3.29) could be valid.

Lemma 1 :

$\Omega(t)$ is assumed analytic in $|t| \leq 1$. Then for $(x, y(x))$ on the vortex sheet location found by integrating (3.7)

(i) Equation (3.29) is valid on the vortex sheet in the neighborhood of $z = -l_1$ where $z = x + iy(x)$.

(ii) Expansion similar to (3.29) is valid at point B ,i.e $z = -l_2 e^{-i\beta}$, where $(-x - l_1)$ and y in equation (3.29) are replaced by the distances from B along OB and the direction perpendicular to OB.

Proof of lemma 1 :

We will only carry out the proof for case (i) since the proof of (ii) follows along similar lines. Locally expanding (3.7) in the neighborhood of $t = 1$, integrating and considering the real and imaginary parts of the resulting expansion for $t = e^{i\theta}$, we arrive at (3.29) upon eliminating θ.

Lemma 2 :

If $\Omega(t)$ is assumed to be analytic for $|t| \leq 1$ and $f(Q)$ defined by (3.28) assumed analytic in $|Q| \leq 1$, then φ is an analytic function of θ, where $t = e^{i\theta}$ and $Q = e^{i\varphi}$.

Proof :

From local expansion of $z_i(Q)$ using (3.28) and inversion, we obtain $(Q - 1)$ to be an analytic function of $(z_i - l_1)^{\frac{1}{2}}$. From expansion and integration of (3.7) in the neighborhood of $t = 1$, we obtain $(z + l_1)^{\frac{1}{2}}$ to be an analytic function of t in the neighborhood of $t = 1$. Substituting $Q = e^{i\varphi}$ and $t = e^{i\theta}$, we obtain φ as an infinitely differentiable function of θ. Carrying out a similar expansion and integration at B, we arrive at the conclusion that φ is analytic function of θ around $\theta = \pi$ as well. Analyticity at other θ values in $[0,\pi]$ follow readily from regularity of mapping functions $z_i(Q)$ and $z(t)$ on the free streamline away from the separation and reattachment points A and B.

Lemma 3 :

If the assumptions of lemma 2 hold, then $|\nabla\Psi|$ calculated in (3.19) is a smooth infinitely differentiable function of φ and hence of θ in $[0, \pi]$.

Proof:

From known regularity principles of solution to poisson's equation, it is clear that the only places where $|\nabla\Psi|$ could fail to be infinitely differentiable are $\theta = 0$ and $\theta = \pi$. We only carry out the proof for differentiability at $\theta = 0$ since the proof for differentiability at $\theta = \pi$ is very similar.

Since $\frac{dz_i}{dQ}$ is an analytic function of Q in the neighborhood of $Q = 1$ (because f is so), inspection of (3.19) reveals that all the terms with the possible exception of $\frac{\partial\Psi_h}{\partial\rho}$ are smooth functions of φ. Now Ψ_h satisfies boundary data in (3.16) which are smooth in the variable φ in the interval $[0, \pi]$. From Schwarz reflection principle, it follows that the same is true for the boundary data of Ψ_h in the φ interval $[-\pi, 0]$. Thus the fourier coefficients in (3.20) and (3.21) decay exponentially with k for large k and therefore $\frac{\partial\Psi_h}{\partial\rho}$ in (3.21) must be an analytic function of φ. Since Ψ_h and therefore $\frac{\partial\Psi_h}{\partial\rho}$ are 2 π-periodic odd functions of φ, it follows that they vanish at 0 and π and therefore the term $\left|\frac{dz_i}{dQ}\right|^{-1} \frac{\partial\Psi_h}{\partial\rho}$ continues to be an analytic function of φ in the interval $[0, \pi]$. It follows therefore that $|\nabla\Psi|$ is a smooth function of φ around $\varphi = 0$. From previous lemma, it follows that it is also an analytic function of θ at 0.

Theorem 1:

We assume conjecture 1 to be true. An iterative scheme described below is used to determine Ω :

For given analytic n-th iterate $\Omega^{(n)}$, we find constants Γ, l_2, etc. using equations (3.8) through (3.13). Equation (3.7) then determines the boundary of region II and (3.19) used to calculate the velocity $\nabla\Psi$, where $z_i\ (Q)$ is determined

as in section 3.4. Equation (3.14) then determines the coefficients a_0, a_1, etc. for the next iterate $\Omega^{(n+1)}$.

Then if $\Omega^{(n)}$ is analytic is the compact set $|t| \leq 1$, then so is the next iterate $\Omega^{(n+1)}$.

Proof of theorem:

If $\Omega^{(n)}$ is analytic up to the unit circle, lemma 1 holds and therefore we obtain the expansion (3.29) for $(x, y(x))$ on the vortex sheet location in the neighborhood of A. Similar expansion holds at B as mentioned earlier. From conjecture 1, it follows that f is analytic in the neighborhood of $Q = 1$ and $Q = -1$. From regularity of the Riemann mapping function $z_i(Q)$ at points on the upper half semicircle other that A and B, it follows that f is analytic in the entire upper half unit circle including its boundaries. Since f is real on the real axis, it follows that f is analytic in the entire unit circle including its boundary. Lemma 3 then implies that $|\nabla\Psi|$ is an analytic function of θ in $[0, \pi]$ and therefore from (3.14), we obtain the coefficients of the next iterate $\Omega^{(n+1)}$ to be analytic in the compact set as desired. Thus the theorem is proved.

Now a sequence of analytic function converging in the max. norm sense in a compact set $|t| \leq 1$ converges to an analytic function in the same set. Thus if there is convergence of the sequence $\Omega^{(n)}$ as $n \to \infty$, the resulting solution $\Omega(t)$ will be analytic. We were unable to prove the convergence of the sequence $\Omega^{(n)}$ rigorously. Numerical calculations as presented in the following sections however suggest that indeed there is such a convergence and so from theorem 1, the solution Ω is analytic up to the unit circle. As a corollary, we have φ to be an infinitely differentiable function of θ in the closed interval $[0, \pi]$ if conjecture 1

is assumed to be true since lemma 2 holds.

3.6. Numerical Procedure

We use an iterative scheme to find solutions to our equations, as sketched in the last section. We start with an initial guess of N coefficients $a_0, a_{1,\ldots}, a_{N-1}$ and obtain an approximate $\Omega(t)$ by truncating (3.5). For ω small, the guess for Ω and hence these N coefficients is zero. For bigger values of ω, we use values of the coefficients obtained from the converged solution for slightly smaller ω. In the following, we describe the procedure used to find the $(n+1)$st iterate given the nth iterates $a_0^n, a_1^n \cdots a_{N-1}^n$ and therefore $\Omega^n(t)$.

We use (3.8) through (3.13) to determine Γ, l_2, q, M, t_∞, t_p consistent with $\Omega=\Omega^n$, where U, l_1, α, β are considered known and fixed. Newton iteration is used for that purpose . Equation (3.7) then determines $z(\theta) = x(\theta) + iy(\theta)$ and hence $z_i(\theta) = -x(\theta) + iy(\theta)$ on the vortex sheet for N_1 points where $\theta_k = (k-1)\pi/(N_1 - 1)$, $k=1, 2,\ldots N_1$. and N_1 is chosen of the form $N_1= 1 + 2\,N\,l$, where l is any positive integer. A subset of these θ values of the form $\theta_{k_j} = (((2j - 1)l + 1) - 1)\pi/(N_1 - 1)$ obtained for $k = (2j - 1)l + 1$ for $j=1,2,\cdots N$ are the θ values at which velocities will be calculated and (3.14) used to find the N coefficients a_j . A little simplification shows that $\theta_{k_j} = (j - 1)\pi/N + \pi/(2N)$ and are therefore points at which the N calculated velocities can be fast Fourier transformed to obtain the Fourier cosine series of (3.14). We avoid calculating velocities at $\theta = 0$ and π, where (3.19) has numerically awkward removable singularities. Now, we find the images $R_w(\nu_k)\, e^{i\nu_k}$ in the W_3 plane for these N_1 points in the z_i plane, using equations (3.22) through (3.24). The ν values in the W_3-plane image of the subset of z_i points characterized by the angles θ_{k_j}, are denoted by ν_{k_j}. Reflection on the real axis provides us with a set of $N_1 - 2$ new points on the near-circular boundary of the extended

W_3 region . All together, we then have $2N_1 - 2$ points at which $R_w(\nu_k)$, ν_k are known. For large enough N_1, this provides a very accurate description of the function $R_w(\nu)$ for arbitrary ν through cubic spline interpolation. We then take N_3 points on the unit circle of the extended Q-plane , evenly spaced in the angular variable φ, and carry out the process of solving Theodersen's integral equation (3.25) exactly as described by Henrici (1979). In the process, we obtain the first $\frac{1}{2}N_3$ b_n coefficients in (3.26). The b_n coefficients define $W_3(Q)$ in (3.27). We then start with N_2 uniformly spaced points on the circumference of the unit Q-circle with $Q_m = e^{2\pi i(m-1)/N_2}$ for $m=1, 2,\ldots N_2$. We calculate $W_3(Q_m)$, $z_i(W_3(Q_m))$ using (3.22), (3.23), (3.24) and (3.27) at those points. Using (3.15), (3.16), (3.18) we calculate Ψ_h at those boundary points and use them in (3.20) and (3.21) to find $\frac{\partial \Psi_h}{\partial \rho}$ at N_2 points. At the $(\frac{1}{2}N_2 - 1)$ points which lie entirely in the upper half Q semi-circular boundary , we calculate $\frac{dz_i}{dQ}$ using (3.22), (3.23), (3.24) and (3.27). These, together with values of other terms in (3.19) already calculated provide the velocities at the $(\frac{1}{2}N_2 - 1)$ points on the upper half semicircle If ν_m, $m=1, 2,\ldots, (\frac{1}{2}N_2 - 1)$ denote the angular positions of the images of those Q points in the W_3 plane , we use these to interpolate velocities at the N points ν_{k_j} through cubic splines. Because of the correspondence of ν_{k_j} with N uniformly spaced out points in the θ variable as discussed earlier, we therefore arrive at the velocities from the inner side of the vortex sheet at the physical z locations corresponding to N equispaced points in the θ variable. This is exactly as desired since (3.14) allows calculation of the $(n+1)$st iterate for $a_0, a_1,\ldots a_{N-1}$ by fast Fourier transforms as in Henrici (1979) .

Thus we have a full description of the iteration scheme. It may be noted that the use of spline interpolation in the variable ν is suitable because , as argued in the last section , the velocity is a smooth function of φ and θ.

3.7. Numerical results and discussion

The object of the present work is to demonstrate the existence of Prandtl-Batchelor flows and we only present results here for the case β = 1.5 radians, α = 0.3 radians, although solutions do exist for a range of β and α. Future calculations for other values of parameters would be dictated by practical interest and necessity. It appears that for these values β and α, solutions exist when the vorticity in region II is in the range $0 \leq \frac{\omega l_1}{U} \leq 10$. The iteration procedure described in the last section was used to solve for $\Omega(t)$. When the successive calculated values of the coefficients $a_0, a_1, \ldots, a_{N-1}$ and other constants were within 10^{-8} of each other, convergence was assumed. Initially, in our calculations, we used $N_1 = 385$, $N = 64$, $N_2 = 4096$, $N_3 = 512$. Changing each of N_1, N, N_2, N_3, made little difference in the converged numerical values. For instance when $N_1 = 385$, $N = 48$, $N_2 = 2048$, $N_3 = 512$, the calculated values of the constants $\Gamma/(l_1 U)$, q/U, etc. and the values that Ω assumed on a host of different points on the t-circle were identical to the originally obtained values upto seven significant figures. Thus we conclude that the calculations have a seven digit accuracy.

The values of different quantities obtained from calculation are presented in Table 1 for four different values of vorticity ω . The streamlines are shown in figures 5a and 5b for the cases $\omega l_1/U = 8$ and $\omega l_1/U = 10$. The results suggest that the vortex sheet moves outwards and hence the value of l_2 needed to assure reattachment at B increases with $\omega l_1/U$. It is of interest to note that l_2/l_1 and the location of the free streamline does not depend critically on $\omega l_1/U$. This means that as far as the exterior flow is concerned the free streamline flows calculated in the earlier chapters present reasonably accurate values of lift and other such characteristics of the exterior flow in the limit of infinite Reynolds number if the flow remains attached on top of the flap.

The extensive use of fast Fourier transforms and spline interpolation avoided the use of any integrations in the calculation of the velocity in region II, and therefore we believe that the method is comparatively very efficient compared to the integro-differential equation techniques used by others who tried calculation of these type of flows. For each value of $\omega l_1 / U$, the entire calculation took between 10 to 20 minutes of CPU time on a VAX 11/750. We obtained numerical convergence in our iteration scheme upto $\omega l_1 / U = 10$. For larger values the rate of convergence slowed down considerably suggesting that there was a critical value of $\omega l_1 / U$ above 10 for which there will be no convergence in the iteration scheme. For $\omega l_1 / U = 8$, the method needed 8 iterations to produce a seven figure accurate result. A different set of values for N_1, N, N_2, N_3 made small differences in the convergence rates provided those integer values were large enough.

3.8. Conclusion

We have presented calculations of a so called Prandtl- Batchelor flow for flow past a flatplate with a flap attached at its rear edge . This is to our knowledge the first such fully consistent calculation of a Prandtl-Batchelor flow past a physical body. For given angle of attack and angle between the plate and the flap , there exists a one-parameter family of such flows, depending on the assumed vorticity in the recirculating region of the flow. If the flow is the zero viscosity limit of a Navier-Stokes solution, it is expected that only one such value of the vorticity will be consistent with the fitting of boundary layers. This question appears to be rather difficult and is not addressed here. Alternatively, the ratio l_2 / l_1 over a certain range, could be supposed to be given in addition to the angles α and β, and the value of ω could be regarded as determined by the requirement that the streamline that separates at A reattaches at B.

Our method provides an accurate and reasonably efficient method of calculation of two dimensional Prandtl-Batchelor flows that incorporate possible singularities at the separation and reattachment points. The function theoretic approach taken allows us to reduce the entire exterior flow problem with unknown boundary into one function of one complex variable on a fixed domain. Further, this function was shown to be a smooth function up to the boundary of a circle and this facilitates its numerical calculation without much trouble. The procedure is general and could possibly be applied to other two dimensional geometries of interest an example of which is presented in the next chapter.

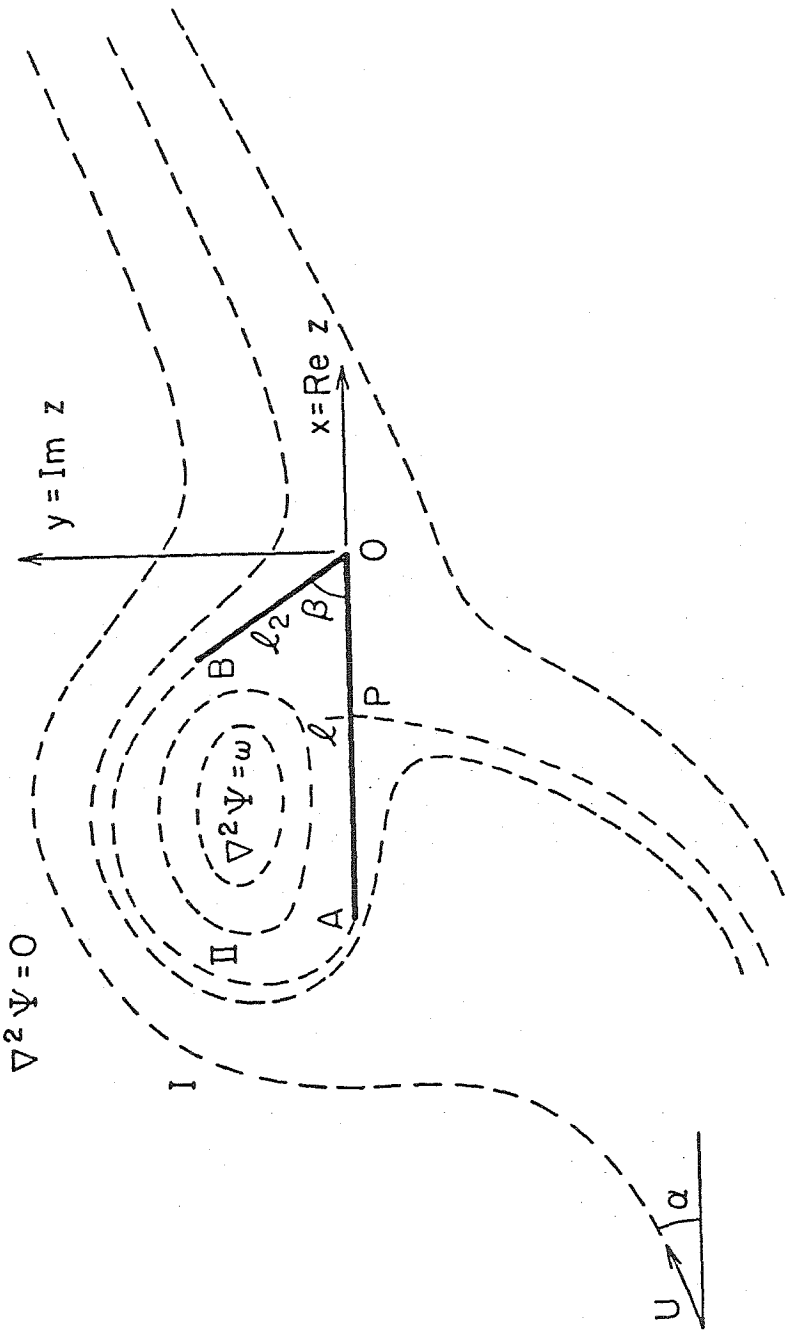

Fig.3.1 : Sketch of flow under consideration. AOB denotes the plate-flap combination, while streamline joining A to B is the vortex sheet location.

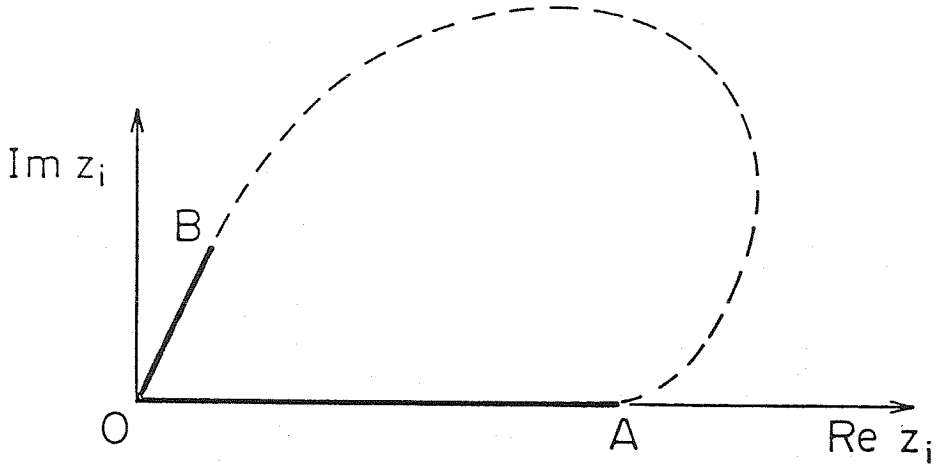

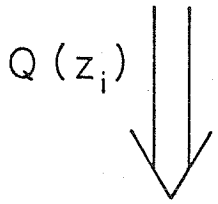

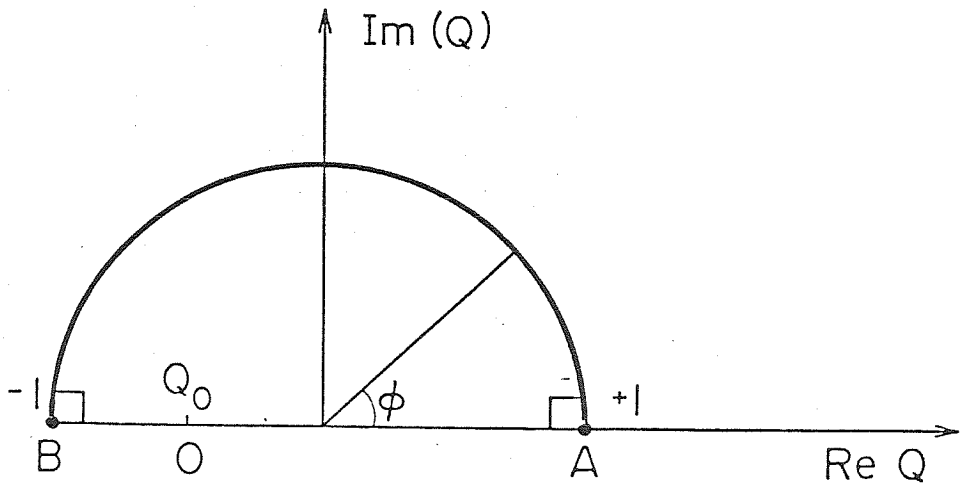

Fig.3.2 :

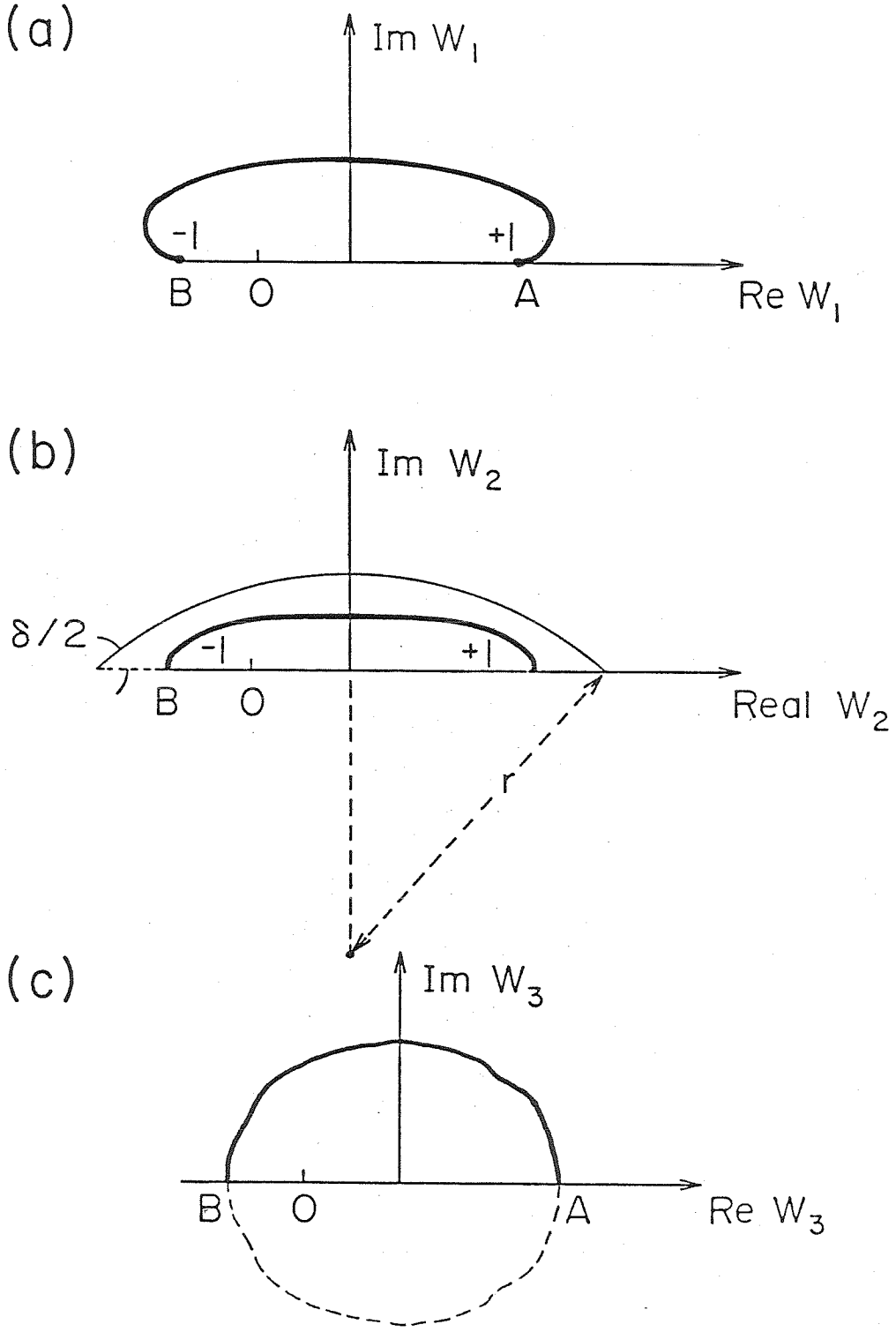

Fig.3.3 : W_1, W_2 and W_3 planes shown in (a),(b) and (c) respectively. r denotes the radius of the circular arc that, together with real axis, encloses the geometry of interest in (b). $\delta/2$ is the angle between the circular arc and the real axis.

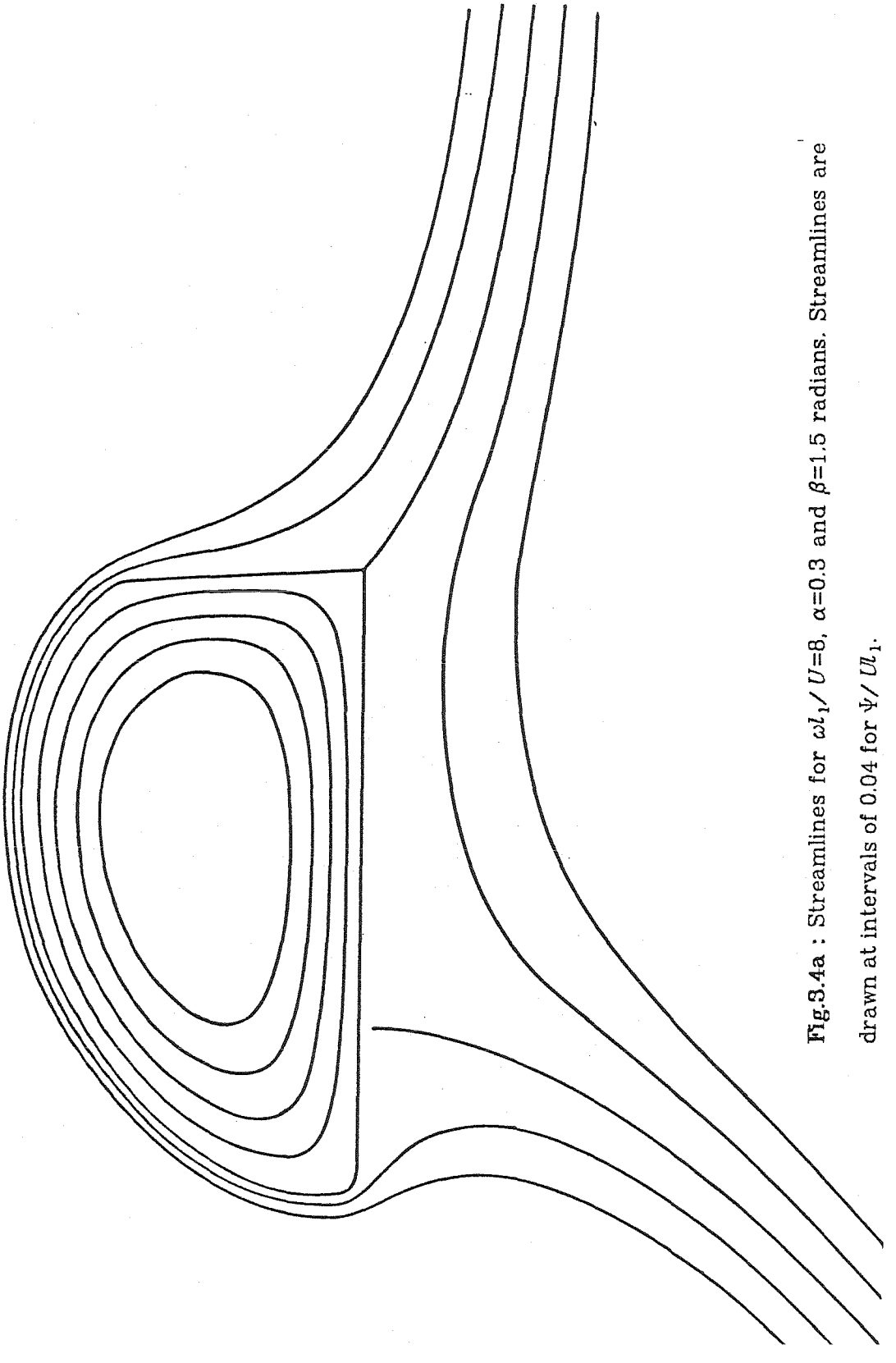

Fig.3.4a : Streamlines for $\omega l_1 / U = 8$, $\alpha = 0.3$ and $\beta = 1.5$ radians. Streamlines are drawn at intervals of 0.04 for $\Psi / U l_1$.

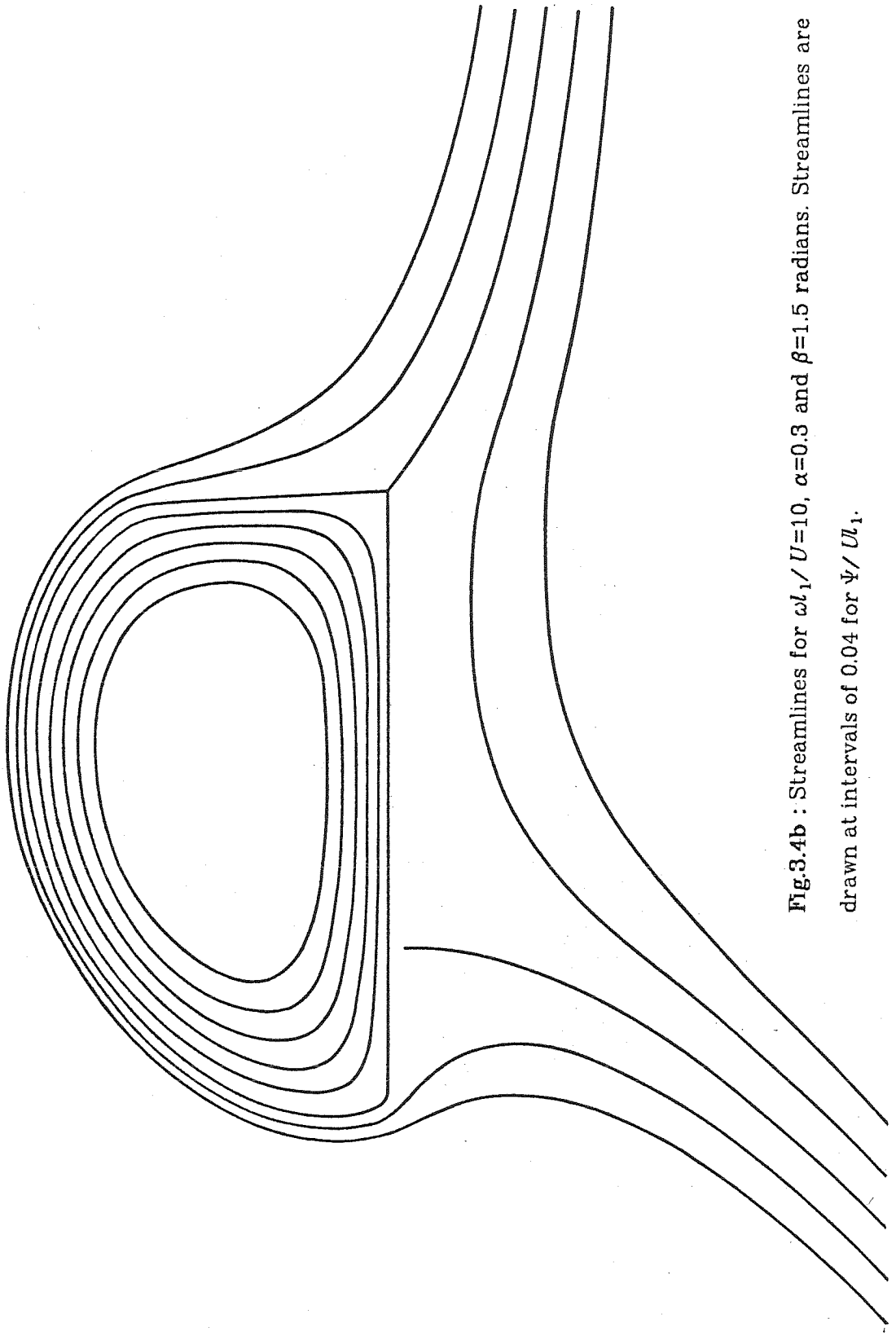

Fig.3.4b : Streamlines for $\omega l_1 / U = 10$, $\alpha = 0.3$ and $\beta = 1.5$ radians. Streamlines are drawn at intervals of 0.04 for $\Psi / U l_1$.

TABLE 3.1

	$\omega l_1/U$ =0	$\omega l_1/U$ =4	$\omega l_1/U$ =8	$\omega l_1/U$ =10
Γ/Ul_1	3.774983	3.832852	4.040451	4.243160
q/U	2.738574	2.669800	2.400910	2.097837
Re t_∞	0.1756735	0.1733073	0.1652458	0.1578012
Im t_∞	0.4323535	0.4343168	0.4416190	0.4491662
Re M/ql_1	-0.1703347	-0.1772941	-0.2068618	-0.2466787
Im M/ql_1	-0.1449536	-0.1491897	-0.1677067	-0.1937230
t_p	0.4187071	0.4180502	0.4172719	0.4190171
l_2	0.3445046	0.3522005	0.3791436	0.4044527
a_0	0.0	0.0183422	0.0966727	0.2006016
a_1	0.0	-0.0039603	-0.0241468	-0.0539812
a_2	0.0	-0.0167881	-0.0776793	-0.1388259
a_3	0.0	-0.0024419	-0.0125488	-0.0260786
a_4	0.0	0.0045678	0.0162926	0.0208911
a_5	0.0	0.0023665	0.0099788	0.0152292
a_6	0.0	-0.0004640	0.0001409	0.0022860
a_7	0.0	-0.0008054	-0.0021805	-0.0017057
a_8	0.0	-0.0002034	-0.0011002	-0.0012923
a_9	0.0	0.0001294	-0.0000245	-0.0002766
a_{10}	0.0	0.0000974	0.0001879	-0.0000072
a_{11}	0.0	0.0000102	0.0001080	0.0000350
a_{12}	0.0	-0.0000222	0.0000034	-0.0000109
a_{13}	0.0	-0.0000107	-0.0000121	0.0000058
a_{14}	0.0	-0.0000009	-0.0000151	-0.0000063
a_{15}	0.0	0.0000027	-0.0000030	0.0000015
a_{16}	0.0	0.0000004	-0.0000043	-0.0000088
a_{17}	0.0	-0.0000001	0.0000002	-0.0000027
a_{18}	0.0	-0.0000008	-0.0000023	-0.0000066
a_{19}	0.0	-0.0000001	0.0000000	-0.0000014
a_{20}	0.0	-0.0000003	-0.0000018	-0.0000041
a_{21}	0.0	0.0000000	-0.0000002	-0.0000008

Table 3.1 : Values of quantities of interest for four different values of vorticity, each for α=0.3 and β=1.5 radians.

Chapter IV

A steadily translating vortex pair with equal but opposite vorticity.

4.1. Introduction

The dynamics of a steady translating pair of equal but opposite vortices have been considered previously by Pocklington (1898) and more recently by Deem & Zabusky (1978) and Pierrehumbert (1980). Pocklington found exact solutions for the case of a pair of hollowed vortex, while Deem & Zabusky and Pierrehumbert consider uniformly distributed vortex cores with continuity of velocity at the boundary. Such a study is of relevance to the vortex pair formed by roll up of vortex sheets shed by a jumbo jet. Besides, their study furthers understanding of vortex interactions, which have in recent years, been considered crucial to better understanding of turbulence.

In this chapter, we consider a pair of vortices with opposite vorticity such that the tangential velocity is discontinuous at the boundary, i.e. the uniform vortex core is surrounded by vortex sheet. Thus the solutions we are seeking form a continuum between the cases considered by Pocklington and Deem & Zabusky and Pierrehumbert. In the special case of a stagnant core, our method of solution is found to give the same results as found by applying Pocklington's method. However, some numerical values quoted in Pocklington's paper do not agree with ours. In Appendix I, the disagreement is shown to be due to errors in Pocklington's calculations. In the last section of this chapter, we present corrections to the results of Pierrehumbert for a pair of touching vortices with equal and opposite vorticity. The letter to the Physics of Fluids (Saffman and Tanveer,1982) presenting the correction is reproduced without any modifications.

While the relevance of the calculations of vortex pair with vortex sheet on their boundary to physically observed phenomena remains doubtful at best because there seems to be no physical mechanism for its creation, the calculations carried out here present yet another instance where the function theoretic

approach of complex variables can be exploited for studying flows where the velocity on the vortex sheet (the separating streamline) is not a constant. Generally, the method used here is similar to the one used in Chapter III for the calculation of Prandtl-Batchelor flows.

4.2. Mathematical formulation

In the frame of reference of a steady translating two-dimensional vortex pair, the velocity at infinity approaches a constant U. All the calculations are carried out in this frame. We are then considering a steady inviscid incompressible flow past a vortex pair. The center of mass of the vortex pair is chosen as the origin of the coordinate system and the y-axis is aligned with the line joining the center of masses of each of the vortex. The uniform stream at infinity is aligned along the positive x-direction. Since the flow is symmetric about the x-axis, it suffices to consider the flow only for y positive. Further, we will only consider vortices with fore and aft symmetry, i.e. the flow is symmetric with respect the y axis as well. The existence of asymmetric vortex solutions is an open question and is not addressed here. Thus, it is enough to consider the flow only in the first quadrant of the z-plane ($z = x + i\,y$)as in fig.4.1. As in the flow in chapter III, we have an exterior irrotational region I and an inner rotational but inviscid region II with constant vorticity ω. For region I, we may introduce the complex velocity potential $W = \Phi + i\,\Psi$, where Φ and Ψ are the velocity potential and the stream function respectively, each of them being harmonic functions of x and y. The uniform flow at infinity implies that as $z \to \infty$,

$$W(z) \to U\,z + O(1) \tag{4.1}$$

Without any loss of generality, we may choose the stream function $\Psi = 0$ on the x-axis and the velocity potential $\Phi = 0$ on the y-axis for $y \geq y_A$, where y_A is the y-value for the point A in fig.4.1. Therefore, on the curved boundary of the exterior flow in the first quadrant which coincides with the right half of the upper

vortex boundary

$$\Psi = \Psi_o \tag{4.2}$$

where Ψ_o is a negative constant. At point B, we denote the corresponding Φ by Φ_o, where Φ_o is positive number. Clearly from considerations of flow symmetry again, we have $\Phi = \Phi_o$ on the imaginary z-axis for $0 \leq y \leq y_B$. For region II, inside the vortex in the upper half plane, the stream function Ψ satisfies

$$\nabla^2 \Psi = \omega \tag{4.3}$$

where ω is a positive constant. Equation (4.2) is once again satisfied on the right half of the upper vortex boundary, while

$$\frac{\partial \Psi}{\partial x} = 0 \tag{4.4}$$

holds on the y-axis for $y_B \leq y \leq y_A$. Clearly Ψ satisfying (4.4) is extendable to the entire vortex with Ψ satisfying (4.2) everywhere on the vortex boundary while (4.3) is satisfied everywhere in the vortex interior. As in chapter III, the pressure condition for the determination of the vortex boundary becomes

$$\left|\frac{dW}{dz}\right|^2 - (\nabla\Psi)^2 = q^2 \tag{4.5}$$

where q^2 is a constant equalling twice the jump of the Bernoulli's constant across the vortex sheet. Before considering procedures to solve this boundary value problem with an unknown boundary, we proceed to show that if there exist Ψ and $W(z)$ that satisfy equations (4.1) through (4.5), then there will be one stagnation point in region I at D (as in fig.4.1), a point on the boundary of the region.

4.3. Number of stagnation points

Consider the contour integral

$$\int_C \left(\frac{1}{2\pi i} \frac{d^2 W}{dz^2} \Big/ \frac{dW}{dz} \right) dz \tag{4.6}$$

where C is a closed contour in fig (4.2). Since the integral is simply the number

of zeroes minus the number of poles of the analytic function $\frac{dW}{dz}$ within the contour C, it is real and therefore we will restrict our attention to the real part of the contribution from each segment that is a constituent of C since the imaginary parts are bound to cancel each other out. C is composed of straight segments L_1, L_2, L_3, L_4, curved segment C_v coinciding with the vortex boundary and a circular arc C_R of radius R. Besides C consists of detours of circular arcs of radius ε wherever $\frac{dW}{dz}$ equals zero. We will consider contribution from each segment in the limit of $\varepsilon \to 0$ and $R \to \infty$.

Clearly the real contribution from each of the straight line segments equals zero since there is no change in the argument of $\frac{dW}{dz}$ between the ends of L_j, where $j = 1,\ldots,4$. As in chapter I, it is easy to see that for each of the small ε semi-circular detours around a simple zero *, the real contribution equals $-\frac{1}{2}$. The real contribution from C_v is $\frac{1}{2}$, since the argument of $\frac{dW}{dz}$ changes from 0 to π as we move along C_v from A to B. The real contribution from C_R is zero since the integrand is seen to decay faster than $1 / R$ as $R \to \infty$. Summing up all the different contributions from each segment composing the contour C and equating it to the number of zeroes minus the number of poles of $\frac{dW}{dz}$, we obtain

$$+ \tfrac{1}{2} - \tfrac{1}{2} n_s = N_s \qquad (4.7)$$

where n_s and N_s are the number of boundary and interior stagnation points. We find that the only nonnegative integral value possibility for n_s and N_s is $n_s = 1$ and $N_s = 0$. Thus, there is one stagnation point on the boundary of region I at D.

4.4. Method of solution

The method of solution is very similar to that in chapter III. As before, we

* For multiple zeroes at a point, we only need to multiply $-\frac{1}{2}$ by the multiplicity of the zero.

map t (z) of region I in the z-plane into the interior of the unit semi-circle such that $z = \infty$ is mapped to 0, A is mapped to +1, and B is mapped to -1. The points corresponding the origin C and the stagnation point D are at $t = c$ and d respectively, where each of them is a negative number. These are unknown a priori and will be determined as part of the problem. Consider $\frac{dW}{dz}$ as a function of t. We introduce the analytic function Ω by the relation

$$\frac{dW}{dz} = \frac{(t - d)}{(1 - t\ d)} e^{\Omega} \tag{4.8}$$

Considerations of the argument of both sides of the above equation on the real axis shows that Im $\Omega = 0$ on the real t-axis and therefore Ω is extendable to the entire unit circle from Schwarz reflection principle. Thus we may write Ω in a taylor series expansion involving t. We do not do so, instead, for convenience of numerical calculations we introduce

$$\tilde{t} = \frac{(t + t_p)}{(1 + t\ t_p)} \tag{4.9}$$

where t_p is a real number in the open interval (-1,1), chosen suitably as described later. Since $\tilde{t}$ (t) maps the unit circle into the unit circle with -1 and +1 getting mapped to -1 and +1, Ω is an analytic function of $\tilde{t}$ on the unit circle and hence

$$\Omega(\tilde{t}) = a_0 + a_1 \tilde{t} + a_2 \tilde{t}^2 + \cdots \tag{4.10}$$

where $a_0, a_1, \cdots$ are all reals and the power series is convergent for any $\tilde{t}$ inside the unit circle. From continuity of $\frac{dW}{dz}$ it follows that the power series is convergent even on the unit circle.

Now, we wish to find W as a function of t. This is more easily facilitated by introducing the conformal map T (t) defined by

$$T = -\tfrac{1}{2}\,(\,t + 1/t\,) \tag{4.11}$$

which maps the unit semi-circle into the upper half plane. We now consider W as a function of T. If we consider the flow boundaries of region I in the W-plane

shown in fig.4.3, we find from Schwarz-Christoffel transformation

$$\frac{dW}{dT} = \bar{K}\,(T+1)^{-\frac{1}{2}}\,(T-1)^{-\frac{1}{2}}(T-C)^{-\frac{1}{2}}\,(T-D) \tag{4.12}$$

where $\bar{K}$ is an unknown real and C and D are real constants related to c and d through (4.11). Using (4.11) and (4.12), we find

$$\frac{dW}{dt} = -i\,K\,t^{-3/2}\,(t-d)\,(1-t\,d)\,(t-c)^{-\frac{1}{2}}\,(1-c\,t)^{-\frac{1}{2}}, \tag{4.13}$$

where K is just a positive constant. Since $\frac{dz}{dt} = \frac{dW}{dt} \Big/ \frac{dW}{dz}$, it follows that

$$\frac{dz}{dt} = \frac{-i\,K\,(1-d\,t)^2\,e^{-\Omega}}{t^{3/2}\,(t-c)^{\frac{1}{2}}\,(1-t\,c)^{\frac{1}{2}}} \tag{4.14}$$

The condition that the vortex pair combination be a steady one implies that there be no total force on each of the vortices. From Blasius theorem, the forces along x and y directions F_x and F_y are given by

$$F_x - i\,F_y = \tfrac{1}{2}\,i \oint_C \left(\frac{dW}{dz}\right)^2 dz \tag{4.15}$$

for C a closed contour around a vortex. From symmetry considerations, we find that F_x, the force along the x-direction will be automatically zero for any vortex boundary with the assumed symmetry. Hence we only have to impose the requirement that F_y on the upper vortex equals zero, which implies

$$\mathrm{Re}\left[\int_0^{\pi} d\theta\,\frac{e^{\Omega}\,(t-d)^2}{t^{\frac{1}{2}}\,(t-c)^{\frac{1}{2}}\,(1-t\,c)^{\frac{1}{2}}}\right] \tag{4.16}$$

where $t = e^{i\theta}$. From (4.8) and the knowledge of velocity at $t = 0$ (i.e. $\tilde{t} = t_p$), we have

$$U = -d\,e^{\,\Omega(t_p)} \tag{4.17}$$

Further, from geometric considerations

$$-i\,y_B = \int_{-1}^{c} \frac{dz}{dt}\,dt \tag{4.18}$$

For given Ω, equations (4.16), (4.17) and (4.18) constitute three real equations to determine the three unknowns c, d and K for given U and y_B. It is easy to see

that U and y_B are only linear scaling factors and that their absolute values have no bearing on the values of any nondimensional quantities that characterize the flow. Hence, each of them were set equal to unity without any loss of generality. Thus the problem is completely determined in terms of Ω and hence the coefficients $a_0, a_1, \cdots$.

For the special case $\omega = 0$, i.e. the case of hollow vortices, the pressure condition (4.5) becomes on the circumference of the unit $\tilde{t}$ semi-circle

$$q = e^{\mathrm{Re}\Omega} \tag{4.19}$$

Since Im $\Omega = 0$ on the real diameter, it follows that Ω is identically a constant equalling $\log q$, where q, in this case, also equals the magnitude of the velocity of the vortex boundary. Thus in terms of a single parameter q, we may determine the constants d, c and K describing the hollowed vortex flow by solving equations (4.16) through (4.18). The case of the hollow vortex pair was considered earlier by Pocklington and his method of solution involves extensive use of properties of elliptic functions.

For the general case $\omega \neq 0$, the determination of $\Omega(t)$ is more complicated since the velocity in region II has to be taken into account in the pressure condition (4.5). For a vortex boundary point corresponding to $\tilde{t} = e^{i\vartheta}$ for $\vartheta \in [0,\pi]$, (4.5), (4.8) and (4.10) imply

$$a_0 + a_1 \cos\vartheta + a_2 \cos 2\vartheta + \cdots = \tfrac{1}{2} \ln (q^2 + (\nabla\Psi)^2) \tag{4.20}$$

Thus the velocity on the inner side of the vortex sheet $\nabla\Psi$ needs to be determined as a function of ϑ in order that the coefficients in the expansion of (4.20) may be determined for given q. The problem now reduces to determining the right hand side of (4.20) and its Fourier cosine expansion with respect to ϑ in terms of $a_0, a_1, \cdots$. In the next section, we describe how the inner velocity and hence the right hand side of (4.20) is determined for given $a_0, a_1, \ldots$ and c, d and K.

4.5. Determination of the velocity in region II on the vortex sheet

For given a_0, a_1,..... and c, d and K, we integrate $\frac{dz}{d\tilde{t}}$ using equations (4.9), (4.14) and using $z\ (-1) = i\ y_B$, to determine $z\ (e^{i\vartheta})$, the location of the vortex boundary for $\vartheta \varepsilon\ [0,\pi]$. Using reflection on the y axis, the other half of the vortex boundary is located. We are then left with the problem of computing the velocity $|\nabla\Psi|$ on the inner side of the vortex sheet where Ψ satisfies (4.3) in the interior and (4.2) on the boundary. Since the vorticity ω equals a constant, it is convenient to separate Ψ into a particular solution Ψ_p and a harmonic function Ψ_h. Conformal transformation of the interior of the vortex into a full circle then converts the problem into one of determination of a harmonic function from given boundary data on a circle. For the purpose of such conformal mapping, once again as in chapter III, we introduce the complex variable $z_i = -x + i\ y$ defined in region II of the physical plane and its reflection on the y-axis. We take particular solution Ψ_p defined by

$$\omega^{-1}\Psi_p = \frac{1}{2}(Imz_i - y_c)^2 \tag{4.21}$$

where $y_c = \frac{1}{2}\ (y_A + y_B)$

Consider the conformal map $Q(z_i)$ that maps the z_i plane interior of the vortex into the unit circle so that A gets mapped to -1, B gets mapped to +1. The third degree of freedom in the Riemann mapping function is automatically decided by the conformal mapping procedure to be described later in which some point in the imaginary z_i axis is mapped to the origin of the Q-plane. The details of the the mapping function $z_i(Q)$ will be discussed in the next section. It will be seen that the real diameter in Q plane corresponds to the imaginary z_i-axis between B and A. We now consider Ψ_h as a function in the Q plane which satisfies boundary conditions as follows:

$$\Psi_h\ (e^{i\varphi}) = -\Psi_p\ (z_i\ (e^{i\varphi})) \tag{4.22}$$

where $\varphi \in [-\pi,\pi]$ and $Q = \rho\, e^{i\varphi}$ in the Q-plane. As in chapter III, we can express the velocity in terms of $z_i\,(Q)$, $\frac{dz_i}{dQ}$ and the normal derivative of Ψ_h in the Q-plane. For our choice of Ψ_p, this becomes

$$|\nabla\Psi| = (\,\mathrm{Im} z_i - y_c\,)\,\frac{\mathrm{Im}\left(Q\,\frac{dz_i}{dQ}\right)}{\left|\frac{dz_i}{dQ}\right|} + \left|\frac{dz_i}{dQ}\right|^{-1}\frac{\partial\Psi_h}{\partial\rho} \qquad (4.23)$$

for $Q = e^{i\varphi}$ on the unit circle boundary. Now (4.22) determines the data for the harmonic function Ψ_h on the boundary of the unit circle. Using (3.20) and (3.21) of chapter III, $\frac{\partial\Psi_h}{\partial\rho}$ in (4.23) is determined. Thus determination of $z_i\,(Q)$ and $\frac{dz_i}{dQ}$ as described in the following section allows us to compute the right hand side We note that in (4.20) we need $|(\nabla\Psi)|^2$ as a function of ϑ and not φ, as given by (4.23). However, for each ϑ , (4.14) and (4.9) determines $(x(\vartheta),y(\vartheta))$ on the physical vortex sheet and therefore the corresponding position in the z_i plane. The conformal map $Q(z_i)$ provides the relation $\varphi(z_i(\vartheta))$ needed to determine the velocity as a function of ϑ. The details of this correspondence and its usage are discussed in section 4.7.

4.6. Mapping into a circle in the Q-plane

As mentioned before, we wish to find $Q(z_i)$ that maps the z_i-plane interior of the vortex into a circle with A mapped to +1, B to -1 and some point on the imaginary z_i axis to the origin. This will be done here by first mapping the vortex boundary in the z_i plane into a near circle through some explicit readily invertible transformations. The mapping from the near circle to an exact circle is then done by solving Theodersen's integral equation exactly as in the last chapter.

Since the shapes of each of the vortices is likely to be elongated as for the case of uniform vortex core with no vortex sheet (see Pierrehumbert, 1980) with large curvature close to the major axis when the distance between the the

vortices is small, we carry out some explicit transformation to get rid of large curvatures. However, for both the hollow vortex or the uniform vortex limit the vortex shape is not quite symmetric about a straight line parallel to the x axis passing through the center of mass of a vortex (especially for small separation of the vortices). Thus the transformation (3.24) cannot be immediately applied to wipe out regions of large curvature. In order to make the geometry more symmetric about its centerline, a bilinear transformation is introduced as follows:

$$W_1(z_i) = \frac{(i\, z_i + y_c)}{(z_i - z_c)} \tag{4.24}$$

where $y_c = \frac{1}{2}(y_A + y_B)$ and z_c is as shown in fig. 4.4. Fig.4.5a shows t;he approximate shape of the boundary in the W_1-plane. Once a more symmetric boundary is obtained we further transform

$$W_2(W_1) = -i\, \frac{\left(r \sin\frac{\delta}{2} + W_1\right)^{\pi/\delta} - \left(r \sin\frac{\delta}{2} - W_1\right)^{\pi/\delta}}{\left(r \sin\frac{\delta}{2} + W_1\right)^{\pi/\delta} + \left(r \sin\frac{\delta}{2} - W_1\right)^{\pi/\delta}} \tag{4.25}$$

Fig.(4.5b) shows the approximate shape of the transformed boundary with appropriate choice of r and δ. This is nearly circular with the real axis corresponding to the imaginary axis in the z_i-plane. If $W_2 = R_w\, e^{i\nu}$ and $Q = e^{i\varphi}$, $-\pi \leq \nu$, $\varphi \leq \pi$, characterize corresponding points on the vortex boundary in the W_3 plane and the unit circle respectively, then as in chapter III, Theodersen's integral equation (3.25) is satisfied by $\nu(\varphi)$. As in chapter III, the solution to this integral equation is conveniently found in the Fourier space and once the iterations converge we obtain the complex Fourier series for $\log(R_w(\nu(\varphi)))$ which allows us to find the coefficients of the Fourier cosine series in φ as well, since it is an even periodic function. From such a series, we obtain the coefficient b_n in

$$\log\left(\frac{W_2}{Q}\right) = \sum_0^\infty b_n Q^n \tag{4.26}$$

inverting the relations in the equations (4.24), (4.25) and using (4.26) we arrive at $z_i(Q)$ from which $Q(z_i)$ is known in principle . The velocity is therefore

determined from the inside of the vortex sheet for a given vortex sheet location. Equating the coefficients of $\cos n\tilde{\theta}$ in (4.20) the coefficients a_0, a_1,... are determined in the same way as in chapter III..

4.7. Numerical Procedure

The procedure used for numerical calculation is quite similar to the one in chapter III. However, it differs in some details. For purposes of clarity, we describe the entire procedure without reference to chapter III even though some steps are exactly the same as in the last chapter. We start with an initial guess of N coefficients $a_0, a_1, \ldots, a_{N-1}$ and obtain an approximate $\Omega(\tilde{t})$ by truncating (4.10). For each q and ω, we use a value of t_p such that the coefficients in the series expansion (4.10) decay rapidly. As ω and q are changed, t_p is adjusted so that the coefficients of Ω in (4.10) continue to decay rapidly. No fine tuning was done, but the degree of freedom offered by arbitrary choice of t_p in the interval (-1, 1) helped tremendously in some cases as far as the decay rate and hence the number of terms in (4.10) needed to describe Ω to the desired level of accuracy. For fixed q and ω small, the guess for Ω and hence a_0 is $\ln q$. The guess for all other coefficients is zero. For bigger values of ω corresponding to the same q, we use values of the coefficients obtained from the Fourier transform with respect to $\tilde{\theta}$ of the boundary values of converged solution Ω for slightly smaller ω. Note that an initial guess of a_0, a_1,... equalling the converged values of these coefficients for slightly different ω or q may be unsatisfactory because of greatly differing values of t_p used in the two cases. In the following, for fixed q and ω, we describe the procedure used to find the $(n+1)$st iterate given the nth iterates a_0^n, $a_1^n \cdots a_{N-1}^n$ and therefore $\Omega^n(\tilde{t})$.

We use (4.16), (4.17) and (4.18) to determine K, c and d for given values of a_0, a_1,... and hence Ω where (4.9) is used to find $\tilde{t}$ for given t. This determination is easily made by first using (4.17) to determine d. Since equation (4.16) is

independent of K, the left hand side is a nonlinear implicit function of one variable c. Newton iteration was used for solving (4.16). Once d and c are determined, only one integration in needed to determine K from (4.18). Equations (4.14) and (4.9) then determines $z(\vartheta) = x(\vartheta) + i\, y(\vartheta)$ and hence $z_i(\vartheta) = -x(\vartheta) + i\, y(\vartheta)$ on the vortex sheet for N_1 points where $\vartheta_k = (k-1)\pi/(N_1-1)$, $k=1, 2,\ldots N_1$. and N_1 is chosen of the form $N_1 = 1 + N\,l$, where l is any positive integer. A subset of these ϑ values of the form $\vartheta_{k_j} = (j-1)\,l\,\pi/(N_1-1)$ for $j=1,2,\cdots N+1$ are the ϑ values at which velocities will be calculated and (4.20) used to find the N coefficients a_j. The uniform spacing of ϑ_{k_j} over a semicircle allows usage of fast Fourier transform for the calculation of Fourier cosine series coefficients of the function on the right hand side of (4.20) once the the velocity $\nabla\Psi$ is calculated at those points. Now, we find the images $R_w(\nu_k)\, e^{i\nu_k}$ in the W_2 plane for these N_1 points in the z_i plane, using equations (4.24) through (4.25). The ν values in the W_2-plane image of the subset of z_i points characterized by the angles ϑ_{k_j}, are denoted by ν_{k_j}. Reflection on the real axis provides us with a set of $N_1 - 2$ new points on the near-circular vortex boundary in the W_2-plane. All together, we then have $2N_1-2$ points at which $R_w(\nu_k)$, ν_k are known. For large enough N_1, this provides a very accurate description of the function $R_w(\nu)$ for arbitrary ν through cubic spline interpolation. We then take N_3 points on the unit Q-circle, evenly spaced in the angular variable φ, and carry out the process of solving Theodersen's integral equation (3.25) exactly as described by Henrici (1979). In the process, we obtain the first $\frac{1}{2}N_3$ b_n coefficients in (4.26) . The b_n coefficients define $W_3(Q)$ in (4.26). We then start with N_2 uniformly spaced points on the circumference of the unit Q-circle with $Q_m = e^{2\pi i(m-1)/N_2}$ for $m=1, 2,\ldots N_2$. We calculate $W_2(Q_m)$, $z_i(W_2(Q_m))$ using (4.24), (4.25) and (4.26) at those points. Using (4.21) and (4.22) we calculate Ψ_h at those boundary points and use them in (3.20) and (3.21) to find $\dfrac{\partial\Psi_h}{\partial\rho}$

at N_2 points. At the $(\frac{1}{2}N_2 + 1)$ points which is part of the upper half Q semi-circular boundary including those on the real axis, we calculate $\frac{dz_i}{dQ}$ using (4.24), (4.25) and (4.26). These, together with values of other terms in (4.23) already calculated provide the velocities at the $(\frac{1}{2}N_2 + 1)$ points on the upper half semicircle If ν_m, m=1, 2,..., $(\frac{1}{2}N_2 + 1)$ denote the angular positions of the images of those Q points in the W_3 plane , we use these to interpolate velocities at the $N + 1$ points ν_{k_j} through cubic splines. Because of the correspondence of ν_{k_j} with $N + 1$ uniformly spaced out points in the θ variable as discussed earlier, we therefore arrive at the velocities from the inner side of the vortex sheet at the physical z locations corresponding to $N + 1$ equispaced points in the θ variable from which the first N coefficients of the Fourier cosine series in (4.20) are determined.

4.8. Numerical results and discussions.

The values of the coefficients completely characterizing the flow for the hollow vortex is listed against parameter q in table (4.1). The corresponding shape of the upper half vortex is shown in fig.4.6 where y_B were set equal to the same value.

Table (4.2) lists the various quantities of interest corresponding to several different ω with q held fixed at 3.0. The corresponding vortex geometries is shown in figure 4.7. The iteration scheme failed to converge when ω was increased beyond some critical number, 9 being the critical value corresponding q = 3.0. Small values of q and ω correspond to the small separation between the vortices. It was considered interesting to find out whether there exist very elongated vortices without vortex sheet in the limit of zero separation between the vortices. Unfortunately, our method of solution did not shed any light on this possibility because the iteration scheme failed to converge even for

relatively small ω when q/U approached the limiting value of 1.

However, we believe the reduction of the entire exterior flow with unknown boundaries into one unknown function Ω of one variable on a fixed domain opens a lot of possibilities and deserves to be investigated further. As a possibility, Newton iteration could be be applied for the determination of Ω to find whether vortices can continue to get elongated as their separation is reduced, a question raised by Saffman (1979). More generally, the function theoretic approach introduced in the last two chapters offers great hopes for solving a wide class of flows with vortex sheet and distributed vorticity, problems which may otherwise be considered almost intractable.

In the following section, we calculate a pair of touching vortices with no vortex sheet. The calculation is done using contour dynamics technique due to Zabusky.

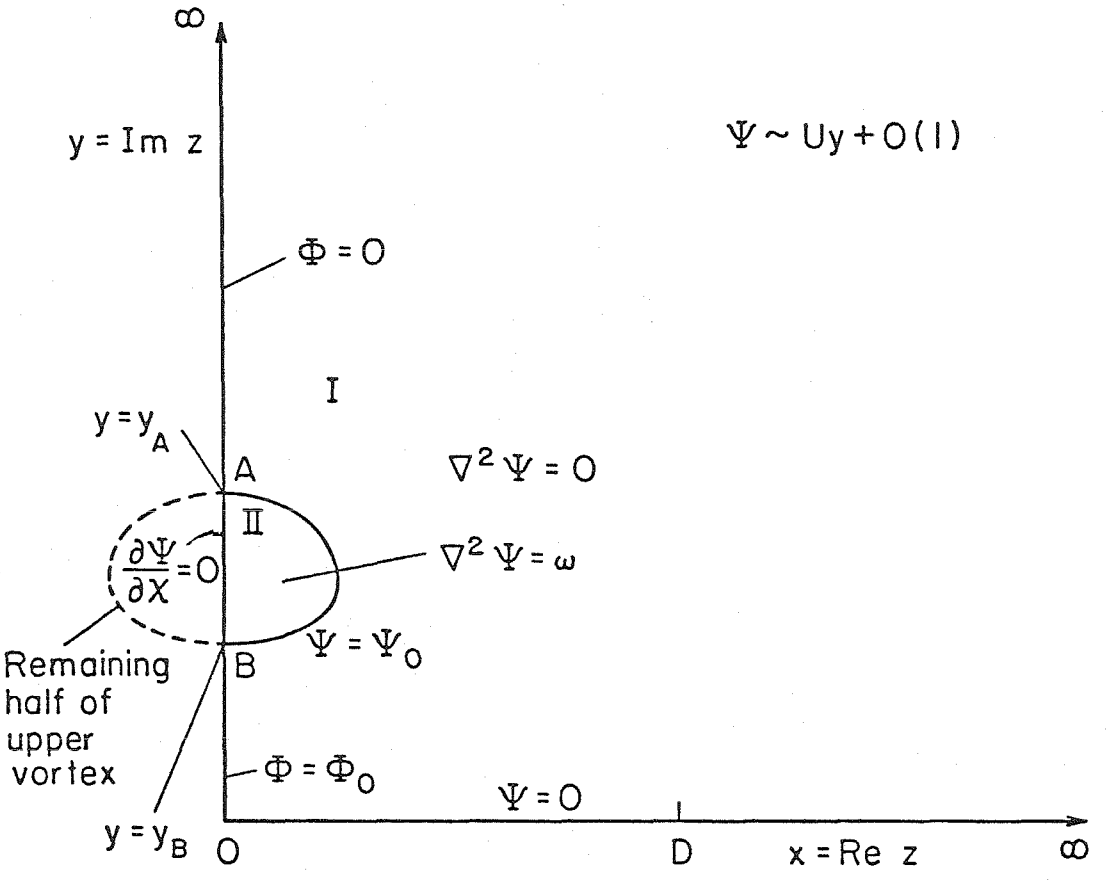

Fig.4.1 : The flow region in the first quadrant of the z-plane (physical plane).

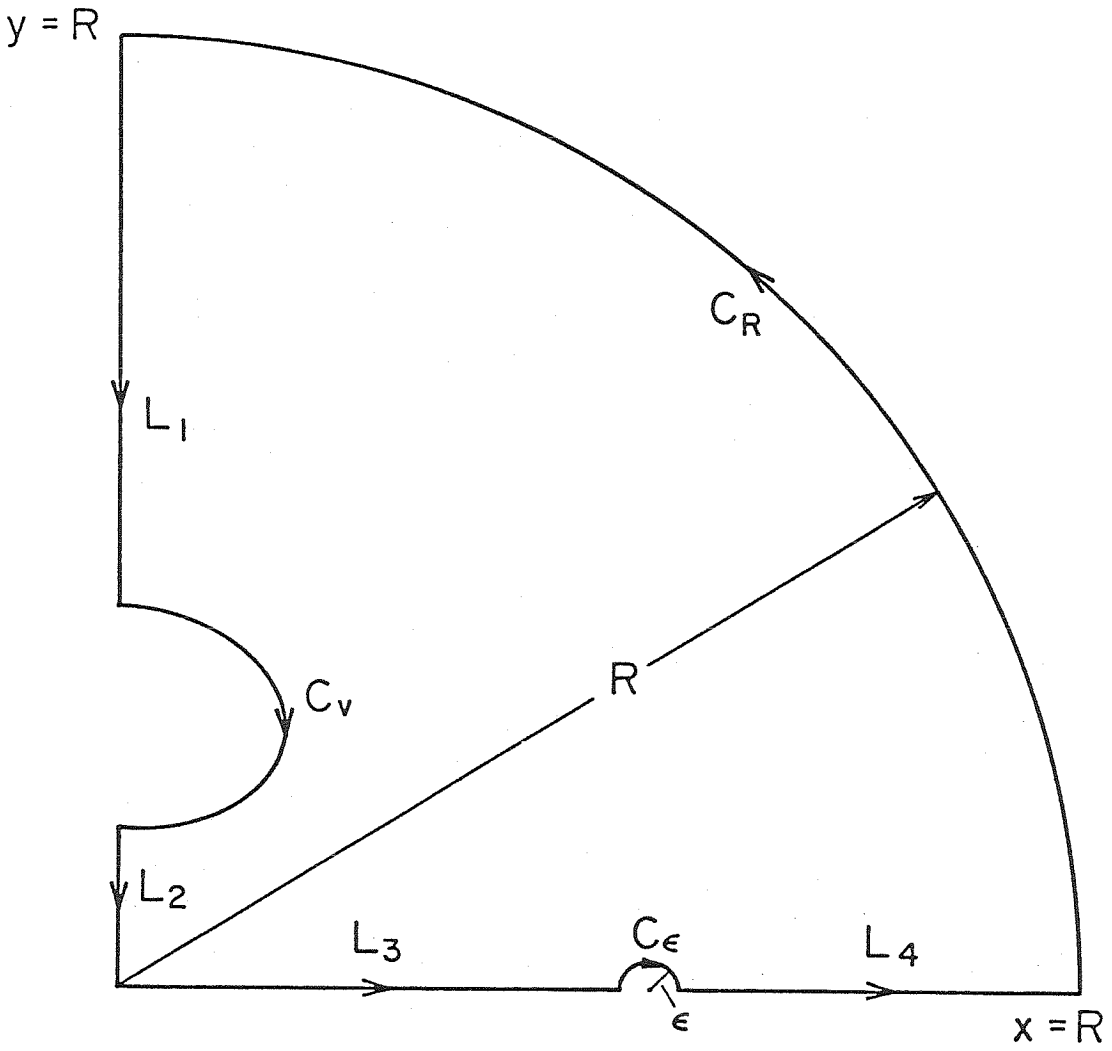

Fig.4.2 : The closed contour C for integration of $\frac{1}{2\pi i} \frac{\frac{d^2 W}{dz^2}}{\frac{dW}{dz}}$.

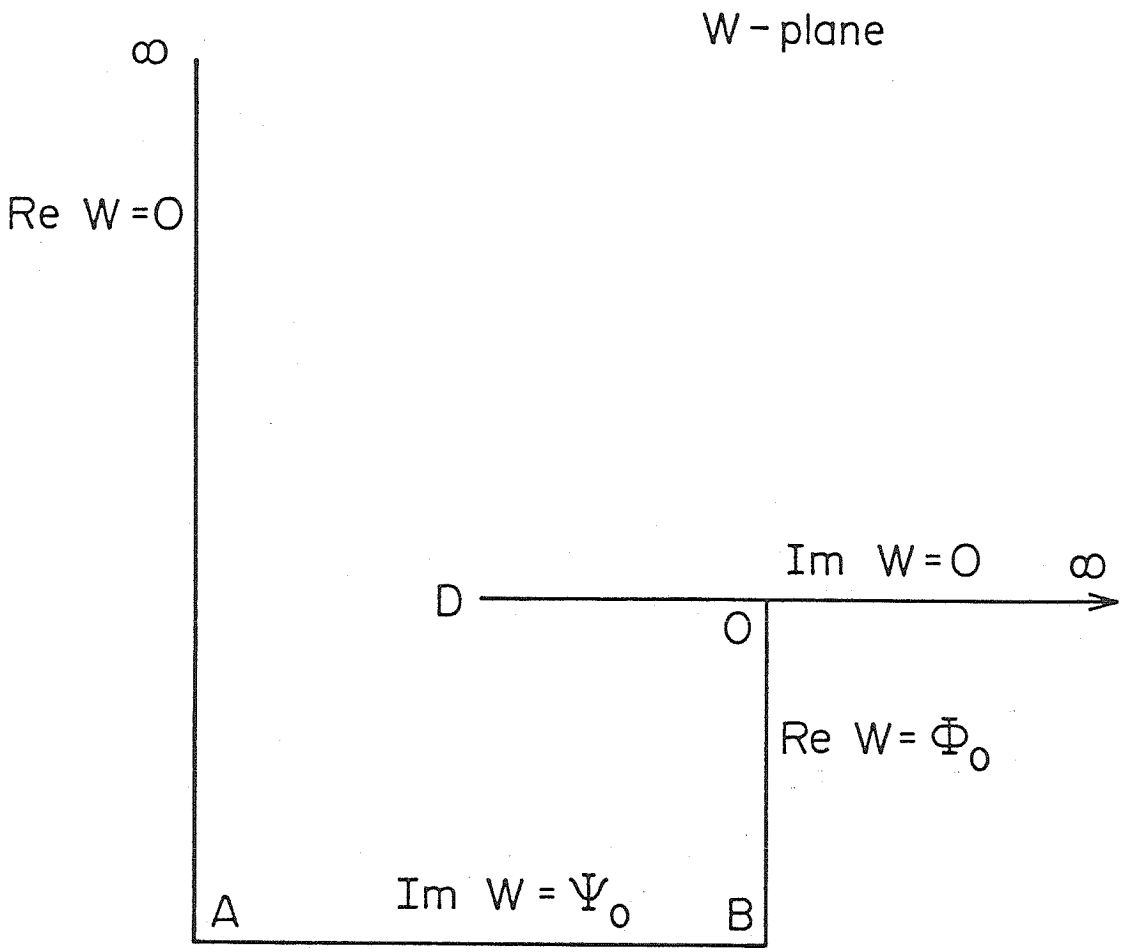

Fig.4.3 : The flow region in the W-plane.

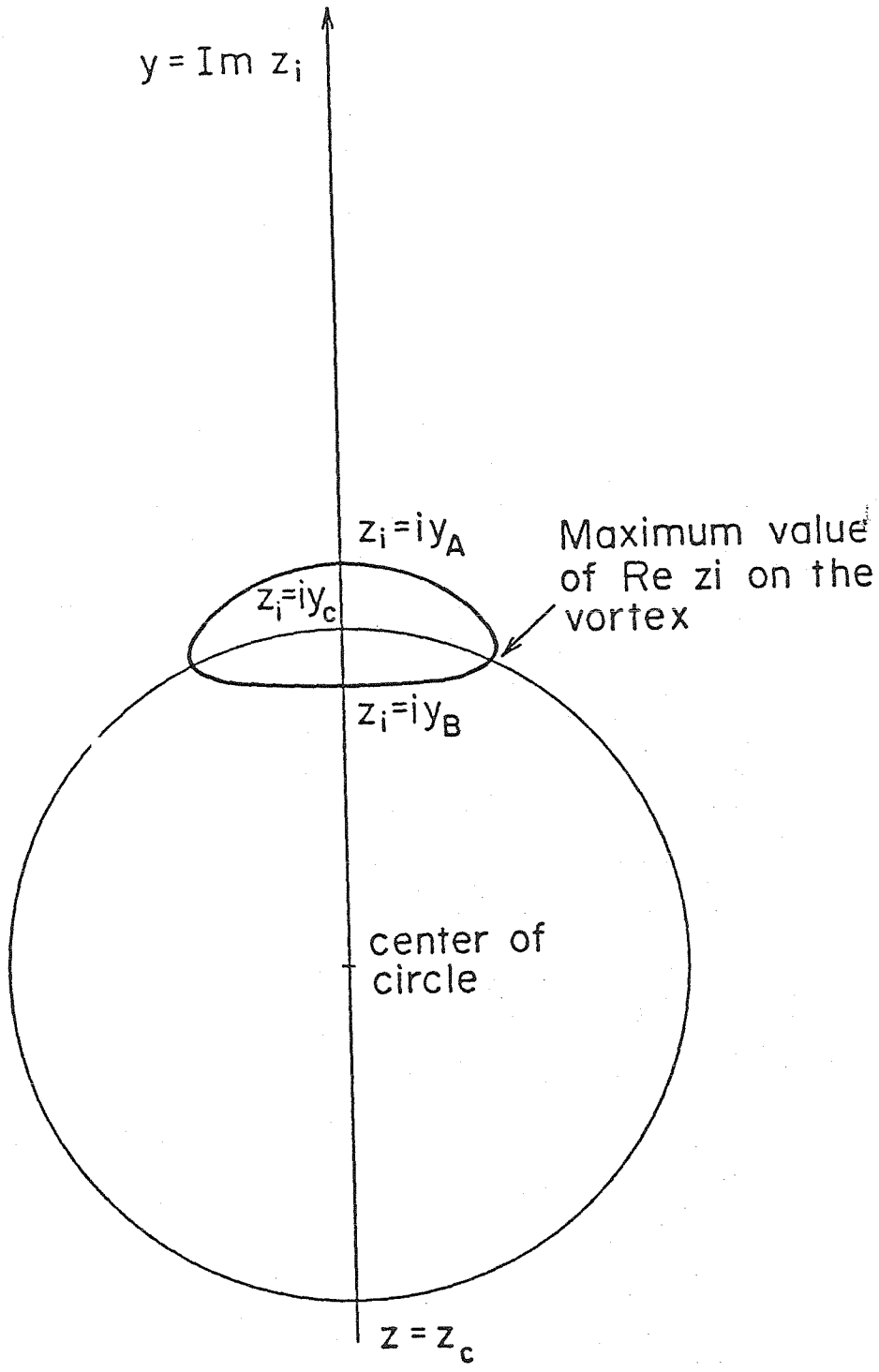

Fig.4.4: The dark solid lines show the upper vortex boundary in the z_i -plane. A circle is drawn such that it passes through $y_c = \frac{1}{2}(y_A + y_B)$ and points on the vortex boundary for which the real part of the z_i are maximum and minimum. z_c denotes the is the location of the other intersection point of the circle with the y-axis.

(a)

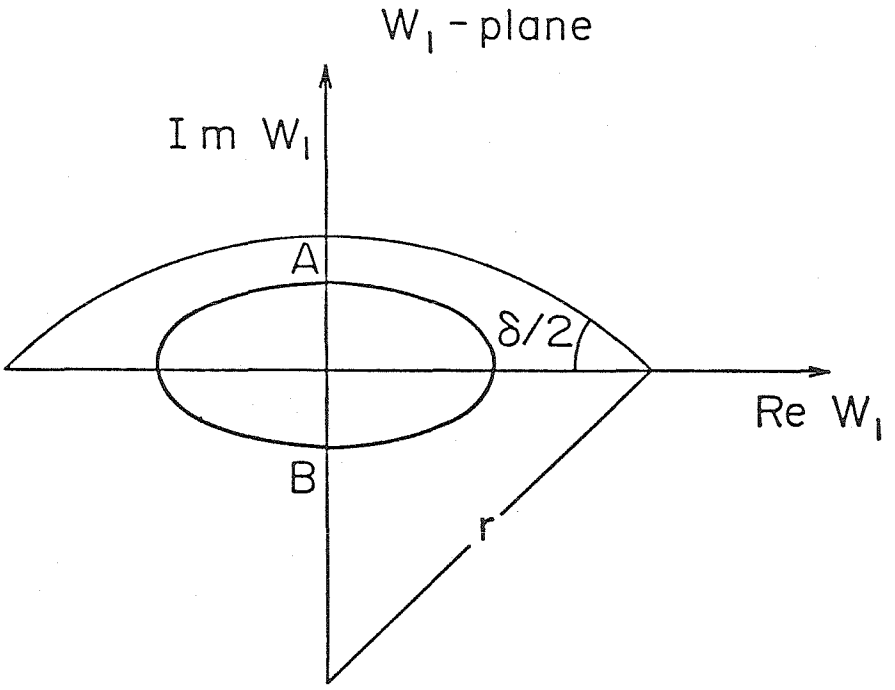

(b)

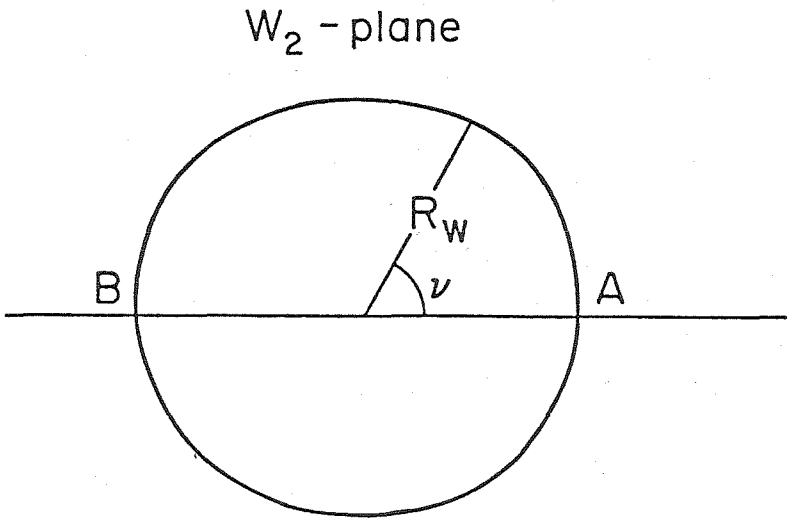

Fig.4.5: The shape of the vortex in the W_1 and W_2 planes.

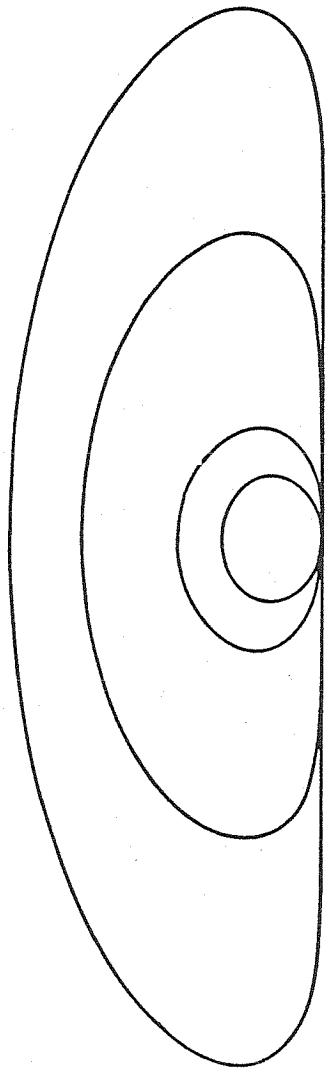

Fig.4.6 : The shapes of hollowed vortices in the upper half z-plane for values of $q / U = 1.7, 2.0, 3.0$ and 4.0 and for the same value of q / U. As q / U increases, the vortex becomes smaller.

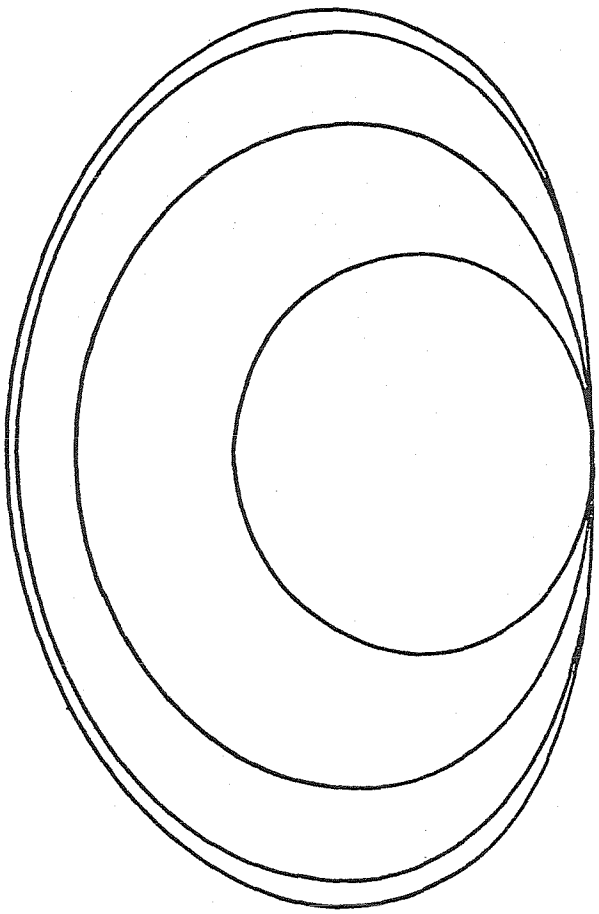

Fig. 4.7 : The shapes of upper half vortices for $q / U = 3.0$ and for $\omega l_1 / U = 0.0, 1.0, 3.0, 9.0$. For fixed q / U, as $\omega l_2 / U$ increases the vortex gets smaller.

Values of constants characterising hollowed vortex pair			
-	$q\ /\ U = 1.7$	$q\ /\ U = 2.0$	$q\ /\ U = 3.0$
c	-0.99999898	-0.9996368	-0.947143
d	-0.588235	-0.500000	-0.333333
K	6.383068	5.088503	3.905521

Table 4.1.

Physical properties of Vortex pair for $q\ /\ U = 3.0$.				
-	$\omega\, y_B\ /\ U = 0$	$\omega\, y_B\ /\ U = 1$	$\omega\, y_B\ /\ U = 3$	$\omega\, y_B\ /\ U = 9.0$
$\Psi_o\ /\ \Gamma$	-0.0982	-0.1019	-0.1197	-0.1612
$\omega S\ /\ \Gamma$	0.0000	0.2219	0.5008	0.7489
$(S\ /\ \pi)^{1/2}\ /\ y_{cm}$	0.6893	0.6693	0.5860	0.4436
$y_B\ /\ y_A$	0.3017	0.3041	0.3280	0.4134
$y_{cm}\ /\ y_A$	0.6375	0.6402	0.6573	0.7046
$x_s\ /\ y_{cm}$	1.9023	1.8773	1.8033	1.7494
$y_s\ /\ y_{cm}$	2.1063	2.1040	2.0961	2.0895
$4\,\pi\, U\, y_{cm}\ /\ \Gamma$	0.9319	0.9413	0.9701	0.9925
$S_t\ /\ (2S)$	4.2726	4.4613	5.5581	9.3366
$T\ /\ (\rho\Gamma^2)$	0.1721	0.1784	0.2064	0.2623

Table 4.2. Γ is the total circulation around the upper half vortex, S the area of each vortex, x_s and y_s are the x and y intercept values of the separating streamline, S_t the total area enclosed by the separating streamline, y_{cm} the y value of the center of mass and T the total kinetic energy in a frame of reference where the vortices move with velocity U.

The touching pair of equal and opposite uniform vortices

P. G. Saffman and S. Tanveer
Department of Applied Mathematics, California Institute of Technology, Pasadena, California 91125

(Received 16 July 1982; accepted 13 August 1982)

The shape and speed of a pair of touching finite area vortices are calculated and an error in previous work corrected.

Pierrehumbert[1] presents steady-state solutions for two-dimensional finite area vortex pairs of equal and opposite uniform vorticity in an inviscid incompressible fluid. He claims that as the gap between the vortices decreases, the shapes approach a limit in which the pair touch along the axis of symmetry with a cusp at each end. The purpose of this letter is to point out that Pierrehumbert's analysis is incomplete and that there exist solutions without cusps, the vortex boundary being perpendicular to the axis as sketched in Fig. 1, although the curvature is infinite. We have recalculated the shapes and find, however, that apart from the behavior near the axis, our shape and his are in good agreement (see Fig. 2) and the calculated speeds also agree to two significant figures.

The flow can be reduced to rest by superposing a velocity U equal and opposite to the speed of the pair. The axis of symmetry is a streamline and it is sufficient to consider the flow in the upper half-plane. We shall also assume fore and aft symmetry. (The existence of nonsymmetrical solutions is an open question.) To consider the shape near the end A of the axis of symmetry, take polar coordinates r, θ centered on A. The stream function ψ satisfies $\nabla^2\psi = 0$ in region I and $\nabla^2\psi = -\omega$ in region II. Take the local expansions in the form

$$\omega^{-1}\psi_{\rm I} = (2\pi)^{-1}(r^2 \ln r \sin 2\theta + \theta r^2 \cos 2\theta) + \alpha r^2 \sin 2\theta + \beta_1\left(\frac{r^2 \ln r \sin 2\theta - \theta r^2 \cos 2\theta}{(\ln r)^2 + \theta^2}\right) + O(r^2/(\ln r)^2), \quad (1)$$

$$\omega^{-1}\psi_{\rm II} = (2\pi)^{-1}(r^2 \ln r \sin 2\theta + \theta r^2 \cos 2\theta) - \tfrac{1}{2}r^2 \sin^2\theta - \tfrac{1}{2}r^2 \cos 2\theta + \alpha r^2 \sin 2\theta + \beta_2\left(\frac{r^2 \ln r \sin 2\theta - \theta r^2 \cos 2\theta}{(\ln r)^2 + \theta^2}\right) + O(r^2/(\ln r)^2). \quad (2)$$

It is easily verified that $\psi_{\rm I}$ and $\psi_{\rm II}$ satisfy the differential equations. Further $\psi_{\rm I} = 0, \psi_{\rm II} = 0$ on $\theta = 0, \pi$, respectively. The velocity has to be continuous on the boundary of the vortex, i.e., $\psi_{\rm I} = \psi_{\rm II} = 0$ and $(\partial\psi_{\rm I}/\partial\theta) = (\partial\psi_{\rm II}/\partial\theta)$ when $\theta = \Theta(r)$ say (continuity of pressure is then automatically satisfied). A little algebra shows that these equations are satisfied to $O(r^2/\ln r)$ accuracy if the boundary is taken to be

$$\Theta(r) = \pi/2 - \pi/(4\ln r) + \gamma/(\ln r)^2 + \ldots, \quad (3)$$

provided $\beta_2 - \beta_1 = \pi/8$ and $\gamma = \pi/8 + \frac{1}{4}\alpha\pi^2$. The assumption that the leading order term for $\psi_{\rm I}$ and $\psi_{\rm II}$ is $r^2 \ln r \sin 2\theta$ can be checked by local expansion around A of $w(z)$ given in Eq. (5), provided the slope of the boundary at A is nonzero. Pierrehumbert's argument for the nonexistence of solutions with nonzero slope overlooked the possibility of logarithmic terms.

The equation to be solved for the determination of the vortex boundary is

$$\mathrm{Im}[w(z)] = 0, \quad (4)$$

where

$$w(z) = -Uz - \frac{\omega}{4\pi}\int_C [(z-z')\ln(z-z') + (z+z')\ln(z+z')]\,d\bar{z}' + [(z-\bar{z}')\ln(z-\bar{z}') + (z+\bar{z}')\ln(z+\bar{z}')]\,dz', \quad (5)$$

and C is the anticlockwise contour in the first quadrant of Fig. 1. Deem and Zabusky[2] first used a similar formula to determine vortex boundaries. Equation (4) is a nonlinear in-

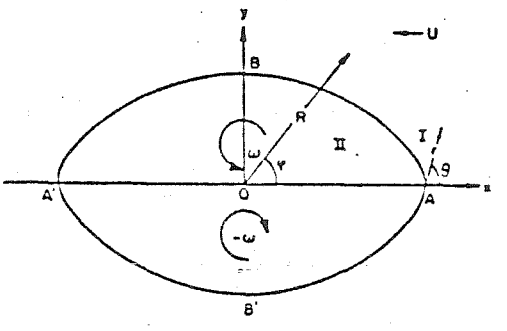

FIG. 1. Sketch of flow geometry and coordinate system for touching vortex pair.

 0031-9171/82/111929-02$1.90

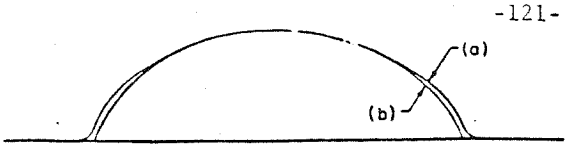

FIG. 2. Comparison of Pierrehumbert's[1] solution (a) and present solution (b) for vortices of the same width.

tegral equation for the vortex boundary. The only length scale in the problem is (U/ω). Given U and ω, the flow and vortex boundary are completely determined and in particular the area S of each vortex is given by

$$S = kU^2/\omega^2, \tag{6}$$

where k is a constant to be determined.

We introduce polar coordinates R, φ centered on 0 (Fig. 1). We constructed numerical solutions by writing R as:

$$R(\bar{\varphi}) = \sum_{n=0}^{N-1} R_n \cos(2n\bar{\varphi}), \tag{7}$$

where $\bar{\varphi}$ is related to the actual angle φ by

$$\varphi = \bar{\varphi} - 0.5 \sin(2\bar{\varphi}). \tag{8}$$

Equation (4) was then satisfied at the points $\bar{\varphi}_j = j\pi/2N$; $j = 1,2,...,N$. The stretching Eq. (8) concentrated the collocation points close to the axis. Notice also that $d\varphi/d\bar{\varphi} = 0$ at $\varphi = 0$ and therefore a Fourier cosine series in $\bar{\varphi}$ does not preclude cases with cusps on the axis. Approximating the integrals in Eq. (5) by sums then reduces Eq. (4) to set of N nonlinear equations in the N unknowns $R_0, R_1,...,R_{N-1}$. Since, irrespective of the vortex boundary choice, the imaginary part of $w(z)$ given by Eq. (5) is close to zero near the axis, we chose

$$\mathrm{Im}\{f_j w\{R(\bar{\varphi}_j)\exp[i\varphi(\bar{\varphi}_j)]\}\} = 0 \tag{9}$$

for $j = 1,...,N$ as our modified nonlinear system, where the numbers f_j were made appropriately big for points close to the axis. In this way, sensitivity of the left-hand side of Eq. (9) to the boundary curve near the axis was ensured. The system was solved by Newton iteration. Here $N = 20$ was found sufficient to give $R(\bar{\varphi})$ to 6 significant figures. Our numerical results support the analytical result that $\theta \sim \pi/2 - \pi/(4 \ln r)$ near A. For $r = 1.3 \times 10^{-2}$ in units of U/ω, the 2-term approximation gives $\theta = 1.689$ and numerical calculation yielded $\theta = 1.697$. Comparison over a range of r between 10^{-3} to 10^{-2} revealed about the same kind of agreement. For smaller r, the agreement was a little worse for the quantity $(\theta - \pi/2)$ because of limitations of numerical accuracy. The value of k in Eq. (6) was found to be 37.11. Pierrehumbert's value is 37, inferred from his numbers.

Saffman and Szeto[3] argued that this solution with touching vortices may be isolated and not the limit of a vortex pair. This question still remains open.

This work was supported by the U. S. Department of Energy (Office of Basic Energy Sciences) and the Office of Naval Research.

[1]R. T. Pierrehumbert, J. Fluid Mech 99, 129 (1980).
[2]G. S. Deem and N. Zabusky, Phys. Rev. Lett. 40, 859 (1978).
[3]P. G. Saffman and R. Szeto, Phys. Fluids 23, 2339 (1980).

APPENDIX 1

Here, we point out a few errors in the paper by Pocklington (1898). In this appendix we use exactly the same notation as in Pocklington. Rather than repeating all the arguments, we will refer the reader to Pocklington's paper and assume familiarity with it.

Up to equation (3) on page 181, we found no errors except for a possible misprint in the first paragraph on page 181, where it is mentioned that $+k, -k$ corresponds to G' and C'. Actually, it is $+1/k, -1/k$ that corresponds to those two points. A more serious error occurs in first paragraph on page 182, where it is mentioned that points D'', and F'', B'' and H'', A'' or I'' correspond to points $t = 1, -1$, $t = +a, -a$ and $t = \infty$ respectively. A correct statement would be, if D'' exchanged places with F'' and B'' with H'' in the above statement in Pocklington. This is less likely to be a printing error, since based on the above incorrect assumption, the statement on page 182 regarding the imaginary part of Ω diminishing by πi follows. Actually, the imaginary part of Ω increases by πi as t increases through the value a. Clearly the statement about D'' being mapped to $t = 1$, etc., could not be correct since the flow region in the Ω plane and the t- plane would not be oriented properly for a conformal mapping to exist. The consequence of these errors, fortunately, is minimal and eventually, all the major derived equations, namely (4), (5), (6), (7) and the expression for $\frac{dz}{dW}$ on the last line of page 182 are correct.

On page 187 of the paper, it is claimed that corresponding to $k = \sin 89°$, the velocity of vortex translation V is 0.97 U, where U is the velocity of the vortex boundary. Also, it is mentioned that figure 7 corresponds to this value of k. Both of these claims are incorrect. Using values of K and E as given in

Abramowitz and Stegun (1970), we calculated a^2 and substituting into $V/U = (2a^2 - 1 - 2a\,(a^2 - 1)^{\frac{1}{2}})$, we found V/U (U/q by the notation of chapter IV) to be 1.0 / 2.8072 and not 0.97. Further, for this value of V/U, it was found by applying the method of chapter IV that the vortex boundary corresponding $k = 89°$ is as given in fig.7 below. Pocklington's method was not applied because the numerical values of the Jacobi Zeta function was not readily available for the argument $k = \sin 89°$. However, the two methods were found to produce identical shapes of the vortex for $k = \sin 88°$, for which V/U = 1.0 / 3.13439.

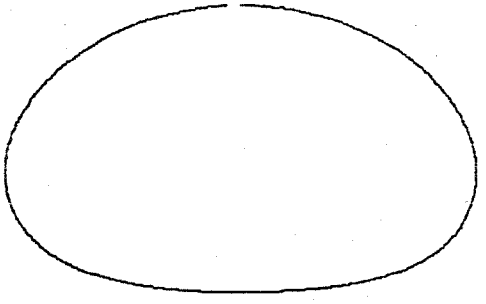

Fig. 7

References

1. Abrahomowitz,M. and Stegun,I., 1970, *Handbook of Mathematical functions*, National Bureau of Standards

2. Batchelor,G.K.,1956a, *On steady laminar flow with closed streamlines at large Reynolds number*, J.Fluid Mech.,1, 177-190.

3. Batchelor,G.K.,1956b, *A proposal concerning laminar wakes behind bluff bodies at large Reynolds number*, J.Fluid Mech.,1, 388-398

4. Birkhoff, G. and Zarantonello, E.H.,1957, *Jets, Wakes and Cavities*, Academic Press.

5. Cox, J.,1973 *The Revolutionary Kasper Wing* Soaring 37, 20

6. Deem,G.S. & Zabusky, N.,1978 *Stationary 'V-states', interactions, recurrence and breaking.* Solitons in Action, (eds: Longren & Scott), Academic

7. Dzugaev,H.,1982, *Solution of flow over a diaphragm in a two dimensional channel*, Izvestiya Akademii Nauk SSSR, Mekhanika Zhidkostii Gaza, July-August,134-137.

8. Goldstein, S., 1948, *On laminar boundary layer flow near a position of separation*, Quarterly J. Mech., 1, 43-69.

9. Henrici,P.,1979, *The use of fast Fourier transform in computational complex analysis*, Siam Review, 21, 4, 481-527.

10. Herwig, H.,1982 *Die Anwendung der asymptotischen Theorie auf laminare Stromungen mit endlichen Ablosegebieten*, Z. Flugwiss, Weltraumforsch 6, 4, 266-279.

11. Hurley, D. and Skeat, N.,1957, *A series of Aerofoils designed to develop exceptionally large lift coefficients when boundary layer control by blowing is employed*, ARL /A-102.

12. Hurley, D. and Ruglen, 1958, *The use of boundary layer control to establish free-streamline flows, being an introduction to the free-streamline flap*, ARL /A-109.

13. Pierrehumbert,R.T.,1980, *A family of steady, translating vortex pairs with distributed vorticity*, J.Fluid Mech. 99, 1, 129-144.

14. Pocklington, H.C.,1898, *The Configuration of a pair of equal and opposit hollow straight vortices of finite cross-section, moving steadily through fluid.* Cambridge Phil. Soc., 8, 178-187.

15. Prandtl, L.,1904, *Uber Flussigkeitsbewegung bei sehr kleiner Reibung*, Verh III, int. Math. Kongr., Heidelberg, 484-491, Teubner, Leipzig.

16. Rossow, V.J.,1978, *Lift enhancement by an externally trapped vortex*, Journal of Aircraft, 15, 9, September, 618-625

17. Sadovskii, V.S.,1971, *Vortex regions in a potential stream with a jump of Bernoulli's constant at the boundary*, PMM, 35, 5, 773-779.

18. Saffman, P.G. & Sheffield, J.S.,1977 *Flow over a Wing with an Attached Free Vortex*, Studies in Applied Math, 57, 107-117

19. Saffman, P.G.,1981, *Dynamics of vorticity*, J.Fluid Mech., 106, 49-58.

20. Saffman, P.G., 1979 *The approach of a vortex pair to a plane surface in inviscid fluid*, J.Fluid Mech., 92, 497-503

21. Saffman, P.G. & Tanveer,S.,1982, *The touching pair of equal and opposite uniform vortices* Phy. Fluids, 25, 1929-1930

22. Sheffield, J.S.,1978 *Topics in vortex motion*, Ph.D thesis, Department of Applied Math, California Institute of Technology.

23. Thwaites,1960 *Incompressible Aerodynamics*, Oxford University Press

24. Smith, A.M.O., 1975, *High lift aerodynamics*, AIAA Journal of Aircraft, vol.12, no.6, 501-530

25. Werle, H. ,1974, *Laminar separation in 2-D, comparison between theory and experiment*, DTMB translation 297.